

Award Number: W81XWH-12-1-0527

TITLE: Function of Brg1 Chromatin Remodeling Factor in Sonic Hedgehog-Dependent Medulloblastoma Initiation and Maintenance

PRINCIPAL INVESTIGATOR: Xuanming Shi

CONTRACTING ORGANIZATION:  
University of Texas, Southwestern Medical Center at Dallas  
Dallas, TX 75390-9105

REPORT DATE: December 2015

TYPE OF REPORT: Final

PREPARED FOR: U.S. Army Medical Research and Materiel Command  
Fort Detrick, Maryland 21702-5012

DISTRIBUTION STATEMENT: Approved for Public Release;  
Distribution Unlimited

The views, opinions and/or findings contained in this report are those of the author(s) and should not be construed as an official Department of the Army position, policy or decision unless so designated by other documentation.

REPORT DOCUMENTATION PAGE				Form Approved OMB No. 0704-0188	
Public reporting burden for this collection of information is estimated to average 1 hour per response, including the time for reviewing instructions, searching existing data sources, gathering and maintaining the data needed, and completing and reviewing this collection of information. Send comments regarding this burden estimate or any other aspect of this collection of information, including suggestions for reducing this burden to Department of Defense, Washington Headquarters Services, Directorate for Information Operations and Reports (0704-0188), 1215 Jefferson Davis Highway, Suite 1204, Arlington, VA 22202-4302. Respondents should be aware that notwithstanding any other provision of law, no person shall be subject to any penalty for failing to comply with a collection of information if it does not display a currently valid OMB control number. PLEASE DO NOT RETURN YOUR FORM TO THE ABOVE ADDRESS.					
1. REPORT DATE December 2015		2. REPORT TYPE Final		3. DATES COVERED 15Sep2012 - 14Sep2015	
4. TITLE AND SUBTITLE  Function of Brg1 Chromatin Remodeling Factor in Sonic Hedgehog-Dependent Medulloblastoma Initiation and Maintenance				5a. CONTRACT NUMBER W81XWH-12-1-0527	
				5b. GRANT NUMBER GRANT11011243	
				5c. PROGRAM ELEMENT NUMBER	
6. AUTHOR(S)  Xuanming Shi, Jiang Wu  E-Mail: Xuanming.Shi@UTsouthwestern.edu				5d. PROJECT NUMBER	
				5e. TASK NUMBER	
				5f. WORK UNIT NUMBER	
7. PERFORMING ORGANIZATION NAME(S) AND ADDRESS(ES)  University of Southwestern Medical Center Dallas, Texas 75390-9040				8. PERFORMING ORGANIZATION REPORT NUMBER	
9. SPONSORING / MONITORING AGENCY NAME(S) AND ADDRESS(ES) U.S. Army Medical Research and Materiel Command Fort Detrick, Maryland 21702-5012				10. SPONSOR/MONITOR'S ACRONYM(S)	
				11. SPONSOR/MONITOR'S REPORT NUMBER(S)	
12. DISTRIBUTION / AVAILABILITY STATEMENT Approved for Public Release; Distribution Unlimited					
13. SUPPLEMENTARY NOTES					
14. ABSTRACT Medulloblastoma is the most common malignant pediatric brain tumor. Overactive Shh signaling in cerebellum granule neuron precursors (CGNPs) is the leading cause of the childhood medulloblastoma (Shh-subtype). Current study focuses on the requirement of Brg1 in mouse model of Shh-type medulloblastoma. In vitro evidences showed that Brg1 is required for mitogenic target gene expression and proliferation in primary SmoM2 CGNP and tumor cultures. In vivo deletion of Brg1 through Atoh1-Cre dramatically decreased death rate and prolonged the survival resulted from Shh-type medulloblastoma. Induction of Brg1 deletion in subcutaneous transplantation led to significantly blocked tumor aggression, decreased the tumor proliferation as well. RT-qPCR and Western blot confirmed that Shh-dependent mitogenic target genes are decreased by knocking out of Brg1. RNA-seq analysis in the primary tumor showed the Brg1 deletion efficiently reversed the SmoM2 oncogenic effects in medulloblastoma development. This study provides evidences that chromatin remodeling complex BAF containing Brg1 is a therapeutic target for Shh-type medulloblastoma. Considering H3K27me3 changes by Brg1 deletion, ChIP-seq of Brg1 together with histone modifications will further uncover the molecular mechanisms underlining Shh-type medulloblastoma.					
15. SUBJECT TERMS Medulloblastoma, Sonic Hedgehog, Chromatin remodeling, BAF complex, Brg1, mouse model of shh-subtype medulloblastoma					
16. SECURITY CLASSIFICATION OF:			17. LIMITATION OF ABSTRACT	18. NUMBER OF PAGES	19a. NAME OF RESPONSIBLE PERSON
a. REPORT	b. ABSTRACT	c. THIS PAGE			USAMRMC
U	U	U	UU	121	19b. TELEPHONE NUMBER (include area code)

## Table of Contents

<b>1. Introduction</b>	4
<b>2. Keywords</b>	4
<b>3. Accomplishments</b>	5
<b>4. Impact</b>	14
<b>5. Changes/Problems</b>	15
<b>6. Products</b>	17
<b>7. Participants &amp; Other Collaborating Organizations</b>	18
<b>8. Special Reporting Requirements</b>	19
<b>9. Appendices</b>	20

## 1. Introduction

Brain tumors are the leading cause of cancer-related death in children, and medulloblastoma is the most common malignant pediatric brain tumor. Although overall survival rates have improved in recent years, the mortality rate remains significant. Hence, new insights into the molecular mechanisms controlling medulloblastoma development are essential for improving clinical trial design, and developing molecularly targeted therapies. Shh signaling pathway plays important roles in many development processes and adult homeostasis. Elevation of Shh target gene expression has been associated with the initiation and /or maintenance of a large spectrum of cancer types, among which medulloblastoma is one of the most well-known Shh-dependent cancer type. During early postnatal cerebellum development, Shh is required for CGNP proliferation. However, overactive Shh pathway causes CGNP over-proliferation and medulloblastoma. Among all the genetic defects, mutations resulting in an overactive Shh signaling in cerebellum granule neuron precursors (CGNPs) are the leading cause of the childhood medulloblastoma and are responsible for ~25% of occurrences (Shh-subtype). Shh signaling pathway mediated by Patched (Ptch1) and Smoothened (Smo) controls target gene expression by differentially regulating activity of Gli family of transcription factors. The regulation of mitogenic target genes by Shh/Gli in cerebellum is critical for CGNP proliferation and medulloblastoma formation.

Mammalian SWI/SNF like BAF (Brg1/Brm associated factors) chromatin remodeling complexes regulate transcription by modulating chromatin structures. It has been shown that depending on the tissue contexts, BAF complexes can either promote or suppress tumor development by regulating different sets of target gene transcription in a context-dependent manner. Recently, we have shown that Brg1, the core subunit of BAF complexes, interacts with Gli transcription factors and is required for activating Shh-induced target gene transcription. *Brg1*-deletion resulted in reduced proliferation of CGNPs in developing cerebellum due to impaired Shh-activated target gene expression, indicating that Brg1 is required for Shh-dependent CGNP proliferation. Thus I hypothesize that Brg1 is required for Shh-subtype medulloblastoma growth and progression. In the study I use *SmoM2*-mouse model and breed with Brg1 conditional knockout allele to test the hypothesis. Those studies for molecular mechanism of medulloblastoma growth at chromatin level will provide insights for drug development and therapy of pediatric brain tumor and other Shh-dependent tumor.

## 2. Keywords

BAF complex, Brg1, medulloblastoma, Gli1, Atoh1, CGNP, transplantation

### 3. Accomplishments

#### 3.1 Major goal of the study

The major goal of the study is to investigate the role of a chromatin remodeler Brg1 in medulloblastoma initiation and maintenance.

#### 3.2 Accomplishments under the goals

##### 3.2 .1 Major activities

- I. Design and perform research experiments to determine the role of Brg1 in medulloblastoma initiation and maintenance.
- II. Analyze experiment results and publish the result in peer-review journals
- III. Communicate with the peers in the same field for career development.

##### 3.2 .2 Specific objectives

**Aim1.** Determine the function of Brg1 in SmoM2-induced medulloblastoma formation.

Using a CreER-LoxP system, I will induce Brg1 deletion before tumor formation in a mouse model of Shh-subtype medulloblastoma to determine the function of Brg1 in medulloblastoma formation. Cerebellar medulloblastoma formation rate, tumor size, grade and Shh target gene expression will be compared between the mice with or without Brg1.

**Aim2.** Determine the function of Brg1 in SmoM2-dependent tumor progression and maintenance.

To determine Brg1 function in Shh-subtype medulloblastoma progression and maintenance, I will delete Brg1 after tumor formation in cultures or in transplanted environment to determine the effects on tumor cell proliferation, cell survival, clonogenic growth abilities and the allograft tumor formation in nude mice.

**Aim3.** Identify Brg1/BAF interacting co-activators of Shh signaling in medulloblastoma.

To understand the mechanisms underlying Brg1 function in Shh target gene activation and Shh-dependent medulloblastoma, I will use a state-of-the-art proteomic approach developed by Dr. Wu and others from Dr. Crabtree's lab in Stanford University to identify BAF-interacting proteins in Shh-activated medulloblastoma. These co-factors are candidate regulators of Shh signaling in cancers.

##### 3.2 .3 Significant results or key outcomes

##### **Task 1. Determine the function of Brg1 in SmoM2-induced Medulloblastoma formation (Month 1-36)**

*1A. Determine the function of Brg1 Smo-M2 dependent CGNP over-proliferation in vitro. (Month 1-18)*

Using an inducible mouse model of medulloblastoma with a *SmoM2-YFP* mutant gene (a point mutation in *Smoothed*) knocked-in at the *Rosa26* locus downstream of a *LoxP-flanked* stop signal (1) , and an inducible *Actin-CreER* transgene, as well as a conditional *Brg1* null allele, we bred different genotypes: *wt*, *Brg1<sup>ikO</sup>*, *Smo*, and *Smo Brg<sup>ikO</sup>*, to determine Brg1 function in CGNPs. We showed that cultured *SmoM2* CGNPs

display increased expression of Gli1 (the most faithful and sensitive Shh target gene) compared to wild-type cultures (Figure 1B). Conditional knockout of *Brg1* decreased Gli1 protein level, and CGNP proliferation indicated by BrdU staining. We found *Brg1* deletion reduced the *SmoM2*-dependent mitogenic target gene expression (Figure 1C). In contrast, b-tubulin and GFAP were not changed (Figure 1B). These experiments suggested that *Brg1* is required for *SmoM2*-induced Shh target gene expression and CGNP proliferation.

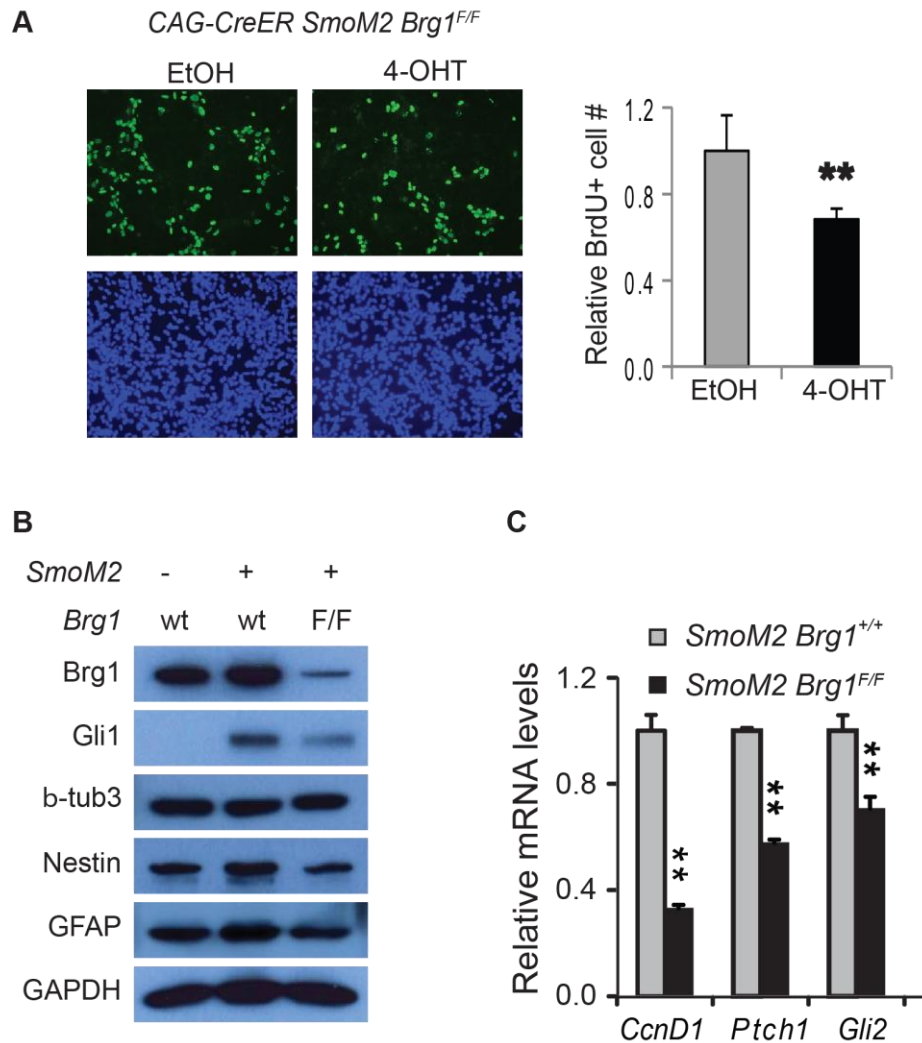


**Figure 1. *Brg1* is required for *SmoM2* CGNP proliferation and the expression of key regulatory genes.**

**A-C.** Deletion of *Brg1* from CAG-CreER *SmoM2* CGNP cultures (after 3 day 4-hydroxytamoxifen treatment) led to decreased proliferation as shown (**A**) by staining of incorporated BrdU (n=3) and by decreased expression of known medulloblastoma genes as shown by (**B**) western blot and (**C**) RT-qPCR.

**1B. Determine the function of *Brg1* in *SmoM2*-dependent medulloblastoma formation.**  
(Month 6-36)

To determine the function of *Brg1* in *SmoM2*-dependent medulloblastoma

formation, we bred above-mentioned mice using *Nestin-creER*. One injection of tamoxifen is expected to induce the expression of *SmoM2* and deletion of *Brg1*. However, since activity of CreER system depends on the Cre expression level and tamoxifen delivery efficiency, deletion of *Brg1* and expression of *SmoM2* may occur in a mosaic pattern. The resulting tumor formation rate and survive curve from *Brg1*<sup>+/+</sup> and *Brg1*<sup>F/F</sup> mice tended to be different but not significant (data not shown). Interestingly our preliminary data showed *Brg1*<sup>+/-</sup> heterozygote may have a different phenotype comparing to *Brg1*<sup>+/+</sup> in *SmoM2*-dependent target gene expression and tumor growth.

As an alternated plan, we bred *SmoM2 Math1-Cre*, *Brg1*<sup>F/F</sup>, F/+ or +/+ mice to analyze the function of *Brg1* in *SmoM2*-dependent medulloblastoma initiation and formation. *Math1-cre* is expressed in CGNP cells. It induces *SmoM2* expression and *Brg1* deletion in the same cells. The data showed so far 66% *Brg1* wild type mice died from medulloblastoma, the percentage of dead *Brg1* F/+, F/F mice was down to 27%, 9% respectively. The survival curve of *Brg1* F/F mice was significantly different from that of *Brg1* +/+ mice (Appendices-1 Figure 2B). These data suggested that *Brg1* deletion can efficiently inhibit growth of medulloblastoma *in vivo*.

## Task 2. Determine function of Brg1 in SmoM2-dependent tumor progression and maintenance (Month13-36).

### 2A. Determine the requirement of Brg1 for SmoM2 medulloblastoma primary culture cancer phenotypes.(Month 13-30)

In this part we have determined the roles of *Brg1* in primary cultured medulloblastoma and in tumor progression by allograft transplantation.

Development of Shh-dependent medulloblastoma requires an active Shh pathway for maintenance and progression. It has been reported that 40% of *SmoM2*, *Actin-CreER* mice develop medulloblastoma due to leakage of the CreER activity (1). Indeed we have observed the occurrence of similar tumors in the *Brg1*<sup>iKO</sup> *SmoM2 Actin-CreER* mice without tamoxifen induction. However, the weak Cre activity without tamoxifen is not sufficient for *Brg1* deletion (data not shown).

To determine the role of *Brg1* in medulloblastoma growth, we first *in vitro* cultured medulloblastoma cells formed due to Cre leakage in *Brg1*<sup>iKO</sup> *SmoM2 Actin-CreER* mice at

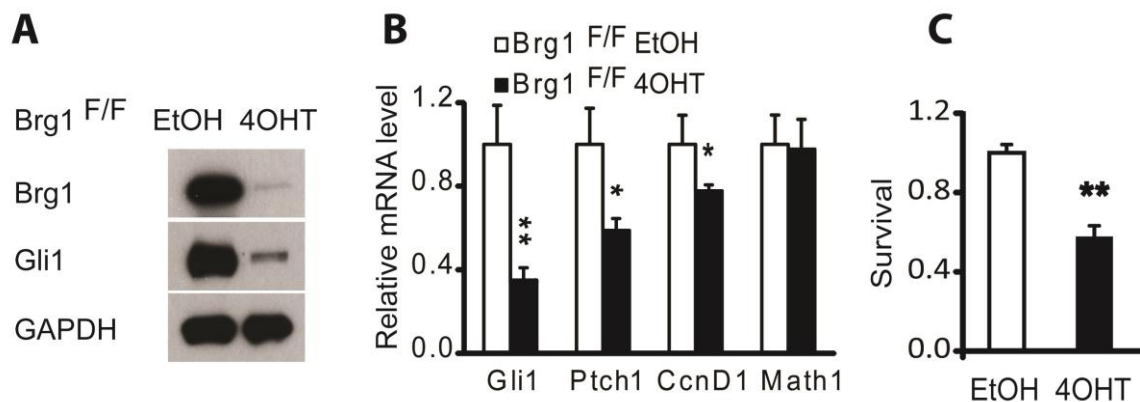


**Figure 1** Brg1-deletion in cultured SmoM2-MB decreased mitogenic target gene expression and tumor growth A) Gli1 protein level decreased by knockout of Brg1 in cultured MB cells showed by Western blot. B) qRT-PCR analysis showed the decrease of mitogenic target genes at the mRNA in cultured MB cells. C) ATP viability assay of MB cultures treated with tamoxifen for 3 days. Student's t-test: \*,  $P < 0.05$ ; \*\*,  $P < 0.01$ .

P60. 4-hydroxy tamoxifen (4OHT) was added to the culture to induce *Brg1* deletion (Figure 2A). After 3 days in culture, *Brg1* was effectively deleted in 4OHT-treated cultures. Deletion of *Brg1* led to significant reduction of *Gli1*, *Ptch1* expression (Figure 2A, B), and the mitogenic target gene *CcnD1* in medulloblastoma cultures (Figure 2B). Deletion of *Brg1* also inhibited medulloblastoma growth as shown by an ATP viability assay in the cultured cells (Figure 2C).

**2B. Determine *Brg1* function in allograft tumor formation by *SmoM2* medulloblastoma after transplantation. (Month 20-36)**

To determine the requirement of *Brg1* for *SmoM2* medulloblastoma allograft tumor formation ability, freshly prepared small tumor pieces of *Brg1*<sup>F/+</sup> *SmoM2* *Actin-CreER* was injected/transplanted subcutaneously into the flank regions of immunodeficient SCID-NOD mice. Three days after transplantation, the recipient SCID-NOD mice were injected with tamoxifen every other day for 10 times to induce *Brg1* deletion in allograft tumors. The *Brg1*<sup>F/+</sup> tumor size after injection of tamoxifen (Tam, (Figure 3A)) was significant smaller than the control in which oil was injected. In contrast, no such changes were found in *Brg1*<sup>+/+</sup> tumor transplantation (Figure 3A). The genotyping of these tumors further confirmed the transplanted tumor type and deletion of one allele *Brg1* after injection of tamoxifen (Figure 3B). These data together indicated *Brg1* reduction inhibited medulloblastoma progression and maintenance.

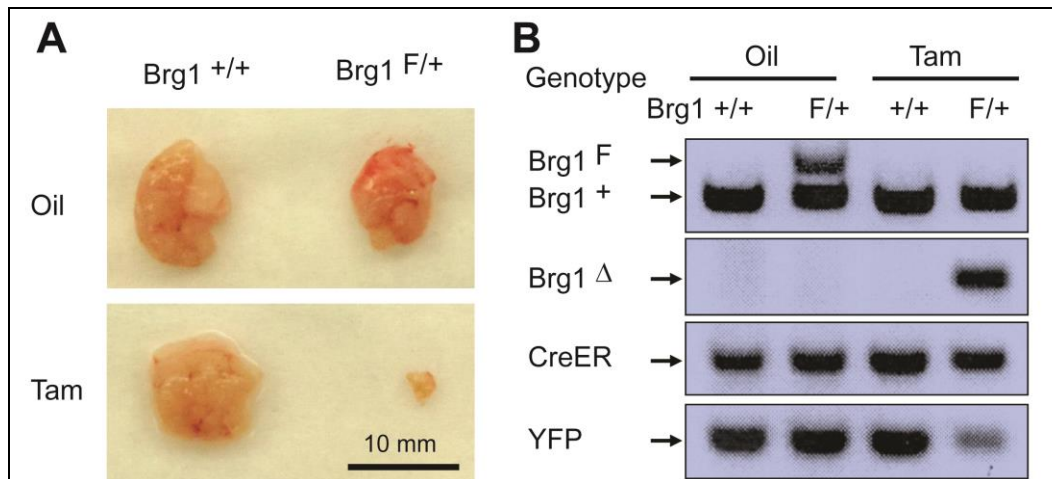


**Figure 3** *Brg1* is required for tumor progression by subcutaneously transplantation in SCID-NOD mice. Tumor A) and the genotyping B) dissected from transplanted mice injected with tamoxifen 3 days after transplantation.

The *Brg1*<sup>F/F</sup> tumor size after injection of tamoxifen was statistically significant smaller than the control in which oil was injected (Appendices-1 Figure 2D). Biochemistry analyses showed *Brg1* was deleted by tamoxifen treatment, and *Shh* target genes *Ptch1*, *CcnD1* and *N-myc* *Gli1* were dramatically decreased by deletion of *Brg1* (Appendices-1 Figure 3A,B). We found the important transcription factor *Gli2* and *Atoh1* decreased by *Brg1* deletion (Appendices-1 Figure 3A,B), suggesting transcription circuits was greatly changed after *Brg1* deletion.



These data together indicated *Brg1* reduction inhibits medulloblastoma progression and maintenance. We then investigated whether the proliferation was decreased by *Brg1* deletion. The transplanted tumor tissue was stained with proliferation marker H3P and BrdU. All these markers were significantly decreased in *Brg1* deleted tumors induced by tamoxifen treatment (Appendices-1 Figure 2E).

### Task 3. Identify Brg1/BAF interacting co-activators of Shh signaling in medulloblastoma (Month 13-36).

Our previous studies have suggested that BAF complex activates Shh-induced transcription by recruiting other unidentified co-activators to Shh target genes, and our previous aim was to investigate the Brg1/BAF complex interacting protein in medulloblastoma development. However, based on the current data, *Brg1* deletion already made systematic changes to limit medulloblastoma growth. To understand the mechanisms underlying Brg1 function in Shh target gene activation and Shh-dependent medulloblastoma, we have modified subaims to use RNA-seq to determine know the global changes of all genes and to use a proteomic approach (2) to identify BAF-interacting proteins in Shh-activated medulloblastoma. Meanwhile, using ChIP-seq we analyze the regulatory mechanism of Brg1 in medulloblastoma development. Regarding proteomic analysis, the BAF-interacting co-activators will be good candidates for mediating Shh-induced gene activation and for Shh-dependent tumor formation. We confirmed interaction between Brg1 and Gli1, Rest and Atoh1 in the medulloblastoma tissue (Figure 4A), indicating the tissue is a feasible resource to probe the interaction proteins important in medulloblastoma development.

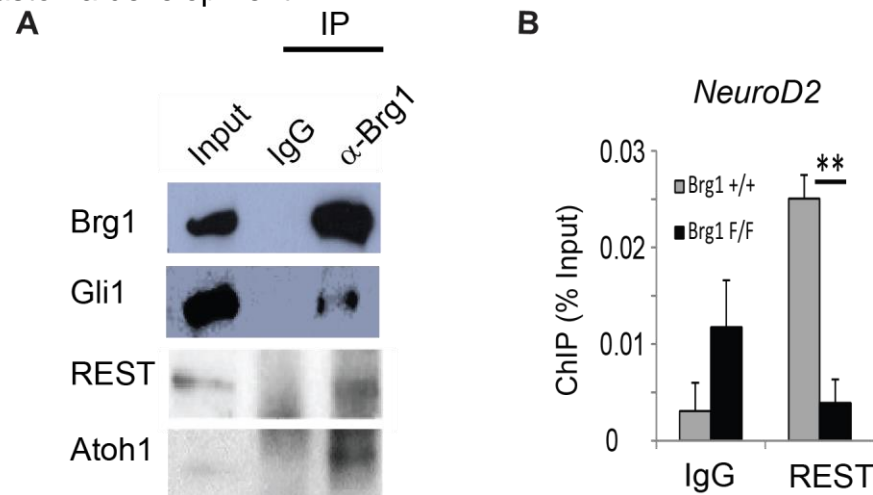


**Figure 4. Endogenous Brg1 interacts with Gli1, Atoh1 and REST in *SmoM2* medulloblastoma.**

**A.** *SmoM2* medulloblastoma lysates were immunoprecipitated with antibodies against Brg1 followed by western blot using antibodies against Brg1, Gli1, Atoh1 and REST. **B.** ChIP-qPCR indicates a reduction of REST binding to the *NeuroD2* regulatory region upon Brg1 deletion in tamoxifen treated *Brg1<sup>F/F</sup>* primary *SmoM2* medulloblastoma.

As to RNA-seq, we injected the mice *Brg1*<sup>+/+</sup> and *Brg1*<sup>F/F</sup> suffering

medulloblastoma with tamoxifen every other days for 20 days. The primary tumor tissue was confirmed with the Brg1 deletion and the decrease of mitogenic genes. Then, total RNA was extracted from the tissue and ran for RNA-seq. Results showed that 1517 genes were changed by deleting Brg1. Almost half of the genes overlapped with SmoM2-regulated genes in medulloblastoma formation (1). Among these 1517 changed genes, the down-regulated genes by Brg1 deletion matched well with the upregulated genes by SmoM2 transgene, and *vice versa* (Appendices-1 Figure 3D). GO analysis clearly showed those downregulated genes by Brg1 deletion consisted of proliferation genes, such as cell cycle, DNA binding, hedgehog, Wnt and Notch signaling (Appendices-1 Figure 3E). The up-regulated genes are most neuronal associated genes. Hence, Brg1 deletion efficiently inhibits the SmoM2 effects in medulloblastoma formation.

To identify direct Brg1 target genes, we performed Brg1 ChIP-seq in *SmoM2* medulloblastoma. Approximately 37 million reads were obtained, and more than 20 million reads were uniquely mapped to the genome. We analyzed the data using the SICER program that is specifically designed for analysis of ChIP-seq data of chromatin regulators(3). We identified 5727 significant Brg1-binding regions with an average size of 2.4 kb; this number of binding regions is similar to those obtained in Brg1 ChIP-seq studies performed in other tissues (4, 5). Most Brg1-binding regions (70%) are in gene bodies or within 5 kb upstream or downstream; 30% are in the intergenic regions (Appendices-1 Figure 4A). The analysis of the distribution of Brg1-binding regions in gene units showed enrichment close to the transcription start sites (Appendices-1 Figure 4B). From the 5727 Brg1-binding regions, we identified 3841 genes with a Brg1-binding region overlapping with the gene body or 5-kb surrounding regions (data not shown). The intersection of the gene set bound by Brg1 with the Brg1-regulated genes identified from primary medulloblastoma yielded 399 genes that are likely direct targets of Brg1 (Appendices-1 Figure 4C, and excel data not shown).

The analyses of Brg1 targetome provide insights into the mechanisms underlying the essential function of Brg1 in Shh-type medulloblastoma. We found that Brg1 regulates important transcriptional regulatory pathways in medulloblastoma including the targetomes of Gli1, Atoh1, and REST. Gli binding sites have been identified in another mouse model of Shh-type medulloblastoma (6). Despite using the different tumor models, we observed a high overlap between Gli1 binding genes and Brg1 binding genes. Within 1169 Gli binding genes, 557 contain Brg1-binding regions (48%,  $p=1.2e-206$ , Appendices-1 Figure 4C). In many target genes, putative Brg1 and Gli1 binding regions are in close proximity (Appendices-1 Figure 4G), suggesting that Gli1 recruits the Brg1 co-activator complex to the Gli regulatory regions. Consistently, we observed an interaction between endogenous Gli1 and Brg1 in medulloblastoma cells (Figure 4A). These data indicate that the essential co-activator function of Brg1 is not limited to a few known Gli1 target genes, but can be applied to the Gli1 targetome in medulloblastoma.

Of the 557 genes co-occupied by Brg1 and Gli1, 82 genes were regulated by Brg1. *Brg1* deletion led to decreases in expression of Gli1-activated known oncogenic genes *Gli1*, *N-myc*, and *Ccnd1* (Appendices-1 Figure 3B, excel data not shown) and potential oncogenic genes such as *Akna*, *Foxo6*, and *Sox18* (6) (Appendices-1 Figure

4H, excel data not shown). In addition, expression levels of Notch and Hippo pathway genes such as *Hes5*, *Hey1* (also Gli1 targets), *Jag1*, and *Tead1* as well as Wnt pathway inhibitors *Wif1* and *SFRP1* (also Gli1 targets) decreased after *Brg1* deletion (Appendices-1 Figure 4H). It has been shown that active Notch and Hippo signaling pathways positively regulate Shh-type medulloblastoma (7), whereas the Wnt pathway inhibits it. Therefore, these data suggest that Brg1 coordinates the crosstalk between signaling pathways to facilitate Shh-activated medulloblastoma development.

In CGNPs and Shh-type medulloblastoma, Atoh1 is necessary for cell-type specification and cell identity maintenance. It also regulates CGNP and medulloblastoma proliferation, mainly by activating *Gli2* expression. The Atoh1 targetome has been identified in early postnatal CGNPs, where Shh signaling is active<sup>29</sup>. Many Atoh1 target genes in CGNPs likely also play important roles in maintaining medulloblastoma cell identity and proliferation. Within the 582 high stringency Atoh1 targets, 251 genes (43%) were also bound by Brg1 (Appendices-1 Figure 4D). Of these, 48 were regulated by Brg1 including potent medulloblastoma oncogenes *Gli2*, *Atoh1*, *CXCR4*, *Tgif1*, and *Aurkb* (Appendices-1 Figure 3B, 4D, 4G, 4H), which are likely direct targets of Brg1. The targeting of Brg1 to Atoh1 binding genes is likely mediated through the interaction between Atoh1 and Brg1. We observed that endogenous Atoh1 co-immunoprecipitated with Brg1 in SmoM2 medulloblastoma (Appendices-1 Figure 4). We next analyzed the specificity of Brg1 in regulating target genes and non-target genes of Gli1 and Atoh1. Of the genes containing neither Gli1 nor Atoh1 binding sites (Gli1-/Atoh1-), less than 15% were occupied by Brg1. In contrast, 38% of the Gli1-/Atoh1+ genes, 46% of the Gli1+/Atoh1- genes, and 66% of the Gli1+/Atoh1+ (73/110) genes were co-occupied by Brg1 (Appendices-1 Figure 4E). The highly enriched Brg1 occupancy in the target genes of Gli1 and/or Atoh1 indicates that Brg1 specifically controls the transcriptional circuitry involved in medulloblastoma identity and proliferation.

Inhibition of several known tumor suppressors significantly enhances the formation and growth of mouse models of Shh-type medulloblastoma. Notably, *Brg1* deletion led to an increase in expression of specific tumor suppressor genes and genes known to be involved in neuronal function and synaptogenesis (Appendices-1 Figure 3E). In medulloblastoma, tumor cells maintain a progenitor state and inhibit neuronal gene expression. It is thought that REST functions as an oncogene by repressing expression of neuronal genes and inhibiting differentiation. Many REST target genes (e.g., *Nrxn2*, *Nrxn3*, and *NeuroD2*) were derepressed upon *Brg1* deletion (Appendices-1 Figure 4F, 4H). Although the target genes of REST in CGNPs and medulloblastomas are not known, the REST targetome identified in embryonic stem cells, where most of the neuronal genes are repressed, may encompass many REST target genes in cerebellum. A comparison between Brg1-repressed genes (1077) with REST binding genes (1775) in embryonic stem cells yielded 198 ( $p=1.8e-32$ ) commonly repressed genes. Of these, 62 are also bound by Brg1 ( $p=4.9e-18$ ) (Appendices-1 Figure 4F). This indicates that Brg1 positively regulates the repression function of REST to inhibit neuronal gene expression and to allow medulloblastoma to grow. We observed the interaction between endogenous Brg1 and REST in smoM2 medulloblastoma (Figure

4A). Deletion of Brg1 led to reduced REST binding to one target gene NeuroD2 (Figure 4B). These results confirmed a previous report that REST recruits BAF complexes to target genes whereas BAF complexes further facilitates REST binding . In addition, Brg1 repressed potential tumor suppressors with mutations identified in Shh-type medulloblastoma such as *LRP1B*, *Syne1*, and *Pde4D*<sup>30</sup>. In contrast, potential tumor suppressor genes such as *DDX3x*, *TCF4*, and *NcoR* found in multiple types of medulloblastomas (8-10) were not significantly changed upon *Brg1* deletion (Appendices-1 Figure 4H). Therefore, by a coordinated regulation of specific oncogenic and tumor suppressing transcription circuits, Brg1 supports *SmoM2* medulloblastoma development.

In addition, recently we found that an H3K27me3 demethylase Jmjd3 is required for Shh signaling pathway in development and medulloblastoma growth through modulating histone modification (11). We hypothesized that Brg1 may coordinate with Jmjd3 to maintain the H3K27me3 around Shh target gene regulatory regions. Indeed, we found that the H3K27me3 levels at global and the *Gli1*, *Atoh1* promoter regions were significantly upregulated (Appendices-1 Figure 5A, C, D). It was reported that Brg1 interacts with Jmjd3 to regulate target gene expression (12). To determine whether Jmjd3 recruitment was affected by BAF complex through *Brg1*, we carried out ChIP-Jmjd3 experiment in primary CGNP cultures treated with 4OHT to delete *Brg1*. Results indicated that Jmjd3 binding at *Gli1* regulatory region was significantly decreased when *Brg1* was deleted (Appendices-1 Figure 5F). These data taken together showed Brg1 cooperates with histone modifiers, such as Jmjd3, to regulate Shh target genes in medulloblastoma development.

In summary, our study reveals an epigenetic mechanism that controls specific transcription programs essential for Shh-type medulloblastoma development. Future functional epigenome studies will elucidate the specific epigenetic regulations of each tumor subtypes and will provide targets for development of the much needed subtype-specific treatments for medulloblastoma patients.

1. J. Mao *et al.*, *Cancer Res.* **66**, 10171 (2006).
2. J. I. Wu *et al.*, *Neuron* **56**, 94 (2007).
3. C. Zang *et al.*, *Bioinformatics.* **25**, 1952 (2009).
4. L. Ho *et al.*, *Proceedings of the National Academy of Sciences of the United States of America* **106**, 5181 (2009).
5. Y. Yu *et al.*, *Cell.* **152**, 248 (2013).
6. E. Y. Lee *et al.*, *Proc Natl Acad Sci U. S. A.* **107**, 9736 (2010).
7. A. Fernandez *et al.*, *Genes Dev.* **23**, 2729 (2009).
8. D. W. Parsons *et al.*, *Science.* **331**, 435 (2011).
9. T. J. Pugh *et al.*, *Nature.* 10 (2012).

10. G. Robinson *et al.*, *Nature* **488**, 43 (2012).
11. X. Shi *et al.*, *Nat. Commun.* **5**, 5425 (2014).
12. S. A. Miller, S. E. Mohn, A. S. Weinmann, *Mol. Cell.* **40**, 594 (2010).

### **3.2 .4 Other achievements**

Promote from Postdoctoral researcher to Instructor.

### **3.3 Opportunities for training and professional development provided by the project**

Nothing to report

### **3.4 How were the results disseminated to communities of interest?**

- I. Present in international meeting
- II Publish high impact papers in peer-reviewed journal

### **3.5 Plan to do during next reporting period**

Nothing to report

#### **4. Impact**

Epigenetic regulation of gene expression provides new mechanisms and therapeutic targets for cancer researches. My proposal focuses on the role of an epigenetic regulator Brg1 in Shh signaling-dependent medulloblastoma, which is the most common brain tumor of childhood. Successfully, my proposal provided significant insights into the epigenetic regulation mechanism of medulloblastoma and also another layer of treatment option by targeting Brg1. Besides medulloblastoma, many other cancers require elevated Shh activity for initiation and/or maintenance. The mechanisms and potential treatments identified in this proposal could readily have a much broader application and profound impact. Thus the findings gained from the project are highly relevant to the health of the military families and their children as well as general public.

## 5. Changes/Problems

Aim1: To determine the function of *Brg1* in *SmoM2*-dependent medulloblastoma formation, we previously bred above-mentioned mice but using *Nestin-creER*. One injection of tamoxifen is expected to induce the expression of *SmoM2* and deletion of *Brg1*. However, since activity of CreER system depends on the Cre expression level and tamoxifen delivery efficiency, deletion of *Brg1* and expression of *SmoM2* occurred in a mosaic pattern. The resulting tumor formation rate and survival curve from *Brg1*<sup>+/+</sup> and *Brg1*<sup>F/F</sup> mice has a trend to be different but the difference is not significant. As an alternated plan, we bred *SmoM2 Math1-Cre*, *Brg1*<sup>F/F</sup>, *F/+* or *+/+* mice to analyze the function of *Brg1* in *SmoM2*-dependent medulloblastoma initiation and formation. *Math1-cre* is expressed in CGNP cells. It induces *SmoM2* expression and *Brg1* deletion in the same cells. The data showed so far 66% *Brg1* wild type mice died from medulloblastoma, the percentage of dead *Brg1* *F/+*, *F/F* mice was down to 27%, 9% respectively. The survival curve of *Brg1* *F/F* mice was significantly different from that of *Brg1* *+/+* mice. These data suggested that *Brg1* deletion can efficiently inhibit growth of medulloblastoma *in vivo*.

Aim 3: Our previous studies have suggested that BAF complex activates Shh-induced transcription by recruiting other unidentified co-activators to Shh target genes, and our previous aim was to investigate the *Brg1*/BAF complex interacting protein in medulloblastoma development. However, based on the current data, *Brg1* deletion already made systematic changes to limit medulloblastoma growth. To understand the mechanisms underlying *Brg1* function in Shh target gene activation and Shh-dependent medulloblastoma, we have modified subaims to use RNA-seq to determine know the global changes of all genes and to use a proteomic approach to identify BAF-interacting proteins in Shh-activated medulloblastoma. Regarding proteomic analysis, the BAF-interacting co-activators will be good candidates for mediating Shh-induced gene activation and for Shh-dependent tumor formation. We confirmed interaction between *Brg1* and *Gli1*, *REST* and *Atoh1* in the medulloblastoma tissue, indicating the tissue is a feasible resource to probe the interaction proteins important in medulloblastoma development.

As to RNA-seq, we injected the mice *Brg1*<sup>+/+</sup> and *Brg1* *F/F* suffering medulloblastoma with tamoxifen every another days for 20 days. The primary tumor tissue was confirmed with the *Brg1* deletion and the decrease of mitogenic genes. Then, total RNA was extracted from the tissue and ran for RNA-seq. Results showed that 1517 genes were changed by deleting *Brg1*. Almost half of the genes overlapped with *SmoM2*-regulated genes in medulloblastoma formation. Among these 1517 changed genes, the downregulated genes by *Brg1* deletion matched well with the upregulated genes by *SmoM2* transgene, and *vice versa*. GO analysis clearly showed those downregulated genes by *Brg1* deletion consisted of proliferation genes, such as cell cycle, DNA binding, hedgehog, Wnt and Notch signaling. The upregulated genes are most neuronal associated genes. Hence, *Brg1* deletion efficiently inhibits the *SmoM2* effects in medulloblastoma formation.

In addition, recently we found that an H3K27me3 demethylase Jmjd3 is required for Shh signaling pathway in development and medulloblastoma growth through modulating histone modification (Shi et al., *Nature communications* 2014). We hypothesized that Brg1 may coordinate with Jmjd3 to maintain the H3K27me3 around Shh target gene regulatory regions. Indeed, we found that the H3K27me3 levels at global and the *Gli1* and *Atoh1* promoter regions were significantly upregulated. It was reported that Brg1 interacts with Jmjd3 to regulate target gene expression. To determine whether Jmjd3 recruitment was affected by BAF complex through *Brg1*, we carried out ChIP-Jmjd3 experiment in primary CGNP cultures treated with 4OHT to delete *Brg1*. Results indicated that Jmjd3 binding at *Gli1* regulatory region was significantly decreased when *Brg1* was deleted. These data taken together showed Brg1 cooperates with histone modifiers, such as Jmjd3, to regulate Shh target genes in medulloblastoma development.

In summary, with small modifications of the original proposal, I successfully accomplished the major goal of the proposal determined the function of Brg1 in Shh-type medulloblastoma and revealed molecular mechanisms underlying its function. This study will also shed light on Brg1 function in many other tumors.



## 6. Products

### Publications

1. Shi, X., Wang, Q., Gu, J., Xuan, Z., Wu, J., Brg1/SmadA4 Coordinates Genetic and Epigenetic Networks Underlying Shh-type Medulloblastoma Development. *Oncogene* (In Press).
2. Shi, X., Zhan, X., Wu, J., A Positive Feedback Loop between Gli1 and Tyrosine Kinase Hck Amplifies Shh Signaling Activities in Medulloblastoma. *Oncogenesis* (2015) 4, e176; doi:10.1038/oncsis.2015.38.
3. Zhang, Z., Cao, M., Chang, C., Wang, C., Shi, X., Zhan, X., Birnbaum, S., Bezprozvanny, I., Huber, K., Wu, J., Autism-Associated Chromatin Regulator Brg1/SmadA4 is Required for Synapse Development and MEF2-mediated Synapse Remodeling. *Molecular and Cellular Biology* 2015 Oct 12. pii: MCB.00534-15.
4. Shi, X., Zhang, Z., Zhan, X., Cao, M., Satoh, T., Akira, S., Shpargel, K., Magnuson, T., Wang, R., Wang, C., Ge, K., Wu, J., An epigenetic switch induced by Shh signalling regulates gene activation during development and medulloblastoma growth. *Nature Communications* 2014; 5:5425.

### Abstract:

5. Shi X, Zhang Z, Wang Q, Wu J. Function of Brg1 chromatin remodeling factor in sonic hedgehog-dependent medulloblastoma development [abstract]. Proceedings of the 105th Annual Meeting of the American Association for Cancer Research; 2014 Apr 5-9; San Diego, CA. Philadelphia (PA): AACR; 2014. Abstract nr 404.

## 7. Participants & Other Collaborating Organizations

### What individuals have worked on the project

Name:	Xuanming Shi
Project Role:	PI
Researcher Identifier	
Nearest person month worked	36
Contribution to Project	Dr. Shi performed most of experiments and analysis
Funding support	American Cancer Society (J. Wu),

Name:	Jiang Wu
Project Role:	PD
Researcher Identifier	
Nearest person month worked	12
Contribution to Project	Dr. Wu designed some of the experiments and performed analysis, and finalized the manuscript
Funding support	grants from March of Dimes Foundation (J. Wu), American Cancer Society (J. Wu), NIMH (J. Wu)

### What other organization were involved as partners

Organization name: **University of Texas at Dallas**

Location of Organization: Richardson Texas 75080

Partner's contribution to the project: **Dr. Zhenyu Xuan** and graduate student **Jiawei Gu** performed the main bioinformatics analyses.

## **8. Special Reporting Requirements**

Nothing to report

## 9. Appendices

1. A copy of manuscript which is in press in Oncogene
2. A copy of paper published in Oncogenesis (2015) 4, e176, doi:10.1038/oncsis.2015.38.
3. A copy of co-author paper published in Molecular and Cellular Biology 2015 Oct 12. pii: MCB.00534-15.
4. A copy of paper published in Nature Communications 2014; 5:5425.
5. Meeting abstract of Proceedings of the 105th Annual Meeting of the American Association for Cancer Research; 2014 Apr 5-9; San Diego.
6. Curriculum Vitae.



# **SMARCA4/Brg1 Coordinates Genetic and Epigenetic Networks Underlying Shh-type Medulloblastoma Development**

## **AUTHORS:**

Xuanming Shi<sup>1</sup>, Qiu Wang<sup>1</sup>, Jiawei Gu<sup>2</sup>, Zhenyu Xuan<sup>2</sup>, Jiang Wu<sup>1\*</sup>

## **AFFILIATIONS:**

<sup>1</sup>Department of Physiology and Developmental Biology, University of Texas Southwestern Medical Center, Dallas, TX 75390, USA

<sup>2</sup>Department of Biological Sciences, Center for Systems Biology, University of Texas at Dallas, Richardson, TX 75080, USA

## **CORRESPONDENCE:**

Jiang Wu

[jiang9.wu@utsouthwestern.edu](mailto:jiang9.wu@utsouthwestern.edu)

Department of Physiology and Developmental Biology

UT Southwestern Medical Center

5323 Harry Hines Blvd.

Dallas TX 75390-9133

Phone: 214-648-1824

Fax: 214-648-1960

**RUNNING TITLE:** Brg1 in Shh-type medulloblastoma

**Conflict of interest:** The authors declare no conflict of interests.

## Abstract

Recent large-scale genomic studies have classified medulloblastoma into four subtypes: Wnt, Shh, Group 3, and Group 4. Each is characterized by specific mutations and distinct epigenetic states. Previously we showed that a chromatin regulator SMARCA4/Brg1 is required for Gli-mediated transcription activation in Sonic hedgehog (Shh) signaling. We report here that Brg1 controls a transcriptional program that specifically regulates Shh-type medulloblastoma growth. Using a mouse model of Shh-type medulloblastoma, we deleted Brg1 in pre-cancerous progenitors and primary or transplanted tumors. *Brg1* deletion significantly inhibited tumor formation and progression. Genome-wide expression analyses and binding experiments indicate that Brg1 specifically coordinates with key transcription factors including Gli1, Atoh1, and REST to regulate the expression of both oncogenes and tumor suppressors that are required for medulloblastoma identity and proliferation. Shh-type medulloblastoma displays distinct H3K27me3 properties. We demonstrate that Brg1 modulates activities of H3K27me3 modifiers to regulate expression of medulloblastoma genes. Brg1-regulated pathways are conserved in human Shh-type medulloblastoma, and Brg1 is important for the growth of a human medulloblastoma cell line. Thus, Brg1 coordinates a genetic and epigenetic network that regulates the transcriptional program underlying Shh-type medulloblastoma development.

## Introduction

Medulloblastoma is the most common malignant childhood brain tumor. Although the survival rate of medulloblastoma patients is relatively high, current treatments have serious side effects<sup>16, 43, 51</sup>. Several large-scale genomic studies have provided rich information about specific transcription profiles and mutations associated with medulloblastoma. Based on these analyses, medulloblastomas are classified into four subgroups: Wnt, Shh, Group 3, and Group 4<sup>26, 44, 46, 48, 49</sup>. Subtypes are characterized by specific mutations, rely on distinct signaling pathways, and possibly have different cell origins. Interestingly, each also displays distinct epigenetic properties, which are likely important for generating and maintaining the transcription program characteristic of each subtype. Functional epigenome studies to identify the molecular mechanisms that regulate the growth of each tumor subtype are required to accelerate the pace of development of much needed, subtype-specific treatment plans for medulloblastoma patients.

Shh-type medulloblastoma accounts for 25% of all medulloblastoma. Mutations that result in constitutively active Sonic hedgehog (Shh) signaling in cerebellum granule neuron precursors (CGNPs) are the essential genetic causes of Shh-type medulloblastoma<sup>2, 30</sup>. During early postnatal development, Shh expressed from Purkinje neurons induces the rapid expansion of CGNPs in the external granule layer (EGL). CGNPs differentiate into granule neurons that migrate to and reside in the internal granule layer (IGL). Active Shh signaling is required for normal CGNP proliferation and for maintenance of CGNPs in an undifferentiated state<sup>8, 9, 65, 66</sup>; however, elevated or constitutively active Shh signaling leads to CGNP over-proliferation and medulloblastoma.

Although various mutations cause Shh-type medulloblastoma and Shh-type medulloblastoma occurs in infants, children and adults, these tumors share certain subtype-specific gene expression patterns that are likely required for tumor proliferation and identity<sup>26, 30, 44, 46, 48, 49</sup>. These include high levels of expression of Shh signaling target genes such as *Gli1* and CGNP specification genes such as *Atoh1*, and relatively low levels of expression of neuronal differentiation genes. Shh signaling mediated by Patched (Ptch1) and Smoothened (Smo) regulates development and cancer by modulating the activities of Gli family transcription factors<sup>4, 15, 22, 24</sup>. Shh activation releases inhibition of Smo by Ptch1 to activate Gli1/2 transcription activators (GliA) and downstream target genes. Shh-induced GliA activities provide a driving force for tumor proliferation by



activating mitogenic genes such as *Gli1*, *CcnD1*, and *N-myc*<sup>2, 24</sup>. The acquisition of CGNP identity is a critical determinant of progenitor cell competence to form Shh-induced medulloblastoma<sup>53</sup>; therefore, Atoh1, an essential transcription factor in CGNP specification, plays an important role in medulloblastoma development<sup>3, 14</sup>. Atoh1 also regulates medulloblastoma proliferation by controlling *Gli2* expression<sup>14</sup>. Compare to Group 3 and Group 4 medulloblastoma, Shh subtype expresses low levels of neuronal genes. The master repressor NRSF/REST is expressed at high levels in Shh-type medulloblastoma and may function as an oncogene to repress expression of certain neuronal genes leading to inhibition of differentiation<sup>7, 42, 52</sup>. Thus, GliA, Atoh1, and REST form a core transcriptional regulatory circuitry to control the identity and proliferation of medulloblastoma. The targetome of this transcription circuitry likely produces medulloblastoma phenotypes, and its coordinated regulation is critical to tumor development.

Previously, we and others have identified several GliA-interacting epigenetic regulators to activate target genes in response to Shh signaling<sup>5, 36, 76</sup>. We have reported that a SWI2/SNF2 like chromatin remodeler SMARCA4/Brg1 functions as a GliA co-activator and is required for Shh-induced target gene activation<sup>76</sup>. As a core subunit of the SWI/SNF-like chromatin remodeling BAF complexes, Brg1 contains an ATPase domain that provides the enzymatic activity to remodel chromatin structures to regulate transcription<sup>17, 72</sup>. In addition, BAF complexes interact with many proteins, including other chromatin regulators and histone modifiers, that might mediate ATPase-independent activities of Brg1 and BAF complexes. BAF complexes have been shown to function as transcription activators or as repressors and play diverse roles during development<sup>72</sup>. In cancers, BAF complexes also play important but context-dependent roles<sup>27, 69, 72</sup>. Recent genomic studies indicated that BAF complexes are mutated in ~20% of all cancer types and represent the most highly mutated chromatin regulator in human cancer<sup>27, 43</sup>. *Brg1* biallelic inactivating mutations have been identified in many cancers such as atypical teratoid/rhabdoid tumors (AT/RT) and ovarian cancers<sup>18, 70</sup>. Heterozygous missense mutations of *Brg1* have been identified in the Wnt and Group 3 medulloblastomas<sup>27, 43</sup>, suggesting a tumor suppressor function of Brg1 in these cancers. In other cancers, however, BAF complexes are required for cancer development and excluded from mutations. Brg1 has been shown to be required for leukemia and small cell lung cancer maintenance by regulating *Myc* expression or *Myc* activities<sup>50, 56</sup>. The requirement of Brg1

for Shh/GliA activation suggests that Brg1 may be required for Shh-type medulloblastoma growth.

Recently we discovered that under basal conditions Shh/Gli target genes poised for activation are marked by a bivalent chromatin domain containing H3K27me3/H3K4me3. The H3K27me3 demethylase Jmjd3/Kdm6b plays a crucial role in removing H3K27me3, recruiting other co-activators, and activating Gli target genes in response to Shh signaling<sup>57</sup>. It has been shown that Brg1 functions together with Jmjd3 to activate transcription of certain genes<sup>35, 39</sup>. Notably, the non-enzymatic activities of both Brg1 and Jmjd3 are required for their co-activator functions in Shh signaling<sup>57, 76</sup>; these two proteins may interact with each other or recruit other co-factors to activate Shh target genes coordinately. Consistent with their co-activator functions in Shh signaling, few mutations in *Brg1* and *Jmjd3* have been identified from pediatric Shh-type medulloblastomas despite a potential tumor suppressor function for both proteins in other medulloblastoma subtypes and other types of cancer<sup>27, 46, 47</sup>.

In this report, using a mouse model of Shh-type medulloblastoma that closely resembles the human tumor, we demonstrate that the chromatin remodeler Brg1 coordinates the core transcriptional circuitry that controls Shh-type medulloblastoma identity and proliferation. Deletion of *Brg1* in CGNPs impaired normal cerebellum development, but considerably extended the survival time of tumor-bearing animals. *Brg1* deletion after medulloblastoma formation significantly inhibited tumor proliferation and growth. Using genome-wide expression and binding experiments, we discovered that Brg1 coordinates with Gli1, Atoh1, and REST to regulate expression of both oncogenes and tumor suppressors specifically required for tumor growth. Brg1-regulated pathways are conserved in human Shh-type medulloblastomas, and Brg1 was also important for the growth of a human medulloblastoma cell line. In addition, we showed that Brg1 modulates activities of H3K27me3 modifiers in regulating medulloblastoma genes. Thus, Brg1 regulates genetic and epigenetic networks that control the transcription program underlying Shh-type medulloblastoma development.

## Results

### **Brg1 is required for cerebellum development and the proliferation of precancerous CGNPs.**

To determine whether the GliA co-activator Brg1 is required for Shh-dependent CGNP proliferation *in vivo*, we deleted *Brg1* using the CGNP-specific *Atoh1-Cre* transgene<sup>73</sup>. *Atoh1-Cre*-induced *Brg1* deletion in CGNPs led to significantly smaller cerebellums at postnatal day 12 (P12) compared to those in wild-type mice despite an overall similar foliation pattern (Figure 1A-B, 1A'-B'). Brg1 protein was deleted in most CGNPs in the EGL and subsequently in granule neurons in the IGL (Figure 1C, 1C'). Brg1-deleted CGNPs also displayed abnormal morphologies such as larger nuclei (Figure 1C, 1C'). The EGL was thinner in *Brg1*-deleted cerebellum, due to impaired CGNP proliferation as indicated by reduced BrdU incorporation (Figure 1D, 1D'). This result indicates an essential function of Brg1 in Shh/Gli-dependent normal cerebellum development. Recently, another genetic study also demonstrated that *Brg1* and *SMARCB1/BAF47/INI1/SNF5* are required for cerebellum development<sup>40</sup>.

The expression of a Cre-inducible *SmoM2* (an activating mutation in *Smo*) transgene in CGNPs results in constitutively active Shh signaling, over-proliferative CGNPs, and medulloblastoma development<sup>37, 53</sup>. In precancerous *SmoM2* CGNPs, Brg1 was required for proliferation (Figure S1A). Cultured CGNPs were obtained from P4 *CAG-CreER* *SmoM2* pups with *Brg1<sup>F/F</sup>* or *Brg1<sup>+/+</sup>*. In both genotypes, tamoxifen treatment induced expression of *SmoM2*, and, in the *Brg1<sup>F/F</sup>* cells, deletion of *Brg1* was induced simultaneously, which significantly reduced CGNP proliferation as indicated by reduced BrdU incorporation (Figure S1A). Consistently, *Brg1* deletion in *SmoM2* CGNPs significantly inhibited the expression of Shh target genes that are induced by the *SmoM2* mutant protein (Figure S1B, S1C).

### **Brg1 is required for *SmoM2* medulloblastoma formation and progression.**

To determine how Brg1 functions in Shh-induced medulloblastoma formation, *Brg1* was deleted in CGNPs in the *SmoM2* mouse model of Shh-type medulloblastoma using *Atoh1-Cre* at the same time that *SmoM2* was induced. Induction of *SmoM2* expression led to abnormal cerebellum development and medulloblastoma growth. At P28, the cerebellum in *Atoh1-Cre SmoM2* mice had no foliation, indicating the requirement of proper Shh signaling for CGNP proliferation and differentiation. Multiple foci of Ki67 positive cells

indicated the initiation of medulloblastoma growth (Figure 2A). In *Atoh1-Cre SmoM2 Brg1<sup>F/F</sup>* mice, the cerebellum is smaller and also lack of foliation. However, no Ki67 positive foci were observed (Figure 2A). In survival studies, all *Atoh1-Cre SmoM2 Brg1<sup>+/+</sup>* mice developed medulloblastoma and died within 3 to 4 months of age (Figure 2B). Deletion of *Brg1* in CGNPs significantly extended survival time of *Atoh1-Cre SmoM2* mice (Figure 2B). In those few *Atoh1-Cre SmoM2 Brg1<sup>F/F</sup>* mice that did suffer from medulloblastoma growth, the *Brg1* allele was not completely deleted in the tumor cells (Figure S2). Deletion of one *Brg1* allele also significantly reduced the lethality rate compared to the mice with wild-type *Brg1* (Figure 2B).

To determine whether *Brg1* is required for medulloblastoma maintenance and progression, we deleted *Brg1* after tumor formation by taking advantage of the leaky CAG-CreER activities (Figure 2C). CAG-CreER *SmoM2* medulloblastomas with *Brg1<sup>+/+</sup>*, *Brg1<sup>F/+</sup>*, or *Brg1<sup>F/F</sup>* alleles were induced by weak Cre activities without tamoxifen treatment. These tumors contain intact *Brg1* alleles (Figures 2C, 2D). When transplanted into SCID-NOD immunodeficient mice subcutaneously, deletion of one or both *Brg1* alleles induced by tamoxifen injection significantly inhibited the growth of tumor allografts (Figures 2D). *Brg1* deletion significantly inhibited tumor cell proliferation as indicated by reduced staining of proliferation markers such as phosphorylated histone H3 (H3P) and by BrdU incorporation (Figure 2E). Deletion of *Brg1* in primary medulloblastomas using the same strategy also significantly inhibited tumor proliferation (Figure S3). Thus, *Brg1* is required for both the formation and progression of *SmoM2* medulloblastoma.

### ***Brg1* is required for the expression of a transcription program specific to *SmoM2* medulloblastoma.**

In medulloblastoma transplantation, as expected, deletion of *Brg1* significantly inhibited the expression of Shh/Gli target genes *Gli1*, *Ptch1*, *Ccnd1*, and *N-myc* (Figures 3A, 3B), which is consistent with the function of *Brg1* as a co-activator of Gli1/2. Interestingly, *Brg1* deletion also inhibited other genes known to be important for medulloblastoma identity and proliferation such as *Atoh1* and *Gli2* (Figure 3B). We next performed RNA-seq to compare the transcription profiles from primary medulloblastomas with or without *Brg1* deletion. Mice with CAG-CreER *SmoM2* medulloblastomas with *Brg1<sup>F/F</sup>* or *Brg1<sup>+/+</sup>* were injected with tamoxifen to induce *Brg1* deletion or to serve as controls. Differential expression analyses showed that levels of expression from 1517 genes were significantly changed

upon *Brg1* deletion (Table S1). These Brg1-regulated genes significantly overlapped with the genes differentially expressed in *SmoM2* medulloblastoma versus normal cerebellum<sup>37</sup> (47%,  $p=2.3e-161$ , Figure 3C). Of the 1517 Brg1-regulated genes, levels of expression of 440 genes were decreased upon *Brg1* deletion (these are Brg1 activated genes), and levels of expression of 1077 genes were increased (these are Brg1 repressed genes). Ranked fold change analyses showed an almost perfect correlation between Brg1-regulated genes and the *SmoM2*-specific gene set (Figure 3D) indicating that Brg1 activates genes specifically expressed in *SmoM2* medulloblastoma and inhibits genes repressed in tumors. These include genes important for cell proliferation and differentiation as shown by the gene ontology analyses (Figure 3E). Thus, the inhibition of tumor growth that resulted from *Brg1* deletion is due to the destruction of the specific transcription program controlling *SmoM2* medulloblastoma.

### **Brg1 regulates key transcriptional regulatory circuits in *SmoM2* medulloblastoma.**

To identify direct Brg1 target genes, we performed Brg1 ChIP-seq in *SmoM2* medulloblastoma. Approximately 37 million reads were obtained, and more than 20 million reads were uniquely mapped to the genome. We analyzed the data using the SICER program that is specifically designed for analysis of ChIP-seq data of chromatin regulators<sup>75</sup>. We identified 5727 significant Brg1-binding regions with an average size of 2.4 kb; this number of binding regions is similar to those obtained in Brg1 ChIP-seq studies performed in other tissues<sup>20, 74</sup>. Most Brg1-binding regions (70%) are in gene bodies or within 5 kb upstream or downstream; 30% are in the intergenic regions (Figure 4A). The analysis of the distribution of Brg1-binding regions in gene units showed enrichment close to the transcription start sites (Figure 4B). From the 5727 Brg1-binding regions, we identified 3841 genes with a Brg1-binding region overlapping with the gene body or 5-kb surrounding regions (Table S2). The intersection of the gene set bound by Brg1 with the Brg1-regulated genes identified from primary medulloblastoma yielded 399 genes that are likely direct targets of Brg1 (Figure 4C, Table S3).

The analyses of Brg1 targetome provide insights into the mechanisms underlying the essential function of Brg1 in Shh-type medulloblastoma. We found that Brg1 regulates important transcriptional regulatory pathways in medulloblastoma including the targetomes of Gli1, Atoh1, and REST. Gli binding sites have been identified in another mouse model of Shh-type medulloblastoma<sup>32</sup>. Despite using the different tumor models, we observed a

high overlap between Gli1 binding genes and Brg1 binding genes. Within 1169 Gli binding genes, 557 contain Brg1-binding regions (48%,  $p=1.2e-206$ , Figure 4C). In many target genes, putative Brg1 and Gli1 binding regions are in close proximity (Figure 4G), suggesting that Gli1 recruits the Brg1 co-activator complex to the Gli regulatory regions. Consistently, we observed an interaction between endogenous Gli1 and Brg1 in medulloblastoma cells (Figure S4A). These data indicate that the essential co-activator function of Brg1 is not limited to a few known Gli1 target genes, but can be applied to the Gli1 targetome in medulloblastoma.

Of the 557 genes co-occupied by Brg1 and Gli1, 82 genes were regulated by Brg1. *Brg1* deletion led to decreases in expression of Gli1-activated known oncogenic genes *Gli1*, *N-myc*, and *Ccnd1* (Figure 3B, Table S1) and potential oncogenic genes such as *Akna*, *Foxo6*, and *Sox18*<sup>32</sup> (Figure 4H, Table S1). In addition, expression levels of Notch and Hippo pathway genes such as *Hes5*, *Hey1* (also Gli1 targets), *Jag1*, and *Tead1* as well as Wnt pathway inhibitors *Wif1* and *SFRP1* (also Gli1 targets) decreased after *Brg1* deletion (Figure 4H). It has been shown that active Notch and Hippo signaling pathways positively regulate Shh-type medulloblastoma<sup>10, 13, 41</sup>, whereas the Wnt pathway inhibits it<sup>1</sup>. Therefore, these data suggest that Brg1 coordinates the crosstalk between signaling pathways to facilitate Shh-activated medulloblastoma development.

In CGNPs and Shh-type medulloblastoma, Atoh1 is necessary for cell-type specification and cell identity maintenance<sup>3, 14</sup>. It also regulates CGNP and medulloblastoma proliferation, mainly by activating *Gli2* expression<sup>14</sup>. The Atoh1 targetome has been identified in early postnatal CGNPs, where Shh signaling is active<sup>29</sup>. Many Atoh1 target genes in CGNPs likely also play important roles in maintaining medulloblastoma cell identity and proliferation. Within the 582 high stringency Atoh1 targets, 251 genes (43%) were also bound by Brg1 (Figure 4D). Of these, 48 were regulated by Brg1 including potent medulloblastoma oncogenes *Gli2*, *Atoh1*, *CXCR4*, *Tgif1*, and *Aurkb* (Figure 3B, 4D, 4G, 4H)<sup>14, 38, 54</sup>, which are likely direct targets of Brg1. The targeting of Brg1 to Atoh1 binding genes is likely mediated through the interaction between Atoh1 and Brg1. We observed that endogenous Atoh1 co-immunoprecipitated with Brg1 in SmoM2 medulloblastoma (Figure S4A). We next analyzed the specificity of Brg1 in regulating target genes and non-target genes of Gli1 and Atoh1. Of the genes containing neither Gli1 nor Atoh1 binding sites (Gli1-/Atoh1-), less than 15% were occupied by Brg1. In contrast,

38% of the Gli1-/Atoh1+ genes, 46% of the Gli1+/Atoh1- genes, and 66% of the Gli1+/Atoh1+ (73/110) genes were co-occupied by Brg1 (Figure 4E). The highly enriched Brg1 occupancy in the target genes of Gli1 and/or Atoh1 indicates that Brg1 specifically controls the transcriptional circuitry involved in medulloblastoma identity and proliferation.

Inhibition of several known tumor suppressors significantly enhances the formation and growth of mouse models of Shh-type medulloblastoma<sup>58, 63, 68</sup>. Notably, *Brg1* deletion led to an increase in expression of specific tumor suppressor genes and genes known to be involved in neuronal function and synaptogenesis (Figure 3E). In medulloblastoma, tumor cells maintain a progenitor state and inhibit neuronal gene expression. It is thought that REST functions as an oncogene by repressing expression of neuronal genes and inhibiting differentiation<sup>7, 42, 52</sup>. Many REST target genes (e.g., *Nrxn2*, *Nrxn3*, and *NeuroD2*) were derepressed upon *Brg1* deletion (Figure 4F, 4H). Although the target genes of REST in CGNPs and medulloblastomas are not known, the REST targetome identified in embryonic stem cells, where most of the neuronal genes are repressed, may encompass many REST target genes in cerebellum<sup>25</sup>. A comparison between Brg1-repressed genes (1077) with REST binding genes (1775) in embryonic stem cells yielded 198 ( $p=1.8e-32$ ) commonly repressed genes. Of these, 62 are also bound by Brg1 ( $p=4.9e-18$ ) (Figure 4F, Table S3). This indicates that Brg1 positively regulates the repression function of REST to inhibit neuronal gene expression and to allow medulloblastoma to grow. We observed the interaction between endogenous Brg1 and REST in smoM2 medulloblastoma (Figure S4A). Deletion of Brg1 led to reduced REST binding to one target gene *NeuroD2* (Figure S4B). These results confirmed a previous report that REST recruits BAF complexes to target genes whereas BAF complexes further facilitates REST binding<sup>45</sup>. In addition, Brg1 repressed potential tumor suppressors with mutations identified in Shh-type medulloblastoma such as *LRP1B*, *Syne1*, and *Pde4D*<sup>30</sup>. In contrast, potential tumor suppressor genes such as *DDX3x*, *TCF4*, and *NcoR* found in multiple types of medulloblastomas<sup>26, 44, 46, 48, 49</sup> were not significantly changed upon *Brg1* deletion (Figure 4H). Therefore, by a coordinated regulation of specific oncogenic and tumor suppressing transcription circuits, Brg1 supports *SmoM2* medulloblastoma development.

**Brg1 regulates the activities of H3K27me3 modifiers in medulloblastoma.**

Human Shh-type medulloblastoma is characterized by low global H3K27me3 levels <sup>49</sup>, which may allow the expression of many H3K27me3-regulated oncogenic genes. Similarly, we observed low global H3K27me3 levels in CGNPs and in *SmoM2* medulloblastoma (Figure 5A) <sup>57</sup>. Interestingly, human medulloblastoma and *SmoM2* tumors contain relatively high levels of SUZ12, a component of the H3K27 methyltransferase complex PRC2 (Figure 5A) <sup>49</sup>. This paradox indicates that high H3K27me3 demethylase activities such as those of Jmjd3 must be present in Shh-type medulloblastoma to remove H3K27me3 and to keep H3K27me3 levels low. Interestingly, we observed a global increase of H3K27me3 levels but decreased PRC2 levels (as indicated by decreased levels of an essential subunit Suz12) when tumor growth was inhibited by *Brg1* deletion (Figure 5A). RT-qPCR analyses showed that *Brg1* deletion in *SmoM2* tumors led to reduced PRC2 subunits mRNA levels (Figure 5B). Thus, *Brg1* may facilitate Jmjd3-mediated removal of H3K27me3 to activate oncogenic genes, whereas *Brg1* may also help maintain the H3K27me3 levels at the repressed gene regulatory regions by positively support PRC2 expression in Shh-type medulloblastoma. In support target gene specific functions of *Brg1* in H3K27me3 regulation, ChIP-qPCR showed increased H3K27me3 levels at *Brg1* activated genes such as *Gli1* and *Atoh1* and decreased H3K27me3 levels at *Brg1* repressed genes such as *NeuroD2* upon *Brg1* deletion (Figure 5C-E). We have previously shown that Jmjd3 directly binds to *Gli1* regulatory regions in Shh-activated CGNPs and is required for maintaining the low local H3K27me3 level and activating *Gli1* expression <sup>57</sup>. Our data indicate that *Brg1* is required for Jmjd3 binding to *Gli1* regulatory regions since Jmjd3 binding in Shh-activated CGNPs was significantly impaired when *Brg1* was deleted (Figure 5F). This reduction of Jmjd3 binding was not due to a decrease of Jmjd3 expression level, since *Jmjd3* mRNA level was even slightly increased in *Brg1* deleted medulloblastoma (Figure 5B). By regulating Jmjd3 activities and PRC2 expression levels, *Brg1* may control expression of certain target genes through modulation of H3K27me3 levels.

### **Conserved functions of Brg1 in human Shh-type medulloblastoma.**

To determine whether *Brg1*-regulated transcriptional pathways in *SmoM2* tumors are also specifically expressed in human Shh-type medulloblastoma, we compared the expression levels of human homologs of *Brg1* targets in different medulloblastoma subtypes. Using a publicly available microarray dataset of 76 pediatric medulloblastoma samples (GSE37418) <sup>49</sup>, we ranked the average expression levels of the human homologs of each



Brg1-activated Gli1 or Atoh1 targets as well as Brg1-repressed REST targets in four types of human medulloblastoma (Table S4). Both Brg1-activated Gli1 and Atoh1 targets have significantly more #1 ranked genes in Shh-type medulloblastoma than other subgroups, whereas significantly more Brg1-repressed REST targets have lowest expression in Shh type tumors compared to other subgroups (Figure 6A, 6B). Brg1 was expressed at relatively high levels in all four subgroups (Figure 6B). These results indicate that in Shh-type medulloblastoma, Brg1-regulated Gli1 and Atoh1 target genes are specifically activated and many REST targets are specifically repressed. Thus, the gene programs coordinately regulated by Brg1 and these transcription factors in *SmoM2* tumors are also specifically associated with human Shh-type medulloblastoma and are likely to be important for human tumor growth.

To further determine the function of Brg1 in human medulloblastoma growth, we performed RNAi-mediated *Brg1* inhibition in human medulloblastoma cell lines and examined the effects on target gene expression and cell growth. The DaoY human cell line resembles Shh-type medulloblastoma cells<sup>62</sup>. Although DaoY cells express low levels of *Gli1* and *Atoh1*, exogenous Gli1 significantly activated Gli1 and Atoh1 targets and accelerated growth of these cells (Figure 6C, 6D). RNAi-mediated inhibition of *Brg1* expression in DaoY cells significantly decreased the expression of these oncogenes and impaired the cell growth in the absence or presence of exogenous Gli1 (Figure 6C-G). In contrast, reduction of Brg1 levels in a Group 3/4-like medulloblastoma cell line D283<sup>55</sup> did not affect the cell growth (Figure 6E, 6F). Notably, similar to in *SmoM2* tumors, inhibition of *Brg1* in DaoY cells but not in D283 cells also increased global H3K27me3 levels (Figure 6H), suggesting that Brg1 may also regulate human medulloblastoma through modulating H3K27me3 modifier activities. These results indicate that Brg1 plays a conserved and specific role in coordinating the genetic and epigenetic regulatory programs in Shh-type medulloblastoma.

## Discussion

In this report, we demonstrated that Brg1 is essential for both normal cerebellum development and Shh-type medulloblastoma growth. In both mouse and human Shh-type medulloblastoma, Brg1 regulates expression of GliA and Atoh1 target genes to maintain tumor identity and proliferation. Brg1 also inhibits expression of genes with potential tumor suppressor functions as well as REST-repressed neuronal genes. Furthermore, Brg1 may regulate the activities of H3K27me3 modifiers to maintain the distinct chromatin environment specific to Shh-type medulloblastoma. Therefore, Brg1 is part of a genetic and epigenetic network that controls the specific transcriptional program underlying Shh-type medulloblastoma (Figure 7). Our study demonstrates that a novel epigenetic mechanism controls subtype-specific medulloblastoma development.

BAF complexes are known to target many developmentally important loci, mainly by interacting with transcription factors through its diverse subunits<sup>17, 72</sup>. Our studies provide genetic and genomic evidence indicating an essential function of Brg1 in regulating Shh/Gli signaling and Atoh1 pathway in cancer. The interactions between Brg1 and Gli1 or Atoh1 and the significant enrichment of Brg1 occupancy in genes targeted by Atoh1 and/or Gli1 relative to non-target genes suggests that in medulloblastoma Brg1 could be recruited by Gli1 or Atoh1 and functions specifically to co-regulate Gli1 and Atoh1 target genes. Brg1 also represses a large number of REST target genes in medulloblastoma and prevents tumor cell differentiation. Brg1 interacts with REST and is also required for maximum binding of REST to certain target genes. This is consistent with a previous report that REST recruits BAF complexes whereas BAF complexes further facilitate REST binding<sup>45</sup>. Gli1 and Atoh1 as well as their target genes are over-represented in human Shh-type medulloblastoma than other subtypes, whereas REST target genes are underrepresented, indicating that Brg1 regulated transcription network is also conserved in human cancers. The mechanisms identified in mouse models are likely applicable to human cancers. A direct test in human cancer xenograft model would be very useful to directly test Brg1 function in human medulloblastoma.

The activities of BAF complexes in tumor development appear to be tumor-type dependent, consistent with its diverse subunit compositions and functions in different tissues<sup>71</sup>. Using the ATPase dependent chromatin remodeling activities or ATPase independent functions by interacting with other epigenetic cofactors, BAF complexes could

activate or repress specific target genes in a context-dependent manner<sup>72</sup>. Therefore, depending on the specific roles of BAF subunits in regulating different oncogenes or tumor suppressors that are associated with each type of tumors, BAF subunits may function either to suppress or to support tumor growth. The tumor suppressor functions of BAF subunits have been extensively studied in AT/RT, where biallelic mutations of *SMARCB1/BAF47* as well as *SMARCA4/Brg1* cause cancer development<sup>18, 64</sup>. In AT/RT with Brg1 or BAF47 mutated, increased Shh target gene expression was observed, which may contribute to the AT/RT growth<sup>23</sup>. This notion is consistent with our previous finding that Brg1/BAF complex plays a dual role in Shh signaling by repressing the basal expression and activating signaling-induced target gene expression<sup>76</sup>. In cancers that require active Shh signaling such as Shh-type medulloblastoma, Brg1 is then required for tumor growth. Therefore depending on the Shh signaling activities in different cell types, BAF deletion may cause different effects on Shh target genes and cancer growth<sup>72</sup>. In medulloblastoma, the potential tumor suppressor functions of Brg1 in Wnt and Group 3 subtypes remain unknown.

Transcription profiles classify medulloblastomas into four groups. Interestingly, mutations in a significant number of epigenetic regulators have been identified. Mutations in H3K4me3 methyltransferase *MLL2/3* occur in multiple medulloblastoma subgroups<sup>12, 46</sup>, whereas mutations in other epigenetic regulators occur with strong subgroup bias. For example, the mutations in H3K27me3 demethylase *UTX/Kdm6A* are highly enriched in Group 4 tumors, but are largely absent from Shh-type medulloblastoma<sup>12, 26, 49</sup>. *SMARCA4/Brg1* mutations have been identified in Wnt and Group 3 subgroups but are rare in Shh-type medulloblastoma, likely because of the essential functions that Brg1 plays in the regulation of the Shh-type medulloblastoma transcriptional program. Although mutations in other BAF subunits are rare in pediatric Shh-type medulloblastoma, they are present in adult Shh-type medulloblastoma<sup>30</sup>. It is not clear how these mutations regulate adult tumor progression; they may contribute to the tumor heterogeneity between pediatric and adult medulloblastoma. In Shh-type medulloblastoma with BAF subunit mutations, the function of Brg1 remains to be explored. Interestingly, it has been shown that Brg1 is required for the oncogenesis caused by loss of the *SMARCB1/SNF5* tumor suppressor<sup>67</sup>. Therefore, the aberrant BAF complexes formed with mutated BAF subunits may misregulate oncogenic genes and further deleting Brg1 would inhibit tumor growth.

The extensive and subgroup specific mutations in epigenetic regulators in medulloblastoma implicate the importance of epigenetic regulation in medulloblastoma development and epigenetic therapy holds great promise for the future treatment of medulloblastoma. In our study, we also showed an important function of Brg1 in coordinating the activities of H3K27me3 regulators. Brg1 deletion caused decreased Jmjd3 binding to the regulatory regions of *Gli1* and *Atoh1* and possibly other oncogenes, which may lead to decreased expression of these genes. *Brg1* deletion also led to a significant decrease of PRC2 levels. PRC2 has been shown to repress tumor suppressors and is oncogenic in other cancers. In addition, PRC2 can function as a co-repressor for REST<sup>11</sup>. It is possible that the decreased PRC2 levels contribute to the de-repression of certain tumor suppressor genes and REST target genes such as *NeuroD2* in *Brg1*-deleted tumors. Thus, Brg1 regulates local H3K27me3 levels in a target gene specific manner. The coordinated regulation H3K27me3 by Brg1 is likely one of the key mechanisms underlying Brg1 function in medulloblastoma transcription regulation. The availability of the chemical inhibitors to Jmjd3 and PRC2 may provide new treatment options for medulloblastoma.

In summary, our study reveals an epigenetic mechanism that controls specific transcription programs essential for Shh-type medulloblastoma development. Future functional epigenome studies will elucidate the specific epigenetic regulations of each tumor subtypes and will provide targets for development of the much needed subtype-specific treatments for medulloblastoma patients.

## Materials and Methods:

### Mice

*SmoM2* mice<sup>37</sup> and *CAG-CreER*<sup>19</sup> mice were purchased from Jackson Laboratory. Due to the CreER leakage, the *CAG-CreER SmoM2* mice have a high rate of spontaneous medulloblastoma development before 2 months of age (~40%) even without tamoxifen induction. These mice were crossed to *Brg1*<sup>+/+</sup>, *Brg1*<sup>F/+</sup>, or *Brg1*<sup>F/F</sup> mice<sup>60, 76</sup> and are maintained on a mixed genetic background at UT Southwestern Medical Center Animal Facility. *Atoh1-Cre* mice were generated by knocking-in the *Cre* gene at the *Atoh1* locus<sup>73</sup> and were provided by Dr. Lin Gan (Rochester University) and Dr. Jane Johnson (UT Southwestern). SCID-NOD mice were purchased from UT Southwestern Mouse Breeding Core Facility.

### Cell cultures and lentiviral infection

Primary CGNP cultures were performed as previously described<sup>76</sup>. Briefly, CGNPs were derived from dissociated P4-7 mouse cerebella and cultured in DMEM/F12 media containing 25 mM KCl, N2, and 10% FBS. For Shh stimulation, Shh conditioned medium produced from Shh-CM 293T cells<sup>6</sup> was added at a 1:20 dilution to CGNP cultures. CGNP cells were treated with Shh in high serum media for 2-3 days. The induction of the *Brg1* conditional deletion was performed by treating the cultures with 1  $\mu$ M 4-hydroxytamoxifen for three days. Medulloblastoma cell lines DaoY and D283 were purchased from ATCC and cultured as suggested by the supplier. Lentiviral constructs pGIPZ shBrg1 and shCtrl<sup>59</sup> were generously provided by Dr. Chin-ping Chang (Indiana University) and packaged as described in<sup>76</sup>. Polyjet (Signagen) was used for plasmid transfection in cultured cells. DaoY and D283 cells were infected with viruses at a multiplicity of infection (MOI) of 5 for 24 h in media with 8  $\mu$ g ml<sup>-1</sup> polybrene. The CellTiter-Glo Luminescent Cell Viability Assay (ATP viability assay) kit (Promega) was used to measure the tumor cell survival signals.

### Tumor transplantation

Medulloblastoma grown in *CAG-CreER SmoM2* mice with *Brg1*<sup>+/+</sup>, *Brg1*<sup>F/+</sup>, or *Brg1*<sup>F/F</sup> alleles were dissected and dissociated. Tumor cells (10<sup>6</sup>) were mixed with Matrigel (BD Biosciences) and injected subcutaneously in the flank region of SCID-NOD immunodeficient mice. Recipient mice were monitored daily for tumor growth. Tamoxifen

(75 mg/kg) or oil solvent were injected intraperitoneally when tumor was visible at ~ 20 days post transplantation. Tamoxifen was injected every other day during a 20 day period before sacrificing the recipient mice for tumor analyses.

### **Immunoblotting**

For immunoblotting, cells or ground tissues were lysed in RIPA buffer (50 mM Tris, pH 8, 250 mM NaCl, 0.05% SDS, 0.5% DOC, 1% NP-40). Histone fractions were prepared with standard acid extraction (0.2 N HCl). Cell lysates or histone fractions were separated on SDS-PAGE gels. Antibodies used were against Gli1 (Cell Signaling), GAPDH (Sigma), H3K27me3 (Active Motif), histone H3 (ab1791, Abcam), Brg1 (G7, Santa Cruz), beta-tub3 (Tuj1, Covance), Nestin (Rat-401, BD Pharmingen), GFAP (BD Pharmingen), HSP90 (Pierce), HA tag (ab9110, Abcam), beta-catenin (Santa Cruz), Atoh1 (Gift from Dr. Jane Johnson) and Rest (07-579, Millipore). HRP-conjugated secondary antibodies were purchased from Jackson Immunology.

### **Immunohistology**

Hematoxylin and eosin (H&E) staining and immunostaining were performed on paraffin sections of tumor or brain tissues. Antibodies used were against H3K27me3 (Millipore), H3P (Millipore), Ki67 (eBioscience), BrdU (BD Pharmingen), SUZ12 (Cell Signaling), and Brg1 (G7, Santa Cruz). The images were visualized using an Olympus BX50 microscope. H3P, Ki67 or BrdU positive cells were counted from four sections (>2000 nuclei counted for each stain) and data are given as percentage of total cells (n=3). The semi-quantitative immunohistochemistry densities of H3K27me3 staining were measured using ImageJ program (NIH).

### **Co-immunoprecipitation experiments**

*SmoM2* medulloblastoma samples were lysed with Buffer A (25 mM Tris, pH 7.5, 25 mM KCl, 5 mM MgCl<sub>2</sub>, 10% glycerol, 0.1% NP-40, with protease inhibitor freshly added). Nuclear extracts were prepared in RIPA buffer (150 mM NaCl, 1.0% NP-40, 0.5% sodium deoxycholate, 0.1% SDS, and 50 mM Tris, pH 8.0) with rotation at 4 °C for 1 hour. After centrifugation, rabbit polyclonal antibodies against Brg1/Brm (J1)<sup>28, 33</sup> were added to pre-cleared nuclear extracts and incubated at 4 °C overnight. Samples were incubated with protein A beads (GE Healthcare) for 1 hour; beads were washed with RIPA buffer four

times. Precipitated proteins were eluted by boiling in 2X Sample Buffer before SDS-PAGE and western blot analysis.

### **RT-PCR and q-PCR**

RNA from cells or ground tissues was extracted with TRIZOL (Invitrogen). cDNAs were synthesized by reverse transcription using Iscript (Bio-Rad), followed by PCR or quantitative PCR analysis. A Bio-Rad real-time PCR system (C1000 Thermal Cycler) was used for quantitative PCR. Levels of *GAPDH* mRNA were used to normalize input RNA. Graphics shown are representative of experiments performed in triplicate. The experiments were repeated for at least three times. Standard errors were calculated according to a previously described method <sup>76</sup>.

### **RNA-seq analyses**

*CAG-CreER SmoM2* mice harboring spontaneous medulloblastoma with *Brg1*<sup>F/F</sup> or *Brg1*<sup>+/+</sup> alleles were injected with tamoxifen. The *Brg1*<sup>+/+</sup> and *Brg1*-deleted (*Brg1*<sup>ik<sup>o</sup></sup>) *SmoM2* medulloblastomas were used for RNA-seq analyses. Total RNAs were extracted, and RNA-seq libraries were prepared using the Illumina RNA-Seq Preparation Kit and were sequenced on a HiSeq 2000 sequencer at UT Southwestern Sequencing Core Facility. RNA-seq reads were mapped using TopHat with default settings (<http://tophat.cbcb.umd.edu>). The mapped reads with the Phred quality score < 20 were filtered out, whereas the duplicates were marked but not removed using SAMTOOLS <sup>34</sup> and PICARD (<http://picard.sourceforge.net>). Transcript assembly and transcript abundance quantification were carried out using CUFFLINKS, and then differential expression analysis between *Brg1*<sup>+/+</sup> and *Brg1*<sup>ik<sup>o</sup></sup> *SmoM2* medulloblastomas was performed using CUFFDIFF <sup>61</sup>. The differentially expressed genes with fold change larger than 2 and p<0.05 were selected as *Brg1*-regulated genes (Table S1). Gene ontology analysis was performed using DAVID tools (<http://david.abcc.ncifcrf.gov/>).

### **Chromatin immunoprecipitation and ChIP-seq analyses**

ChIP experiments were performed as described previously <sup>76</sup>. Dounced tissue or dissociated cells were crosslinked with PFA or double crosslinked with DSG (Pierce), and sonicated to fragments (200-500 bp). Antibodies used were against H3K27me3 (Millipore), Jmjd3 (Abcam) and *Brg1*/Brm (J1) <sup>28</sup>. J1 antibody has been used previously for *Brg1* ChIP-seq analyses <sup>20, 74</sup>. Precipitated DNA was purified and subjected to either real-time

PCR or next generation sequencing. NEBNext ChIP-Seq Sample Prep Master Mix Set 1 was used for library generation and a Hiseq 2500 sequencer was used for sequencing at UT Southwestern Medical Center Sequencing Core Facility.

Short reads were mapped to UCSC reference mouse genome with bowtie<sup>31</sup> and then SICER was used to detect the Brg1-binding regions<sup>75</sup>. SICER uses clustering approach to pool together the enrichment signals of ChIP-seq reads from neighboring nucleosomes to increase the power for detecting broad binding domains. Thus it is suitable for analyzing the ChIP-seq data of histone modifications and chromatin regulators, which are usually noisy and contain broad domains. SICER has been successfully used for detecting Brg1 binding regions in hematopoietic cell lineages<sup>21</sup>. Default parameter settings with three 200 bp windows were used to calculate the enrichment of Brg1 binding regions. The corresponding input sample was used as control. Duplicate reads were removed before peak calling by SICER. Statistically significant peaks (FDR<0.05) enriched in the Brg1-ChIP sample relative to its corresponding input sample were annotated for genomic location.

In order to calculate the distribution of binding regions in reference to nearby genes, we used the mouse gene annotation obtained from iGenomes ([http://support.illumina.com/sequencing/sequencing\\_software/igenome.ilmn](http://support.illumina.com/sequencing/sequencing_software/igenome.ilmn)). The mid-point of each Brg1-binding region was compared with the location of genes to identify either the overlapping gene or the closest non-overlapped gene. The distance from the mid-point of each Brg1-binding region to the 5' end of the overlapped or the nearest gene was calculated. The promoter region was defined as 5 kb upstream of the gene, and the downstream was defined as 5 kb downstream of the gene.

### **Bioinformatics analyses**

Ranked fold change analysis was performed to determine the association between Brg1-regulated genes and genes differentially expressed in *SmoM2* MB. The differentially expressed genes (DEGs) detected from either Brg1 RNA-seq or *SmoM2* expression array<sup>37</sup> were ranked based on fold changes. Twenty bins with equal range of fold change were used to count the number of DEGs shared in both gene sets. In order to identify genes regulated by multiple proteins, including Brg1, Gli1, and Atoh1, we used the UCSC mouse genome build mm10 and mouse gene annotation from iGenomes as references to



associate locations of binding regions of each protein with nearby genes. All the reported peak locations were converted to mm10 coordinates with UCSC liftOver tool (<http://genome.ucsc.edu/cgi-bin/hgLiftOver>). We consider that a gene is bound by a protein if there is a binding region or peak overlapping its gene body or within the 5-kb flanking regions. Few previously reported target genes of these proteins were missed due to coordinate conversion of binding regions. Gli1 binding sites were identified using a FLAG-tagged Gli1 transgene in another similar mouse model of Shh-type medulloblastoma arising from *Ptch1*<sup>+/-</sup> mice<sup>32</sup>. From 1059 Gli1 binding regions, we identified 1169 potential Gli1 binding genes. Atoh1 binding gene sets in P5 CGNPs were determined in a previous analysis<sup>29</sup>. REST target genes in embryonic stem cells were determined by ChIP-PET and directly obtained from a previous report<sup>25</sup>. To test the significance of the overlapping between gene sets bound by two proteins, we use Fisher-exact test to calculate p-value. The microarray dataset GSE37418 with 76 subtype-characterized pediatric medulloblastoma samples<sup>49</sup> was analyzed for expression levels of human homologs of Brg1-regulated medulloblastoma genes in different medulloblastoma subtypes. All the human homologs of Brg1-activated Gli1 targets (42 total) and Atoh1 targets (29 total) and Brg1-repressed REST targets (177 total) were analyzed for their average expression in each subgroup. The #1 ranked subgroup for each Brg1-activated gene or the #4 ranked subgroup for each Brg1-repressed genes were identified, counted, and compared (Table S4, Figure 6A). The binominal test was used for calculating p-value. The RNA-seq and ChIP-seq data generated in this study have been deposited in NCBI GEO repository with accession number GSE69674 (GSE69672 for RNA-seq and GSE69673 for ChIP-seq).

### **Statistical analysis**

Data are expressed as means  $\pm$  s.d. (n=3 unless specifically indicated). Statistical analysis was performed by either analysis of variance with ANOVA post hoc t-test for multiple comparisons or a two-tailed unpaired Student's t-test. A p value of <0.05 was considered significant.

## **Acknowledgements**

We thank Drs. Brent Orr (St. Jude Hospital), Wenzhe Niu, and Zilai Zhang, and Mou Cao for technical support and Dr. Chao Xing and the UTSW Sequencing Facility for performing the next generation sequencing and RNA-seq analyses. We thank Drs. Lin Gan and Jane Johnson for providing the *Atoh1-Cre* mice and Dr. Ching-Ping Chang for providing human Brg1 shRNA constructs. This work was supported by grants from March of Dimes Foundation (J. Wu), American Cancer Society (J. Wu), NIMH (J. Wu) and Department of Defense Visionary postdoc fellowship (X. Shi).

## **Contributions**

J.W and X.S. designed the experiments. X.S., Q.W, and J.W. performed the experiments and collected the data. X.S. and J.W. analyzed the results. J.G. and Z.X. performed the main bioinformatics analyses. J.W. wrote the manuscript with help from all authors.

## References:

- 1 Anne SL, Govek EE, Ayrault O, Kim JH, Zhu X, Murphy DA *et al.* WNT3 inhibits cerebellar granule neuron progenitor proliferation and medulloblastoma formation via MAPK activation. *PLoS One* 2013; 8: e81769.
- 2 Barakat MT, Humke EW, Scott MP. Learning from Jekyll to control Hyde: Hedgehog signaling in development and cancer. *Trends Mol Med* 2010; 16: 337-348.
- 3 Ben-Arie N, Bellen HJ, Armstrong DL, McCall AE, Gordadze PR, Guo Q *et al.* Math1 is essential for genesis of cerebellar granule neurons. *Nature* 1997; 390: 169-172.
- 4 Briscoe J, Therond PP. The mechanisms of Hedgehog signalling and its roles in development and disease. *Nat Rev Mol Cell Biol* 2013; 14: 416-429.
- 5 Canettieri G, Di Marcotullio L, Greco A, Coni S, Antonucci L, Infante P *et al.* Histone deacetylase and Cullin3-REN(KCTD11) ubiquitin ligase interplay regulates Hedgehog signalling through Gli acetylation. *Nat Cell Biol* 2010; 12: 132-142.
- 6 Chen JK, Taipale J, Young KE, Maiti T, Beachy PA. Small molecule modulation of Smoothened activity. *Proc Natl Acad Sci U S A* 2002; 99: 14071-14076.
- 7 Chong JA, Tapia-Ramirez J, Kim S, Toledo-Aral JJ, Zheng Y, Boutros MC *et al.* REST: a mammalian silencer protein that restricts sodium channel gene expression to neurons. *Cell* 1995; 80: 949-957.
- 8 Corrales JD, Rocco GL, Blaess S, Guo Q, Joyner AL. Spatial pattern of sonic hedgehog signaling through Gli genes during cerebellum development. *Development* 2004; 131: 5581-5590.
- 9 Dahmane N, Ruiz i Altaba A. Sonic hedgehog regulates the growth and patterning of the cerebellum. *Development* 1999; 126: 3089-3100.
- 10 Dakubo GD, Mazerolle CJ, Wallace VA. Expression of Notch and Wnt pathway components and activation of Notch signaling in medulloblastomas from heterozygous patched mice. *Journal of neuro-oncology* 2006; 79: 221-227.
- 11 Dietrich N, Lerdrup M, Landt E, Agrawal-Singh S, Bak M, Tommerup N *et al.* REST-mediated recruitment of polycomb repressor complexes in mammalian cells. *PLoS Genet* 2012; 8: e1002494.

- 12 Dubuc AM, Remke M, Korshunov A, Northcott PA, Zhan SH, Mendez-Lago M *et al.* Aberrant patterns of H3K4 and H3K27 histone lysine methylation occur across subgroups in medulloblastoma. *Acta neuropathologica* 2013; 125: 373-384.
- 13 Fernandez LA, Northcott PA, Dalton J, Fraga C, Ellison D, Angers S *et al.* YAP1 is amplified and up-regulated in hedgehog-associated medulloblastomas and mediates Sonic hedgehog-driven neural precursor proliferation. *Genes Dev* 2009; 23: 2729-2741.
- 14 Flora A, Klisch TJ, Schuster G, Zoghbi HY. Deletion of Atoh1 disrupts Sonic Hedgehog signaling in the developing cerebellum and prevents medulloblastoma. *Science* 2009; 326: 1424-1427.
- 15 Fuccillo M, Joyner AL, Fishell G. Morphogen to mitogen: the multiple roles of hedgehog signalling in vertebrate neural development. *Nat Rev Neurosci* 2006; 7: 772-783.
- 16 Gajjar A, Chintagumpala M, Ashley D, Kellie S, Kun LE, Merchant TE *et al.* Risk-adapted craniospinal radiotherapy followed by high-dose chemotherapy and stem-cell rescue in children with newly diagnosed medulloblastoma (St Jude Medulloblastoma-96): long-term results from a prospective, multicentre trial. *Lancet Oncol* 2006; 7: 813-820.
- 17 Hargreaves DC, Crabtree GR. ATP-dependent chromatin remodeling: genetics, genomics and mechanisms. *Cell Res* 2011; 21: 396-420.
- 18 Hasselblatt M, Nagel I, Oyen F, Bartelheim K, Russell RB, Schuller U *et al.* SMARCA4-mutated atypical teratoid/rhabdoid tumors are associated with inherited germline alterations and poor prognosis. *Acta neuropathologica* 2014; 128: 453-456.
- 19 Hayashi S, McMahon AP. Efficient recombination in diverse tissues by a tamoxifen-inducible form of Cre: a tool for temporally regulated gene activation/inactivation in the mouse. *Dev Biol* 2002; 244: 305-318.
- 20 Ho L, Jothi R, Ronan JL, Cui K, Zhao K, Crabtree GR. An embryonic stem cell chromatin remodeling complex, esBAF, is an essential component of the core pluripotency transcriptional network. *Proc Natl Acad Sci U S A* 2009; 106: 5187-5191.
- 21 Hu G, Schones DE, Cui K, Ybarra R, Northrup D, Tang Q *et al.* Regulation of nucleosome landscape and transcription factor targeting at tissue-specific enhancers by BRG1. *Genome Res* 2011; 21: 1650-1658.

- 22 Ingham PW, McMahon AP. Hedgehog signaling in animal development: paradigms and principles. *Genes Dev* 2001; 15: 3059-3087.
- 23 Jagani Z, Mora-Blanco EL, Sansam CG, McKenna ES, Wilson B, Chen D *et al.* Loss of the tumor suppressor Snf5 leads to aberrant activation of the Hedgehog-Gli pathway. *Nat Med* 2010.
- 24 Jiang J, Hui CC. Hedgehog signaling in development and cancer. *Dev Cell* 2008; 15: 801-812.
- 25 Johnson R, Teh CH, Kunarso G, Wong KY, Srinivasan G, Cooper ML *et al.* REST regulates distinct transcriptional networks in embryonic and neural stem cells. *PLoS biology* 2008; 6: e256.
- 26 Jones DT, Jager N, Kool M, Zichner T, Hutter B, Sultan M *et al.* Dissecting the genomic complexity underlying medulloblastoma. *Nature* 2012; 488: 100-105.
- 27 Kadoch C, Hargreaves DC, Hodges C, Elias L, Ho L, Ranish J *et al.* Proteomic and bioinformatic analysis of mammalian SWI/SNF complexes identifies extensive roles in human malignancy. *Nat Genet* 2013; 45: 592-601.
- 28 Khavari PA, Peterson CL, Tamkun JW, Mendel DB, Crabtree GR. BRG1 contains a conserved domain of the SWI2/SNF2 family necessary for normal mitotic growth and transcription. *Nature* 1993; 366: 170-174.
- 29 Klisch TJ, Xi Y, Flora A, Wang L, Li W, Zoghbi HY. In vivo Atoh1 targetome reveals how a proneural transcription factor regulates cerebellar development. *Proc Natl Acad Sci U S A* 2011; 108: 3288-3293.
- 30 Kool M, Jones DT, Jager N, Northcott PA, Pugh TJ, Hovestadt V *et al.* Genome sequencing of SHH medulloblastoma predicts genotype-related response to smoothened inhibition. *Cancer Cell* 2014; 25: 393-405.
- 31 Langmead B, Trapnell C, Pop M, Salzberg SL. Ultrafast and memory-efficient alignment of short DNA sequences to the human genome. *Genome Biol* 2009; 10: R25.
- 32 Lee EY, Ji H, Ouyang Z, Zhou B, Ma W, Vokes SA *et al.* Hedgehog pathway-regulated gene networks in cerebellum development and tumorigenesis. *Proc Natl Acad Sci U S A* 2010; 107: 9736-9741.
- 33 Lessard J, Wu JI, Ranish JA, Wan M, Winslow MM, Staahl BT *et al.* An Essential Switch in Subunit Composition of a Chromatin Remodeling Complex during Neural Development. *Neuron* 2007; 55: 201-215.

- 34 Li H, Handsaker B, Wysoker A, Fennell T, Ruan J, Homer N *et al.* The Sequence Alignment/Map format and SAMtools. *Bioinformatics* 2009; 25: 2078-2079.
- 35 Li Q, Wang HY, Chepelev I, Zhu Q, Wei G, Zhao K *et al.* Stage-dependent and locus-specific role of histone demethylase Jumonji D3 (JMJD3) in the embryonic stages of lung development. *PLoS Genet* 2014; 10: e1004524.
- 36 Malatesta M, Steinhauer C, Mohammad F, Pandey DP, Squarrito M, Helin K. Histone acetyltransferase PCAF is required for Hedgehog-Gli-dependent transcription and cancer cell proliferation. *Cancer Res* 2013.
- 37 Mao J, Ligon KL, Rakhlin EY, Thayer SP, Bronson RT, Rowitch D *et al.* A novel somatic mouse model to survey tumorigenic potential applied to the Hedgehog pathway. *Cancer Res* 2006; 66: 10171-10178.
- 38 Markant SL, Esparza LA, Sun J, Barton KL, McCoig LM, Grant GA *et al.* Targeting sonic hedgehog-associated medulloblastoma through inhibition of Aurora and Polo-like kinases. *Cancer Res* 2013; 73: 6310-6322.
- 39 Miller SA, Mohn SE, Weinmann AS. Jmjd3 and UTX play a demethylase-independent role in chromatin remodeling to regulate T-box family member-dependent gene expression. *Mol Cell* 2010; 40: 594-605.
- 40 Moreno N, Schmidt C, Ahlfeld J, Poschl J, Dittmar S, Pfister SM *et al.* Loss of Smar proteins impairs cerebellar development. *J Neurosci* 2014; 34: 13486-13491.
- 41 Natarajan S, Li Y, Miller EE, Shih DJ, Taylor MD, Stearns TM *et al.* Notch1-induced brain tumor models the sonic hedgehog subgroup of human medulloblastoma. *Cancer Res* 2013; 73: 5381-5390.
- 42 Negrini S, Prada I, D'Alessandro R, Meldolesi J. REST: an oncogene or a tumor suppressor? *Trends Cell Biol* 2013; 23: 289-295.
- 43 Northcott PA, Jones DT, Kool M, Robinson GW, Gilbertson RJ, Cho YJ *et al.* Medulloblastomics: the end of the beginning. *Nat Rev Cancer* 2012; 12: 818-834.
- 44 Northcott PA, Shih DJ, Peacock J, Garzia L, Morrissy AS, Zichner T *et al.* Subgroup-specific structural variation across 1,000 medulloblastoma genomes. *Nature* 2012; 488: 49-56.
- 45 Ooi L, Belyaev ND, Miyake K, Wood IC, Buckley NJ. BRG1 chromatin remodeling activity is required for efficient chromatin binding by repressor element 1-silencing transcription factor (REST) and facilitates REST-mediated repression. *J Biol Chem* 2006; 281: 38974-38980.

- 46 Parsons DW, Li M, Zhang X, Jones S, Leary RJ, Lin JC *et al.* The genetic landscape of the childhood cancer medulloblastoma. *Science* 2011; 331: 435-439.
- 47 Popov N, Gil J. Epigenetic regulation of the INK4b-ARF-INK4a locus: in sickness and in health. *Epigenetics* 2010; 5: 685-690.
- 48 Pugh TJ, Weeraratne SD, Archer TC, Pomeranz Krummel DA, Auclair D, Bochicchio J *et al.* Medulloblastoma exome sequencing uncovers subtype-specific somatic mutations. *Nature* 2012; 488: 106-110.
- 49 Robinson G, Parker M, Kranenburg TA, Lu C, Chen X, Ding L *et al.* Novel mutations target distinct subgroups of medulloblastoma. *Nature* 2012; 488: 43-48.
- 50 Romero OA, Torres-Diz M, Pros E, Savola S, Gomez A, Moran S *et al.* MAX inactivation in small cell lung cancer disrupts MYC-SWI/SNF programs and is synthetic lethal with BRG1. *Cancer discovery* 2014; 4: 292-303.
- 51 Rutkowski S, von Hoff K, Emser A, Zwiener I, Pietsch T, Figarella-Branger D *et al.* Survival and prognostic factors of early childhood medulloblastoma: an international meta-analysis. *Journal of clinical oncology : official journal of the American Society of Clinical Oncology* 2010; 28: 4961-4968.
- 52 Schoenherr CJ, Anderson DJ. The neuron-restrictive silencer factor (NRSF): a coordinate repressor of multiple neuron-specific genes. *Science* 1995; 267: 1360-1363.
- 53 Schuller U, Heine VM, Mao J, Kho AT, Dillon AK, Han YG *et al.* Acquisition of granule neuron precursor identity is a critical determinant of progenitor cell competence to form Shh-induced medulloblastoma. *Cancer Cell* 2008; 14: 123-134.
- 54 Sengupta R, Dubuc A, Ward S, Yang L, Northcott P, Woerner BM *et al.* CXCR4 activation defines a new subgroup of Sonic hedgehog-driven medulloblastoma. *Cancer Res* 2012; 72: 122-132.
- 55 Sengupta S, Weeraratne SD, Sun H, Phallen J, Rallapalli SK, Teider N *et al.* alpha5-GABAA receptors negatively regulate MYC-amplified medulloblastoma growth. *Acta neuropathologica* 2014; 127: 593-603.
- 56 Shi J, Whyte WA, Zepeda-Mendoza CJ, Milazzo JP, Shen C, Roe JS *et al.* Role of SWI/SNF in acute leukemia maintenance and enhancer-mediated Myc regulation. *Genes Dev* 2013; 27: 2648-2662.

- 57 Shi X, Zhang Z, Zhan X, Cao M, Satoh T, Akira S *et al.* An epigenetic switch induced by Shh signalling regulates gene activation during development and medulloblastoma growth. *Nat Commun* 2014; 5: 5425.
- 58 Smits M, van Rijn S, Hulleman E, Biesmans D, van Vuurden DG, Kool M *et al.* EZH2-regulated DAB2IP is a medulloblastoma tumor suppressor and a positive marker for survival. *Clin Cancer Res* 2012; 18: 4048-4058.
- 59 Stankunas K, Hang CT, Tsun ZY, Chen H, Lee NV, Wu JI *et al.* Endocardial Brg1 represses ADAMTS1 to maintain the microenvironment for myocardial morphogenesis. *Dev Cell* 2008; 14: 298-311.
- 60 Sumi-Ichinose C, Ichinose H, Metzger D, Chambon P. SNF2beta-BRG1 is essential for the viability of F9 murine embryonal carcinoma cells. *Mol Cell Biol* 1997; 17: 5976-5986.
- 61 Trapnell C, Williams BA, Pertea G, Mortazavi A, Kwan G, van Baren MJ *et al.* Transcript assembly and quantification by RNA-Seq reveals unannotated transcripts and isoform switching during cell differentiation. *Nat Biotechnol* 2010; 28: 511-515.
- 62 Triscott J, Lee C, Foster C, Manoranjan B, Pambid MR, Berns R *et al.* Personalizing the treatment of pediatric medulloblastoma: Polo-like kinase 1 as a molecular target in high-risk children. *Cancer Res* 2013; 73: 6734-6744.
- 63 Uziel T, Zindy F, Sherr CJ, Roussel MF. The CDK inhibitor p18Ink4c is a tumor suppressor in medulloblastoma. *Cell Cycle* 2006; 5: 363-365.
- 64 Versteeg I, Sevenet N, Lange J, Rousseau-Merck MF, Ambros P, Handgretinger R *et al.* Truncating mutations of hSNF5/INI1 in aggressive paediatric cancer. *Nature* 1998; 394: 203-206.
- 65 Wallace VA. Purkinje-cell-derived Sonic hedgehog regulates granule neuron precursor cell proliferation in the developing mouse cerebellum. *Curr Biol* 1999; 9: 445-448.
- 66 Wang VY, Zoghbi HY. Genetic regulation of cerebellar development. *Nat Rev Neurosci* 2001; 2: 484-491.
- 67 Wang X, Sansam CG, Thom CS, Metzger D, Evans JA, Nguyen PT *et al.* Oncogenesis caused by loss of the SNF5 tumor suppressor is dependent on activity of BRG1, the ATPase of the SWI/SNF chromatin remodeling complex. *Cancer Res* 2009; 69: 8094-8101.



- 68 Wetmore C, Eberhart DE, Curran T. Loss of p53 but not ARF accelerates medulloblastoma in mice heterozygous for patched. *Cancer Res* 2001; 61: 513-516.
- 69 Wilson BG, Roberts CW. SWI/SNF nucleosome remodellers and cancer. *Nat Rev Cancer* 2011; 11: 481-492.
- 70 Witkowski L, Carrot-Zhang J, Albrecht S, Fahiminiya S, Hamel N, Tomiak E *et al.* Germline and somatic SMARCA4 mutations characterize small cell carcinoma of the ovary, hypercalcemic type. *Nat Genet* 2014; 46: 438-443.
- 71 Wu JI, Lessard J, Crabtree GR. Understanding the words of chromatin regulation. *Cell* 2009; 136: 200-206.
- 72 Wu JI. Diverse functions of ATP-dependent chromatin remodeling complexes in development and cancer. *Acta Biochim Biophys Sin (Shanghai)* 2012; 44: 54-69.
- 73 Yang H, Xie X, Deng M, Chen X, Gan L. Generation and characterization of Atoh1-Cre knock-in mouse line. *Genesis* 2010; 48: 407-413.
- 74 Yu Y, Chen Y, Kim B, Wang H, Zhao C, He X *et al.* Olig2 targets chromatin remodelers to enhancers to initiate oligodendrocyte differentiation. *Cell* 2013; 152: 248-261.
- 75 Zang C, Schones DE, Zeng C, Cui K, Zhao K, Peng W. A clustering approach for identification of enriched domains from histone modification ChIP-Seq data. *Bioinformatics* 2009; 25: 1952-1958.
- 76 Zhan X, Shi X, Zhang Z, Chen Y, Wu JI. Dual role of Brg chromatin remodeling factor in Sonic hedgehog signaling during neural development. *Proc Natl Acad Sci U S A* 2011; 108: 12758-12763.

## Figure Legends

### Figure 1. *Brg1* is required for CGNP proliferation and cerebellum development.

**A, A'.** Conditional deletion of *Brg1* in CGNPs using *Atoh1-Cre* led to reduced cerebellum size at postnatal day 12 (P12) compared to wild-type mice. **B, B'.** H&E staining of sagittal sections of P12 wild-type and *Brg1*-mutant cerebellum. The *Brg1*-mutant cerebella are significantly smaller than the wild type. **C, C'.** Immunostaining of P12 wild-type and *Brg1* mutant cerebellum demonstrates the deletion of *Brg1* from many CGNPs and granule neuron progenies in the mutant. The extra granule layer (EGL) is thinner in *Brg1*-mutant cerebellum. The higher magnification images of the EGL regions in the boxes are shown at the bottom. **D, D'.** BrdU labeling in P8 *Brg1*-mutant cerebellum EGL is decreased relative to that in wild-type EGL. BrdU was injected 2 hours before sacrifice. The quantification of BrdU-positive cells in EGL is plotted.

### Figure 2. *Brg1* is required for *SmoM2* medulloblastoma formation and progression.

**A.** H&E and Ki67 staining of sagittal sections of cerebella from P28 *Atoh1-Cre SmoM2 Brg1<sup>+/+</sup>* or *Atoh1-Cre SmoM2 Brg1<sup>F/F</sup>* mice. Arrows indicate a few Ki67 positive tumor initiation areas. **B.** Deletion of *Brg1* significantly extended survival time for mice harboring *SmoM2* medulloblastoma. Shown are survival curves of *Atoh1-Cre SmoM2* mice with *Brg1<sup>+/+</sup>*, *Brg1<sup>F/+</sup>*, or *Brg1<sup>F/F</sup>* alleles (n=15, 19, and 13, respectively). Log-rank test was used to determine the significance. **C.** The genetic strategy for deletion of *Brg1* in *SmoM2* medulloblastoma. LoxP sites flanking the stop signal and *Brg1* exons are shown as empty triangles. Leaky CAG-CreER activity induces *SmoM2* expression and medulloblastoma formation with an intact *Brg1* floxed allele. Treatment with tamoxifen activates CreER to induce *Brg1* deletion in tumors. Tamoxifen applied before tumor formation will induce the expression of *SmoM2* and deletion of *Brg1* simultaneously. **D.** CAG-CreER *SmoM2 Brg1<sup>F/F</sup>* medulloblastomas grown in the absence of tamoxifen induction were transplanted subcutaneously into SCID-NOD mice. Mice were injected with tamoxifen (Tam) or oil control after tumors became visible at 20 days after transplantation. Examples of tumors after oil or tamoxifen treatment are shown in top panels. Genotyping results indicate the presence of the recombined *Brg1Δ* allele only in tamoxifen-treated samples. The remaining *Brg1<sup>F</sup>* allele results from partial recombination of *Brg1* allele. The *Brg1<sup>+</sup>* alleles are from the host tissues. Shown right is the quantifications of transplanted *Brg1<sup>F/F</sup>* tumor sizes after tamoxifen or oil treatment. n=6 for oil treatment and n=5 for tamoxifen treatment. **E.** Tamoxifen induced *Brg1* deletion from transplanted CAG-CreER *SmoM2*

*Brg1*<sup>F/F</sup> medulloblastoma led to decreased tumor proliferation as indicated by decreased staining of proliferation markers H3P and BrdU (n=3). Student's t-test. \*: p<0.05; \*\*: p<0.01.

**Figure 3. *Brg1* deletion inhibits the transcription program specifically expressed in *SmoM2* medulloblastoma.** **A-B.** Tamoxifen (Tam) treatment of SCID-NOD recipient mice with *CAG-CreER SmoM2 Brg1*<sup>F/F</sup> medulloblastoma transplantation led to **(A)** decreased Gli1 expression as indicated by western blot and **(B)** decreased expression of Shh target genes and other known medulloblastoma oncogenes as shown by RT-qPCR. Controls were treated with vehicle (Oil). **C.** Significant overlap between *Brg1*-regulated genes and genes differentially expressed in *SmoM2* tumors versus normal cerebellum tissues. *Brg1*-regulated genes were identified by comparing gene profiles between *SmoM2* medulloblastoma with or without *Brg1* deletion. **D.** *Brg1* activates and represses gene sets specifically activated or repressed in *SmoM2* tumors. Genes regulated by *Brg1* and *SmoM2* were placed in a 20x20 matrix with ranked fold changes on both axes. The color key indicates the number of genes falling into each unit. **E.** Gene ontology analysis of the *Brg1*-regulated genes indicates the main categories of genes activated or repressed by *Brg1* in *SmoM2* medulloblastoma. Significance was determined by Student's t-test. \*\*: p<0.01.

**Figure 4. *Brg1* is required for the specific transcriptional regulatory circuitry controlling *SmoM2* medulloblastoma.** **A.** Genomic distribution of *Brg1* ChIP-seq binding regions identified in *SmoM2* medulloblastoma using SICER program. **B.** Distribution of *Brg1*-binding regions in a gene unit. The center of the *Brg1*-binding regions was used for the analyses. **C.** Venn diagram indicating the overlap between *Brg1*-binding genes and *Brg1*-regulated genes in medulloblastoma. Also indicated are genes containing both *Brg1* and Gli1 binding regions. **D.** Significant overlap between *Brg1*-binding genes and Atoh1-binding genes. The number in parentheses indicates the number of genes regulated by *Brg1* in medulloblastoma. **E.** Comparison of the percentages of target genes of Gli1, Atoh1, and Gli1/Atoh1 that are bound by *Brg1*. A significant enrichment of *Brg1* occupancy was observed in the genes with Gli1 and/or Atoh1 binding sites. **F.** A significant number of potential REST target genes are bound and repressed by *Brg1* in medulloblastoma. **G.** Snapshots of *Brg1* occupancy on representative Gli1 and Atoh1 target oncogenes. The genomic structures of the genes are shown below graphs with 5' on the left. *Brg1*-binding

regions identified using SICER are shown as black bars under the ChIP-seq signals. The Gli1 and Atoh1 binding sites close to the Brg1-binding regions are shown as red and green bars, respectively. **H.** Confirmation of the differential expression of Brg1 target genes by RT-qPCR in *SmoM2* medulloblastoma with or without *Brg1* deletion. The classification of the selected genes is listed below the gene names. TS: tumor suppressors. Significance was determined by Student's t-test. \*:  $p < 0.05$ ; \*\*:  $p < 0.01$ .

**Figure 5. Brg1 regulates the activities of H3K27me3 modifiers in medulloblastoma.**

**A.** *Brg1* deletion in primary *SmoM2* medulloblastoma led to increased global H3K27me3 and decreased levels of PRC2 subunits as shown by immunostaining. The quantifications of immunohistochemistry densities normalized to *Brg1*<sup>+/+</sup> tumors are shown on the right. **B.** RT-qPCR analyses of expression levels of PRC2 subunits and H3K27me3 demethylase in *SmoM2* medulloblastoma with or without *Brg1* deletion. **C-E.** ChIP-qPCR experiments indicate increased or decreased H3K27me3 levels at the regulatory regions of Brg1 target genes in *SmoM2* medulloblastoma upon *Brg1* deletion. **F.** Decreased Jmjd3 binding to the *Gli1* gene regulatory region in Shh-treated, *Brg1*-deleted CGNPs as shown by ChIP-qPCR. A region upstream of *Gli1* gene was used as a negative control for Jmjd3 binding. Significance was determined by Student's t-test. \*:  $p < 0.05$ , \*\*:  $p < 0.01$ .

**Figure 6. Brg1 function is conserved in human Shh-type medulloblastoma.**

**A.** The transcription pathways regulated by Brg1 in *SmoM2* mouse medulloblastoma are also specific to human Shh-type medulloblastoma. Using a microarray dataset of 76 human pediatric medulloblastoma samples with known subtypes (GSE37418), the average expression levels of human homologs of Brg1-activated Gli1 or Atoh1 targets as well as Brg1-repressed REST targets in each of the four types of medulloblastoma were compared. The subgroup with the highest expression level for each Brg1-activated genes and the subgroup with the lowest expression for each Brg1 repressed genes were identified and counted. The distributions of #1 or #4 ranked genes in each subgroup for the three Brg1-regulated gene lists are shown. The dash line indicates the expected 25% for each subgroup if there are no specificities. **B.** The average expression levels of example genes in each medulloblastoma subtype in the human microarray dataset. *SMARCA4/Brg1* is highly expressed in all tumor samples. Expression levels of human *GLI1* and *ATOH1* were significantly higher, whereas that of a REST target *CACAN1G* was significantly lower, in Shh-type medulloblastoma than in other subgroups. The numbers in

parentheses indicate the number of tumor samples in each subgroup. **C-D.** RNAi-mediated *Brg1* inhibition in Gli1-activated human medulloblastoma cell line DaoY led to **(C)** reduced Gli1/Atoh1 target gene expression as shown by RT-qPCR and **(D)** decreased cell growth as analyzed by ATP cell viability assays. **E.** RNAi-mediated *Brg1* inhibition did not affect the growth of D283 human medulloblastoma cell line. **F.** RT-qPCR analyses of mRNA levels of *Brg1* in DaoY and D283 cells with or without *Brg1* RNAi inhibition. **G.** Western blot assays show the endogenous Brg1 and exogenous HA-Gli1 protein levels in DaoY cells with or without inhibition of *Brg1* expression. **H.** Western blot assays show global H3K27me3 levels in DaoY and D283 cells with or without inhibition of *Brg1* expression. Significance was determined using t-test or ANOVA with post hoc t-test. \*\* indicates  $p < 0.01$  and \* indicates  $p < 0.05$ .

**Figure 7. Chromatin regulator Brg1 controls the transcriptional regulatory circuits underlying Shh-type medulloblastoma growth.**

A model representing specific functions of Brg1 in regulating the transcriptional regulatory circuits that control Shh-type medulloblastoma. Brg1 activates target genes of two key regulators of Shh-type medulloblastoma, Gli1 and Atoh1. Brg1 represses the expression of Shh-type medulloblastoma specific tumor suppressors and REST-targeted neuronal genes. *Brg1* deletion led to the inhibition of Shh-type medulloblastoma growth by deregulation of the essential transcription program.

Figure 1. Brg1 is required for CGNP proliferation and cerebellum development.

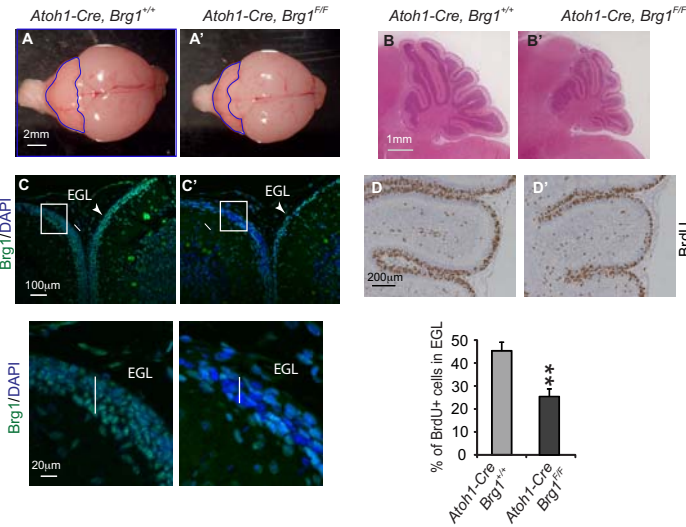


Figure 2. Brg1 is required for *SmoM2* medulloblastoma formation and progression.

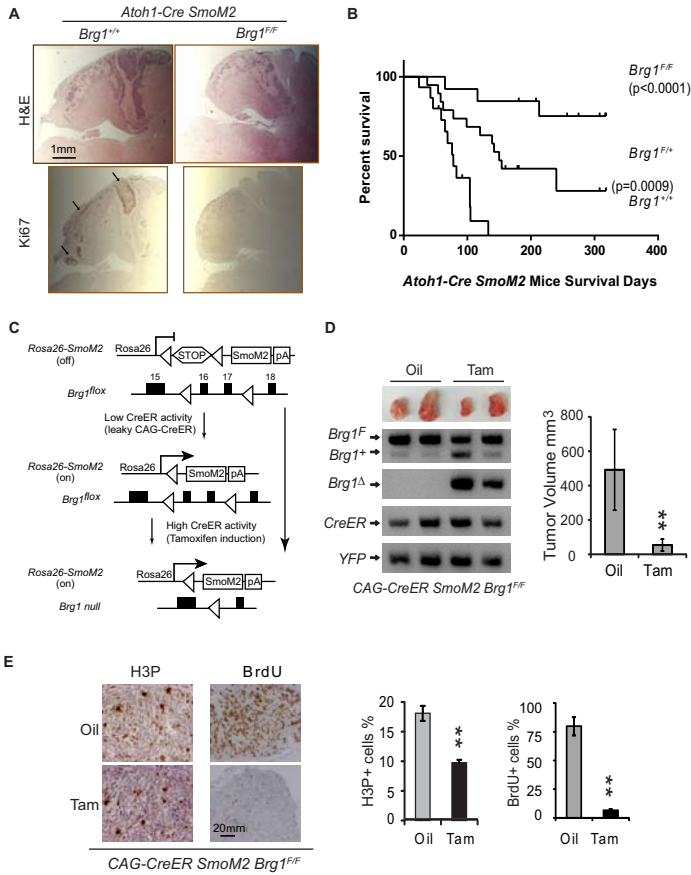


Figure 3. Brg1 deletion inhibits the transcription program specifically expressed in *SmoM2* medulloblastoma.

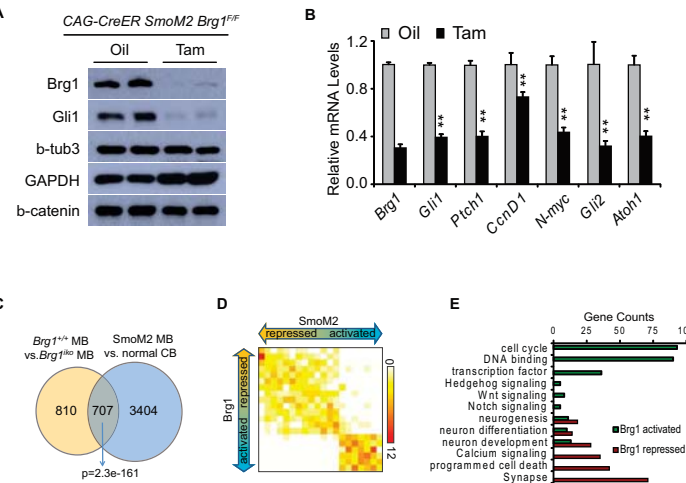


Figure 4. Brg1 is required for the specific transcriptional regulatory circuitry controlling *SmoM2* medulloblastoma.

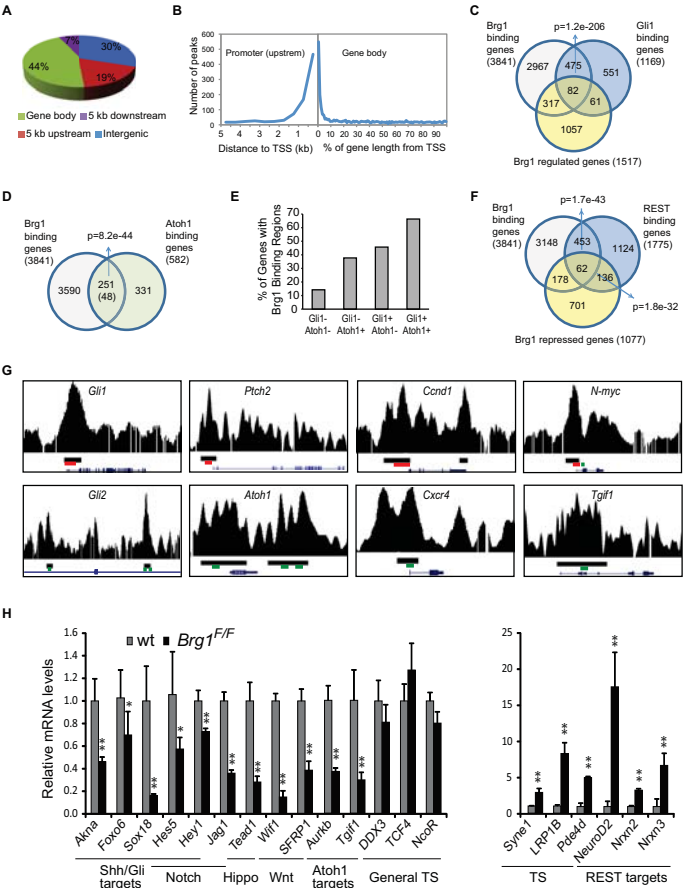


Figure 5. Brg1 regulates the activities of H3K27me3 modifiers in medulloblastoma.

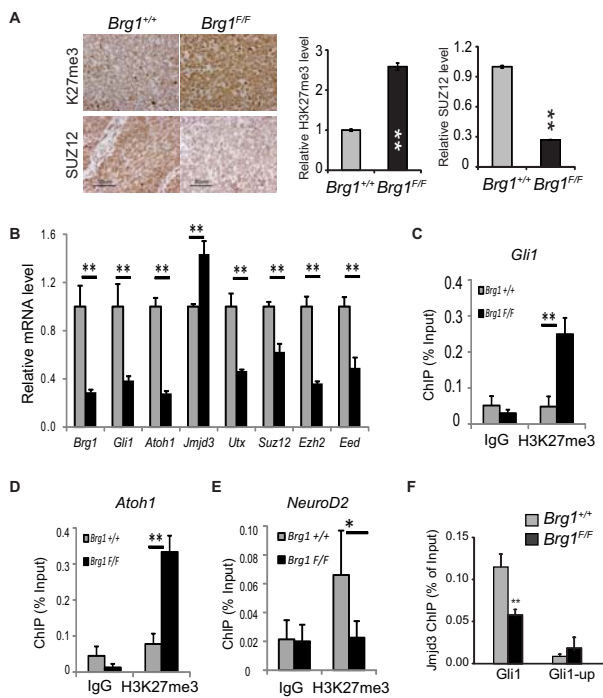


Figure 6. Brg1 function is conserved in human Shh-type medulloblastoma.

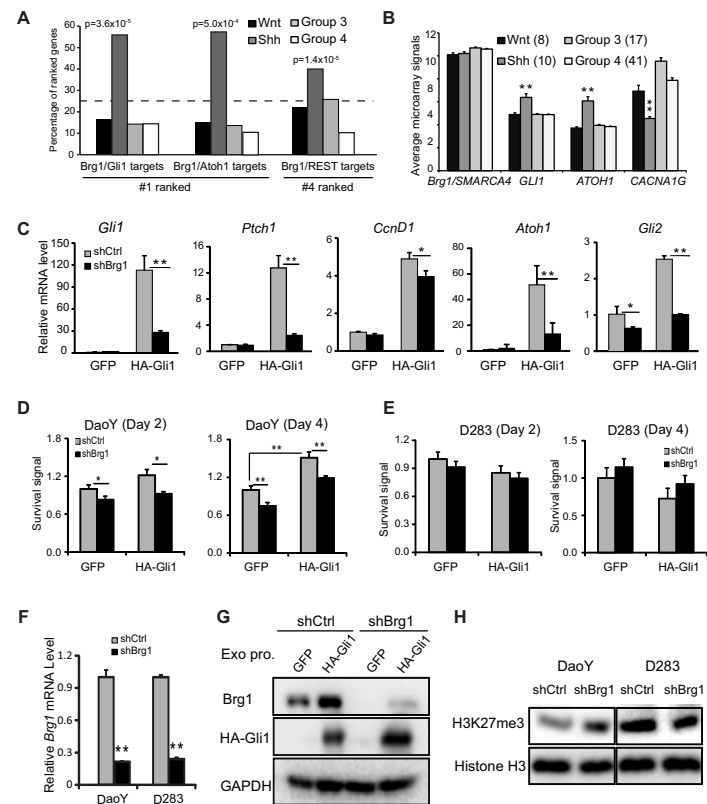
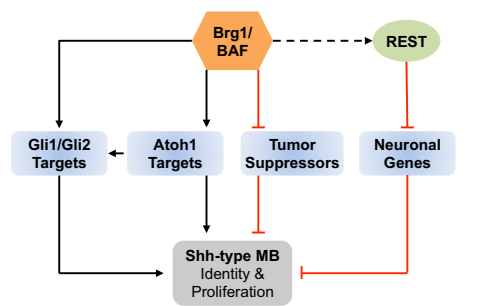


Figure 7. chromatin regulator Brg1 controls the transcriptional regulatory circuits underlying Shh-type medulloblastoma growth.



## ORIGINAL ARTICLE

## A positive feedback loop between Gli1 and tyrosine kinase Hck amplifies shh signaling activities in medulloblastoma

X Shi, X Zhan and J Wu

Sonic hedgehog (Shh) signaling is critical during normal development, and the abnormal activation of the Shh pathway is involved in many human cancers. As a target gene of the Shh pathway and as a transcription activator downstream of Shh signaling, Gli1 autoregulates and increases Shh signaling output. Gli1 is one of the key oncogenic factors in Shh-induced tumors such as medulloblastoma. Gli1 is posttranslationally modified, but the nature of the active form of Gli1 was unclear. Here we identified a Src family kinase Hck as a novel activator of Gli1. In Shh-responsive NIH3T3 cells, Hck interacts with Gli1 and phosphorylates multiple tyrosine residues in Gli1. Gli1-mediated target gene activation was significantly enhanced by Hck with both kinase activity-dependent and -independent mechanisms. We provide evidence showing that Hck disrupts the interaction between Gli1 and its inhibitor Sufu. In both NIH3T3 cells and cerebellum granule neuron precursors, the *Hck* gene is also a direct target of Gli1. Therefore, Gli1 and Hck form a positive feedback loop that amplifies Shh signaling transcription outcomes. In Shh-induced medulloblastoma, Hck is highly expressed and Gli1 is tyrosine phosphorylated, which may enhance the tumorigenic effects of the *Gli1* oncogene. RNAi-mediated inhibition of *Hck* expression significantly repressed medulloblastoma cell growth. In summary, a novel positive feedback loop contributes to maximal Gli1 oncogenic activities in Shh-induced tumors such as medulloblastoma.

*Oncogenesis* (2015) 4, e176; doi:10.1038/oncsis.2015.38; published online 30 November 2015

## INTRODUCTION

Sonic hedgehog (Shh) signaling has critical roles in many development processes, and dysregulation of Shh signaling has been implicated in diseases and cancers such as those in cerebellum, skin, pancreas, prostate and lung.<sup>1–6</sup> In cerebellum during early postnatal development, Shh secreted from Purkinje neurons functions as a mitogen to stimulate the proliferation of cerebellum granular neuron precursor (CGNP) cells.<sup>7–10</sup> Mutations leading to constitutively active Shh signaling in CGNPs cause CGNP over-proliferation and Shh-type medulloblastoma, which accounts for 25% of all medulloblastoma cases and is the most frequent malignant childhood brain tumor.<sup>11–15</sup> Shh signaling transduced by Patched (Ptch1) and Smoothened (Smo) induces target gene expression by activating Gli transcription activators.<sup>1,3,16,17</sup> Gli1 is a sensitive Shh target gene and functions solely as a transcription activator in response to Shh signaling. Thus it forms an auto-positive feedback loop that enhances Shh signaling outcomes.<sup>5,18</sup> Although Gli1 is not essential for development, it is a potent oncogene and is required for Shh-induced tumor growth.<sup>19–21</sup> Gli1 expression is elevated in many cancer types with elevated Shh signaling.<sup>3</sup> Inhibiting Gli1 activity would likely be an effective approach for treating these cancers. Thus, understanding the largely unknown mechanisms of Gli1 activation will provide insights into the mechanism of cancer growth and will guide development of treatments.<sup>22,23</sup>

An important regulator of Gli1 activities is the inhibitor Sufu, which sequesters Gli1 in the cytoplasm and also inhibits Gli1 activities in the nucleus.<sup>22,24–26</sup> In addition, Gli1 activities are regulated by posttranslational modification events such as Ser/Thr phosphorylation. It can also be acetylated, ubiquitinated and sumoylated.<sup>6,26–28</sup> Several posttranslational modifications

potentially interrupt the Gli1–Sufu interactions and release Gli1 from the inhibition by Sufu.<sup>22,26</sup> Gli1 modification enzymes such as histone deacetylases and atypical protein kinase C (aPKC) family members  $\iota$  and  $\lambda$  are promising targets for the treatment of Shh-related cancers.<sup>28,29</sup>

Several Tyr residues in Gli1 are conserved, but until our study, it was not known whether Gli1 was Tyr phosphorylated or whether tyrosine kinases function in regulating Gli1 activities. In mammals, there are 10 families of nonreceptor tyrosine kinases.<sup>30,31</sup> The Src family, consisting of Src, Hck, Lyn, Fyn, Fgr, Blk, Lck, Yes and Ylk, play essential roles in malignant transformation and tumor progression.<sup>32,33</sup> Besides the kinase activities, Src family kinases also display kinase activity-independent functions,<sup>34,35</sup> mostly through protein-protein interactions. The Src family kinase Hck has a known function in hematopoiesis.<sup>36,37</sup> Interestingly, *Hck* was identified in a genome-wide study of potential Gli1 binding genes in CGNPs and in Shh-type medulloblastoma.<sup>38</sup> As Shh/Gli target genes such as *Gli1*, *Ptch1*, *Hhip* and *aPKC- $\iota/\lambda$*  are Shh pathway regulators, it is possible that Hck also regulates Shh signaling.

In this report, we show that *Hck* is a direct target gene of Shh signaling and can be activated by Gli1 in both NIH3T3 cells and in CGNPs. Hck interacts with Gli1 and phosphorylates it at multiple Tyr residues. Hck enhances Gli1-mediated target gene activation through both kinase activity-dependent and -independent mechanisms. We provide evidences showing that Hck releases Gli1 from Sufu inhibition by disrupting the Gli1–Sufu interaction. Therefore, Gli1 and Hck form a positive feedback loop to amplify Shh signaling outcomes. In Shh-induced medulloblastoma, both Gli1 and Hck are expressed at high levels and Gli1 is Tyr phosphorylated. RNAi-mediated inhibition of *Hck* expression significantly inhibited tumor cell growth. Thus, Gli1–Hck positive



feedback loop enhances Gli1 oncogenic effects and contribute to the growth of medulloblastoma.

## RESULTS

*Hck* is a direct target of Gli1 in response to Shh signaling

In an experiment using RNA-seq designed to identify Shh-responsive genes in mouse embryonic fibroblasts (MEFs), we observed that *Hck* expression was induced by Shh treatment.<sup>39</sup> In a previous study, *Hck* was identified as a Gli1 binding gene in both CGNPs and medulloblastoma.<sup>38</sup> To validate that *Hck* is a Shh/Gli target gene, we treated Shh-responsive NIH3T3 cells with Shh-conditioned medium. The *Hck* mRNA (messenger RNA) level was significantly upregulated after Shh treatment. *Gli1* was also upregulated indicating that NIH3T3 cells were activated by Shh (Figure 1a). In CGNP cultures, Shh treatment significantly induced the expression of *Gli1* and *Hck* (Figure 1b). In addition, when we expressed exogenous Gli proteins in NIH3T3 cells, the levels of both *Hck* and another Gli target gene *Ptch1* were significantly increased by Gli1 (Figure 1c). Three Gli transcription factors were evaluated, and *Hck* expression was most sensitive to Gli1 (Figure 1d).

Previous chromatin immunoprecipitation (ChIP)-on-Chip experiments in CGNP and medulloblastoma identified a potential Gli1 binding site ~1.1 kb upstream of the transcription start site of *Hck*; the region harbors a Gli binding motif (Figure 1e, Supplementary Figure S1).<sup>38</sup> To determine whether Gli1 regulates *Hck* through direct binding, we performed ChIP experiments using antibodies against HA-Gli1 in NIH3T3 cells. ChIP quantitative PCR analyses indicate that Gli1 bound to the upstream enhancer region but not the region surrounding the transcription start site (Figure 1f). To further understand the regulation of the *Hck* gene by Gli1, we cloned 1.7 kb of genomic DNA, including the *Hck* transcription start site and the putative Gli1 binding region, into a luciferase reporter vector. The *Hck* reporter was significantly upregulated upon co-transfection of Gli1 (Figure 1g). Truncation or internal deletion of the Gli1 binding region significantly impaired Gli1-induced reporter activities. Mutation of the 9-bp Gli binding motif resulted in a similar loss of the responsiveness to Gli1 activation (Figure 1g). Taken together, our data indicate that Shh-induced *Hck* expression is mediated by direct binding of Gli1 to the regulatory region upstream of the *Hck* promoter.

Acute depletion of *Hck* leads to impaired Shh signaling gene expression

To determine whether *Hck* regulates Shh signaling, we inhibited *Hck* expression using lentivirus-mediated expression of an RNAi agent in NIH3T3 cells. Although *Hck* inhibition did not affect the basal expression of Shh target genes *Gli1* and *Ptch1*, Shh-induced expression of these genes was significantly impaired, indicating that *Hck* functions in Shh-induced Gli target gene activation (Figures 2a and c). Importantly, the defective gene activation in response to Shh was rescued by an RNAi-resistant human wild-type *Hck* (Figure 2d). Significantly higher Gli1 expression was observed in the presence of exogenous wild-type *Hck* than in control cells; this is likely owing to overexpression of *Hck*. Notably, a kinase-inactive form of *Hck* (*Hck*-K269E)<sup>40</sup> did not rescue the defective Gli1 activation that resulted from *Hck* inhibition despite the high levels of expression of the mutant protein (Figure 2d). Thus, *Hck* is required for Shh signaling in NIH3T3 cells, and its kinase activity is required.

*Hck* enhances Gli1-mediated target gene activation to form a positive feedback loop

To delineate how *Hck* regulates Gli-mediated gene transcription in response to Shh signaling, we co-expressed Gli1 and *Hck* in

NIH3T3 cells. Exogenous Gli1 activated the expression of endogenous Shh target genes *Ptch1*, *Gli1* and *Hck* as expected, whereas *Hck* alone had a moderate or no effect on the target gene expression. Expression levels of exogenous human *Hck* and endogenous *Hck* were distinguished by using specific PCR primers in human and mouse *Hck* genes, respectively. Interestingly, co-expression of *Hck* and Gli1 significantly enhanced Gli1 activator activities. All Shh target genes tested were expressed at higher levels in the presence of exogenous *Hck* than in the presence of Gli1 alone (Figures 3a and c). Interestingly, the kinase-dead *Hck*-K269E mutant protein also enhanced Gli1-mediated target gene induction albeit with less fold change than wild-type *Hck* (Figure 3d), suggesting that besides the kinase activities, kinase-independent mechanisms also exist to activate Gli1. Thus, as *Hck* is a target gene of Gli1 and it encodes an activator of Gli1, *Hck* and Gli1 form a positive feedback loop that amplifies Shh signaling outcomes.

*Hck* phosphorylates multiple residues in Gli1 through direct binding

*Hck* is a Src family tyrosine kinase; *Hck* phosphorylates itself and other substrate proteins.<sup>41</sup> To examine whether *Hck* can phosphorylate Gli1, we expressed HA-tagged Gli1 and *Hck* individually or simultaneously in NIH3T3 cells, then immunoprecipitated proteins phosphorylated at Tyr using the antibody 4G10 specific for phosphorylated Tyr residues. Consistent with the previously reported auto-phosphorylation function of *Hck*,<sup>41</sup> HA-*Hck* migrated at ~59 kD was detected in the proteins precipitated with 4G10 from cells expressing exogenous *Hck*. Without exogenously expressed *Hck*, Gli1 was not precipitated with 4G10. With co-expressed *Hck*, HA-Gli1 migrated at ~150 kD was detected in the 4G10 precipitations (Figure 4a), suggesting that Gli1 is phosphorylated by *Hck*. To determine whether *Hck* interacts with Gli1, we performed co-immunoprecipitation experiments. NIH3T3 cells were transfected with vectors for expression of Gli1-GFP and/or HA-*Hck*. Cell lysates were immunoprecipitated with antibodies against the GFP tag. HA-*Hck* was co-immunoprecipitated with Gli1-GFP. Gli1-GFP was Tyr phosphorylated in the presence of HA-*Hck* as it reacted with the 4G10 antibody (Figure 4b).

In the Gli1 protein, there are 32 Tyr residues that are conserved between mouse and human (Supplementary Figure S2). To determine which residues can be phosphorylated by *Hck*, we evaluated phosphorylation of the full-length Gli1 protein, the N-terminal region, the zinc-finger domain and the C-terminal fragment expressed in NIH3T3 cells. Using a western blot analysis, we observed that the full-length Gli1 and the C-terminal fragment were phosphorylated as indicated by multiple slow-migrating bands (Figure 4c, indicated by asterisks). The tyrosine phosphorylation in both the N- and C-terminal regions of Gli1 was also detected with 4G10 antibody western blot following immunoprecipitation with anti-HA antibodies (Figure 4d). These results indicate that multiple Tyr residues in the N- and C-terminal domains of Gli1 are likely phosphorylated by *Hck*. This is consistent with previous findings that Gli proteins are relatively unstructured and interact with other proteins through both N- and C-terminal domains.<sup>27,42</sup> Therefore, *Hck* likely regulates Shh signaling output by interacting and phosphorylating Gli1.

To identify the potential *Hck*-targeted Tyr phosphorylation sites in Gli1, HA-Gli1 co-expressed with *Hck* in NIH3T3 cells were immunoprecipitated with anti-HA antibodies and separated on SDS-PAGE (SDS polyacrylamide gel electrophoresis) gels. Gli1 proteins in gel slices were digested, extracted and subjected for LC/MS/MS. Within 23 Gli1 peptides recovered (26.3% coverage), we identified Y800 as a phosphorylated residue with high confidence (Figure 4e). Y800 is a potential *Hck* target site in Gli1. However, deleting Y800 did not diminish the Gli1 Tyr

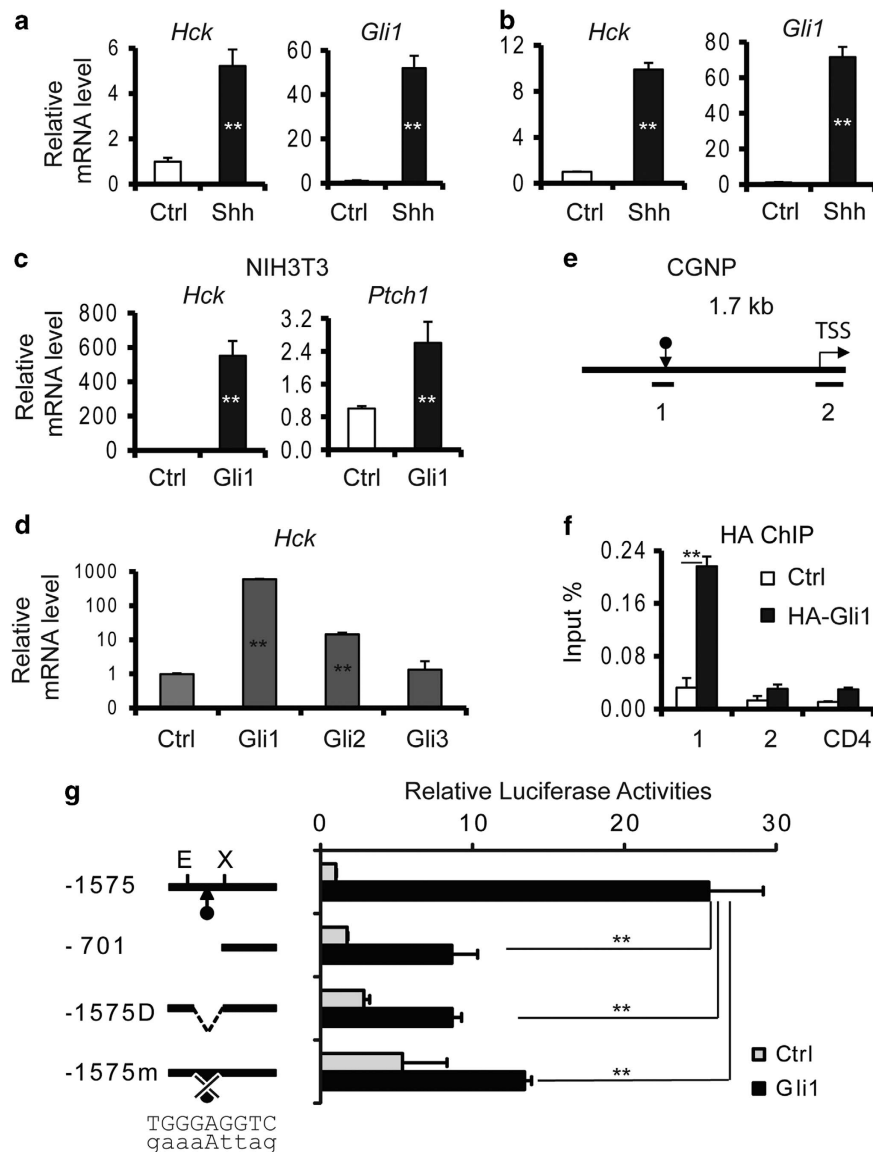


**Figure 1.** *Hck* is a direct Shh/Gli1 target gene. (a) NIH3T3 cells were treated with or without Shh-conditioned media. Levels of *Hck* and *Gli1* mRNAs were determined by RT-qPCR. (b) *Hck* and *Gli1* mRNA levels were determined by RT-qPCR in CGNP cells treated with or without Shh-conditioned media. (c) NIH3T3 cells were infected with empty vector or lentiviruses for expression of Gli1 proteins. Levels of *Hck* and Shh target gene *Ptch1* were determined. (d) Levels of *Hck* were determined by RT-qPCR in NIH3T3 cells infected with lentiviruses expressing different Gli proteins. (e) A schematic map of the 1.7 kb *Hck* regulatory region used for ChIP and reporter assays. The Gli binding site (indicated by the arrow) and the transcription start site (TSS) are shown. Small bars indicate the location of ChIP PCR products. (f) NIH3T3 cells were infected with empty vector control or HA-Gli1 expressing lentiviruses. ChIP-qPCR analyses were performed with anti-HA antibody. A region in *CD4* was used as a negative control. (g) The 1.7 kb wild-type full-length *Hck* enhancer region (–1575; E: EcoRI site; X: XhoI site) and mutants including a truncated construct (–701), a construct with the putative Gli1 binding site deleted (–1575D) or mutated (–1575m) were cloned upstream of a luciferase reporter gene. Plasmids expressing control (empty vector) or Gli1 proteins were co-transfected with reporters into NIH3T3 cells. Relative luciferase activities are shown on the right. Presented are means plus s.d. Statistical analyses were performed using the Student's *t*-test; \*\**P* < 0.01. qPCR, quantitative PCR.

phosphorylation (Supplementary Figure S3). This observation confirmed that Gli1 is Tyr phosphorylated at multiple sites including Y800.

#### Hck disrupts Gli–Sufu interactions

Gli1 activities can be regulated at several different steps. Two critical steps are the activation in cilia and the inhibition by Sufu. Kif3a is required for the formation and function of primary cilia in transducing the Shh signal.<sup>25,43</sup> Interestingly, in *Kif3a*<sup>–/–</sup> MEF cells, *Gli1* transcriptional activation was still enhanced by exogenous Hck (Figures 5a and b), indicating that Hck functions downstream

of Kif3a. On the contrary, in *Sufu*<sup>–/–</sup> MEF cells,<sup>44</sup> Hck failed to enhance Gli1 activities in inducing endogenous *Gli1* expression (Figure 5c). This result indicates that Hck functions at the same level or downstream of Sufu.

Sufu interacts tightly with Gli activators and inhibits their activities at several levels.<sup>22,24–26,42</sup> We next examined whether Hck affects the interaction between Gli1 and Sufu. In NIH3T3 cells expressing tagged Gli1 and Sufu, in the absence of exogenous Hck, ~30% of Gli1 co-immunoprecipitated with Sufu. However, in the presence of Hck, only ~5% of the Gli1 co-precipitated with Sufu (Figure 5d). In a gel with better resolution, it appeared that only unphosphorylated Gli1 co-precipitated with Sufu

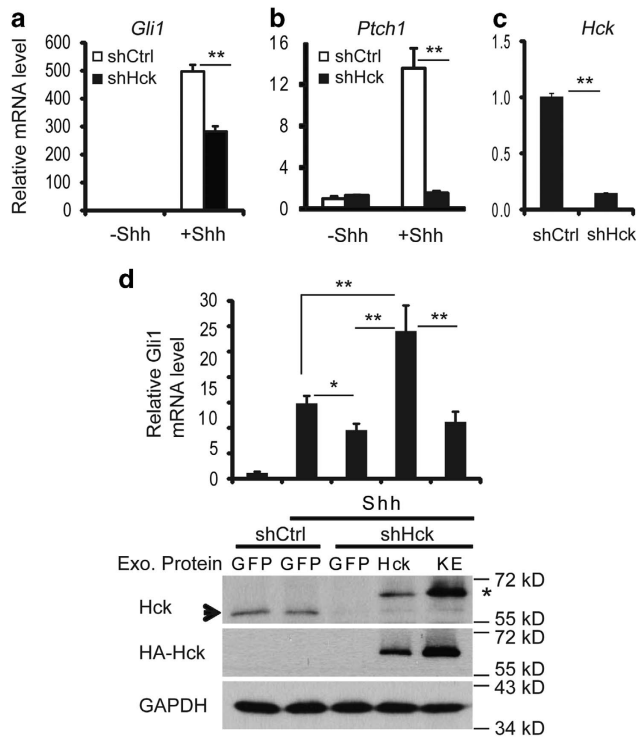


**Figure 2.** Acute knockdown of Hck leads to impaired Shh signaling-induced gene expression. (a–c) NIH3T3 cells were infected with lentiviruses expressing scrambled shRNA (shCtrl) or shRNA designed to target *Hck* (shHck). The cells were treated with or without Shh-conditioned medium. mRNA levels of Shh target genes (a) *Gli1*, (b) *Ptch1* and (c) *Hck* were determined by RT–qPCR. (d) NIH3T3 cells infected with lentiviruses expressing scrambled shRNA or shHck were co-infected with viruses for expression of Hck, Hck-K269E or GFP control. Upper panel: Endogenous *Gli1* mRNA levels under basal or Shh-stimulated conditions were measured by RT–qPCR. Only wild-type Hck, but not the kinase-inactive Hck mutant (KE), rescued defective Shh-induced *Gli1* expression that resulted from expression of shHck. Lower panel: western blot analyses of endogenous and exogenous Hck in samples analyzed by RT–PCR. An arrow points to the endogenous Hck band and a star indicates HA-Hck. Presented are means plus s.d.;  $n = 3$ . Statistical analyses were performed using the Student's *t*-test; \*\* $P < 0.01$  and \* $P < 0.05$ . qPCR, quantitative PCR.

(Supplementary Figure S4). These results suggest that the interaction between Gli1 and Hck or the phosphorylation of Gli1 by Hck disrupts Sufu–Gli1 interaction. To determine whether the kinase activity of Hck is required, we performed the experiments with the kinase-inactive Hck-K269E. Interestingly, co-expressing Hck-KE also significantly reduced the co-immunoprecipitation efficiency of Gli1 with Sufu (Figure 5e). Thus, kinase activity-independent mechanisms could be largely responsible for Hck function in disrupting Gli1–Sufu interaction, possibly through Hck–Gli1 interactions. Similar to Gli1, Gli2 is also inhibited by Sufu. In NIH3T3 cells, both Hck and Hck-KE mutant proteins significantly reduced Gli2 co-immunoprecipitation with Sufu (Figure 5e). Thus, Hck could also disrupt Gli2–Sufu interactions. These results indicate that one mechanism that Hck uses to activate Gli1 and possibly Gli2 is to release Gli proteins from Sufu inhibition.

Hck is highly expressed in Shh-type medulloblastoma and required for tumor cell growth

During early postnatal cerebellum development (postnatal day 0 (P0) to P14 for mouse), Shh signaling induces rapid proliferation of CGNPs, which then differentiate into granule neurons. Mutations such as *Ptch1* loss-of-function or *Smo* gain-of-function lead to

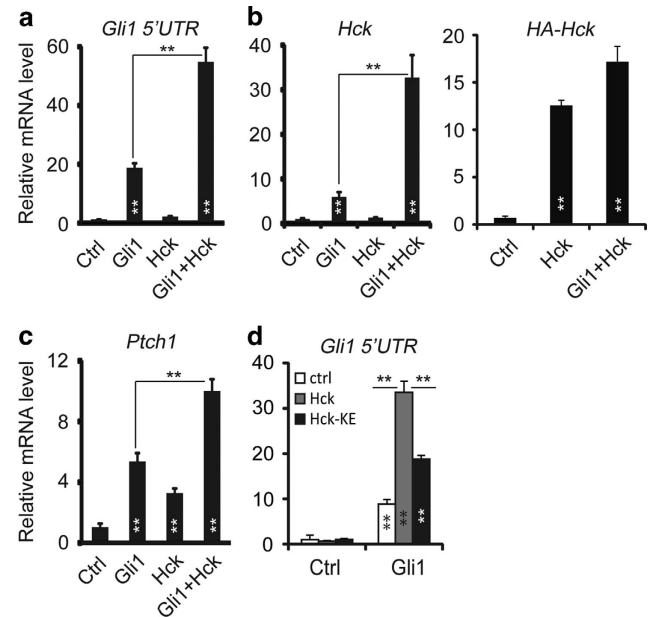


**Figure 3.** Hck enhances Gli1-mediated target gene activation. (a, b, c) NIH3T3 cells were infected with lentiviruses expressing Gli1 alone, Hck alone or the two together. Levels of Shh target genes (a) *Gli1*, (b) *Hck* and (c) *Ptch1* were determined by RT–qPCR. Endogenous *Gli1* levels were measured using primers in the 5'–UTR to distinguish this message from that of the exogenous Gli1. Exogenous human *Hck* levels were measured using primers specific to human genes. (d) Hck kinase activity is required for maximum activation of Gli1. As in a, Gli1-induced expression of endogenous *Gli1* was measured in the presence of wild-type Hck or Hck-K269E kinase-dead mutant (Hck-KE). Presented are means plus s.d.;  $n = 3$ . Statistical analyses were performed using the Student's *t*-test; \*\* $P < 0.01$ . qPCR, quantitative PCR.

constitutively active Shh signaling, which results in CGNP over-proliferation and medulloblastoma.<sup>13</sup> A mouse model of medulloblastoma with an activating SmoM2 mutant transgene closely resembles human Shh-type medulloblastomas.<sup>45</sup> The high *Gli1* levels that we observed in P4 cerebellum and in medulloblastoma samples indicate active Shh signaling during cerebellum development and in Shh-type medulloblastoma formation (Figure 6a). High levels of *Sufu* were also found in developing cerebellum and in medulloblastoma (Figure 6b), indicating inhibition of Shh/Gli1 activities despite activation of Shh signaling. Interestingly, both mRNA and protein levels of Hck were significantly higher in medulloblastoma compared with normal cerebellum and NIH3T3 cells (Figures 6c and d, Supplementary Figure S5), which may contribute to the abnormally high Shh/Gli1 activities in Shh-type medulloblastoma and the uncontrolled proliferation of these cells. Indeed, we found that endogenous Gli1 is Tyr phosphorylated in medulloblastoma as indicated by 4G10 antibody immunoprecipitation (Figure 6e). Importantly, inhibition of *Hck* expression mediated by RNAi in cultured SmoM2 medulloblastoma cells significantly decreased the survival and growth of cancer cells as indicated by cell viability assays (Figure 6f). Key Shh target genes such as *Gli1* and *Ptch1* were significantly decreased upon Hck inhibition (Figure 6g). Our data indicate that high level of Hck is required for maximum Gli1 activities and oncogenic functions in medulloblastoma. Disrupting Gli1–Hck feedback loop would be a promising treatment strategy for Shh-type medulloblastoma.

## DISCUSSION

In the past two decades, significant progress has been made in understanding how Shh signaling contributes to normal

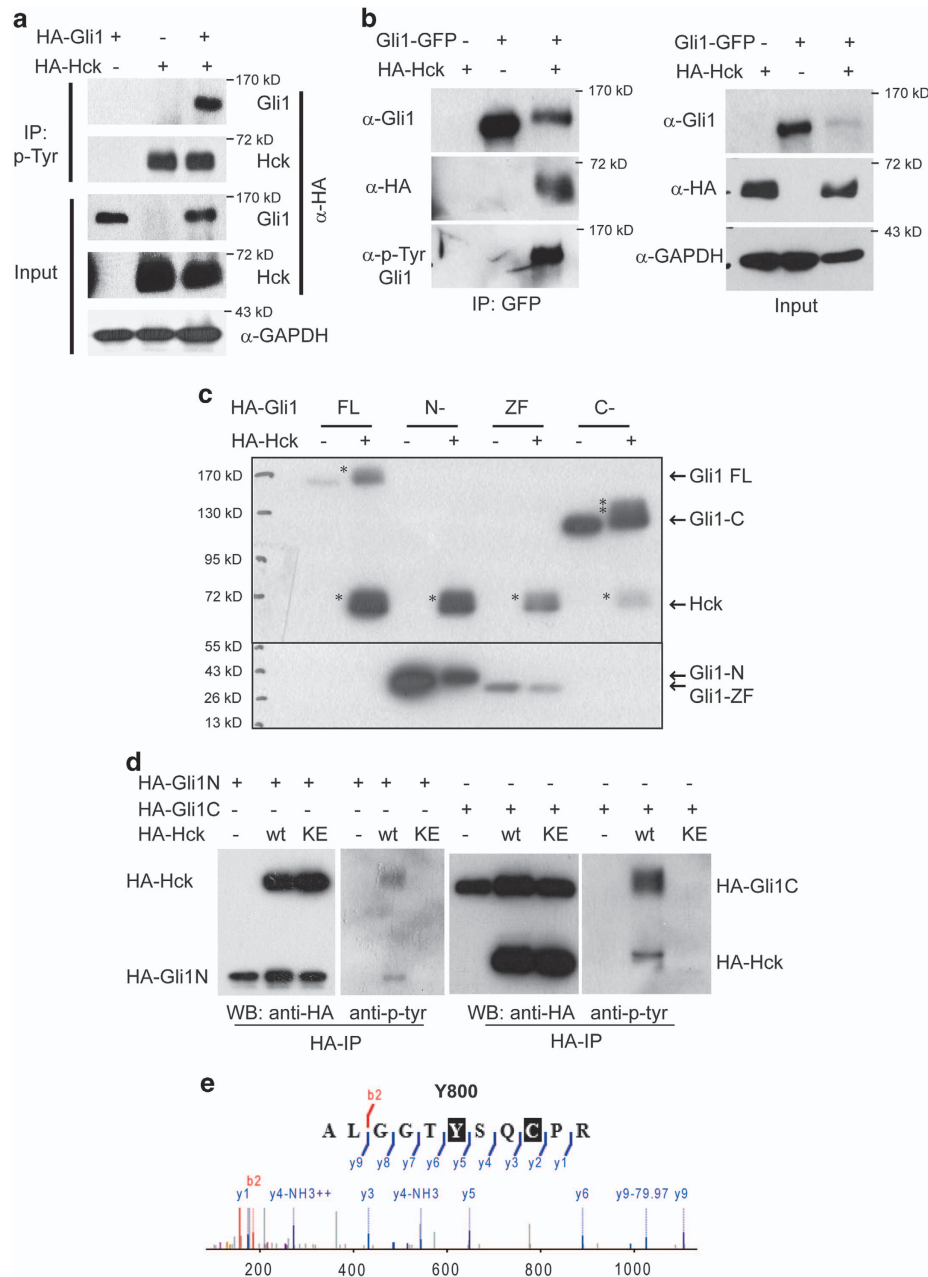


**Figure 4.** Hck phosphorylates multiple residues in Gli1 through direct binding. **(a)** Gli1 is Tyr phosphorylated in the presence of exogenous Hck. NIH3T3 cells were transiently transfected with constructs expressing HA-tagged Gli1 alone, Hck alone or the two together. Cell lysates were immunoprecipitated using 4G10 antibody, followed by western blot using antibody against HA tag. **(b)** Gli1 co-precipitates with Hck. NIH3T3 cells were transfected with constructs for expression of GFP-Gli1, HA-Hck or the two together. Antibodies against GFP were used for the immunoprecipitation and antibodies against Gli1, HA and phospho-Tyr (4G10) were used for western blot. HA-Hck was co-precipitated with GFP-Gli1. Gli1 was Tyr phosphorylated in the presence of Hck as shown by the 4G10-positive band. GAPDH was used as a loading control. **(c)** Western blot analyses of Hck phosphorylated human Gli1 fragments (FL, full-length; N-, N-terminal fragment (1-231 aa); ZF, zinc-finger domain (232-410 aa); C-, C-terminal fragment (411-1106 aa)) separated on an SDS-PAGE gel. NIH3T3 cells were co-transfected with constructs for expression of Gli1 fragments and HA-Hck. Asterisks indicate the phosphorylated bands; arrows point to the corresponding non-phosphorylated protein bands. **(d)** Both the N- and C-terminal fragments of Gli1 were Tyr phosphorylated in the presence of Hck. NIH3T3 cells were transfected with constructs for expression of HA-tagged Gli1 fragments and HA-Hck or the kinase-inactive Hck-K269E. Antibodies against HA were used for the immunoprecipitation and antibodies against HA, and phospho-Tyr (4G10) were used for western blot. **(e)** HPLC-MS/MS spectrum of phosphopeptide ALGGTY(p)SQCP R that contains Y800. The ion peak labeled with minus 79.97 ( $\text{H}_3\text{PO}_4$  mass) serves to confirm the Y800 phosphorylation.

development and cancer progression. Recent genomic studies on the basis of the transcription profiles have shown that ~25% of medulloblastoma cases are characterized by active Shh signaling. In this study, we demonstrate that a tyrosine kinase Hck forms a positive feedback loop with the transcription activator Gli1 to

amplify Shh signaling outputs; this feedback loop contributes to the tumorigenic function of Shh signaling (Figure 7). We found that Hck is a direct Shh target gene that is sensitive to Gli1 activation. We provide evidence that Hck enhances Gli1 activities and that this function of Hck is mediated by both phosphorylation



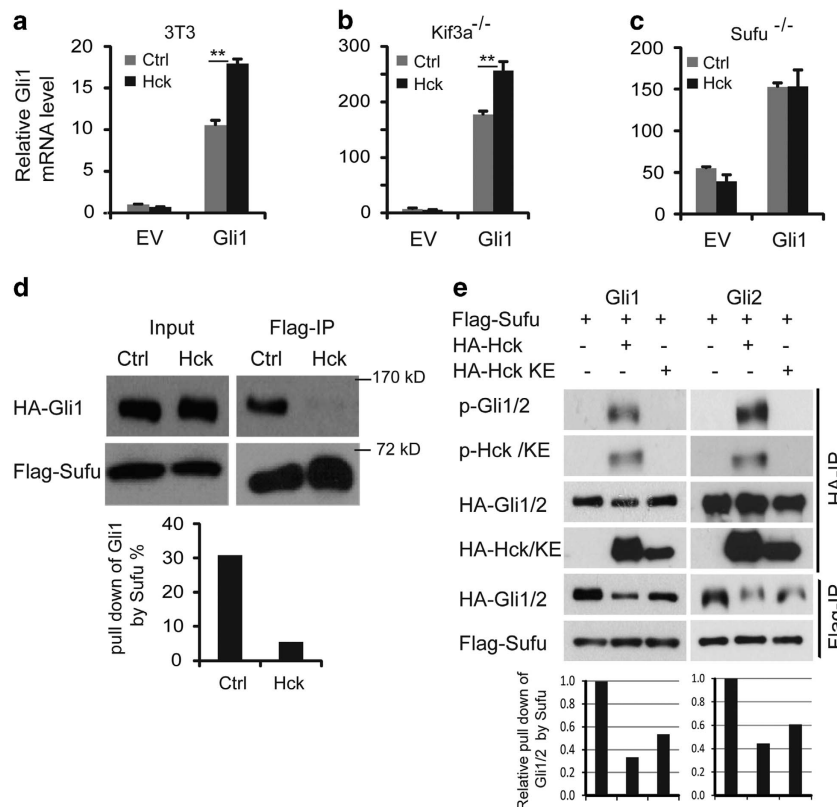


**Figure 5.** Hck disrupts Gli-Sufu interactions. (a–c) Hck activates Gli1 downstream of Kif3a in a Sufu-dependent fashion. (a) NIH3T3 cells, (b) immortalized *Kif3a*<sup>-/-</sup> MEFs and (c) *Sufu*<sup>-/-</sup> MEFs were co-infected with a control or with lentiviruses designed to express Gli1 and/or Hck. Endogenous *Gli1* levels measured using primers in the 5'-UTR were determined by RT-qPCR. Presented are means plus s.d.; *n* = 3. Significance was determined by Student's *t*-test; \*\**P* < 0.01. (d) Hck disrupts Gli1-Sufu interactions. NIH3T3 cells were transfected with constructs expressing HA-Gli1 and Flag-tagged Sufu in the presence or absence of exogenous HA-Hck. Cell lysates were precipitated with anti-Flag antibodies and western blotted with antibodies against HA or Flag. The western blot bands were quantified with NIH Image J software and the percentage of Gli1 precipitated with Flag-Sufu was compared with the input. (e) NIH3T3 cells were transfected with constructs expressing HA-Gli1/2 and Flag-Sufu in the presence of exogenous HA-Hck or kinase-inactive Hck-K269E. Cell lysates were precipitated with anti-Flag or anti-HA antibodies and western blotted with antibodies against HA, Flag or 4G10 antibodies. Quantifications of western blot are shown below. qPCR, quantitative PCR.

of Gli1 and kinase-independent activities. High level of Hck disrupts the interaction between Gli1 and its inhibitor Sufu with kinase activity-independent mechanisms. Importantly, Hck is highly expressed in Shh-type medulloblastoma and required for tumor cell growth. Thus, disrupting the Gli1-Hck feedback loop may inhibit progression of Shh-type medulloblastoma.

In this study, we demonstrate that Gli1 is activated by novel mechanisms through tyrosine phosphorylation and interaction with a tyrosine kinase. We showed that tyrosine kinase Hck activates Gli1 and the kinase activity is required for its maximum effect. In medulloblastoma in which Gli1 is highly expressed and activated, we observed Tyr phosphorylation of endogenous Gli1. There are 32 conserved Tyr residues throughout the Gli protein. Our truncation analyses indicated that multiple residues are likely phosphorylated by Hck. We identified Y800 in human Gli1 as a potential Hck target site. This is consistent with a report from the PhosphoSitePlus database that the conserved Y798 in rat was phosphorylated in ischemic esophagus. In Gli1, Y800 is located in the proline-rich region that may be important in both the active Gli1 conformation and its interactions with other regulators. However, it is likely that additional functional Tyr residues are phosphorylated by Hck. Notably, Y121 in the SYGH Sufu binding motif is important for maintaining the hydrophobic interacting surface between Gli1 and Sufu.<sup>46,47</sup> Although we confirmed the importance of Y121 in Gli1-Sufu interaction by mutagenesis analyses (data not shown), we did not observe the phosphorylation of the Tyr by mass spectrometry. Thus, analyses of

combinations of Tyr mutations or more targeted mass spectrometry studies may reveal the entire Gli1 phosphorylation pattern that activates Gli1 function. In addition, our data do not definitively exclude the possibility that Hck phosphorylates other Gli1 regulators and activates Gli1 indirectly.

In the study, we observed that Hck could activate Gli1 through kinase-independent activities as both wild-type and kinase-inactive Hck could activate Gli1-mediated target gene activation and disrupt the interaction between Gli1 and its inhibitor Sufu. As Hck interacts with Gli1, it is possible that high levels of Hck could compete with Sufu for interaction. Similarly, Hck could also interrupt Gli2-Sufu interactions, which may contribute to Hck functions in amplifying Shh signaling outputs. Although Sufu is a major Gli1 inhibitor, Hck may further activate Gli1 through phosphorylation as the kinase activity is required for maximum Gli1 activation by Hck. Hck may phosphorylate Gli1 to promote its transcription activities or to affect its interaction with other regulators or co-factors.

Although both Gli1 and Hck are important for Shh target gene activation, they are not required for normal development.<sup>19,37,48,49</sup> During normal development, Gli2 is sufficient for Shh-induced gene activation.<sup>19</sup> Gli1 is required for medulloblastoma formation and is more potent than Gli2 at inducing cell transformation.<sup>50</sup> Thus Gli1 activity is important for the abnormally high transcription output of Shh signaling that are required for tumorigenesis. We speculate that Hck is induced by high levels of Gli1 and that the positive feedback loop with Gli1 operates only in the presence

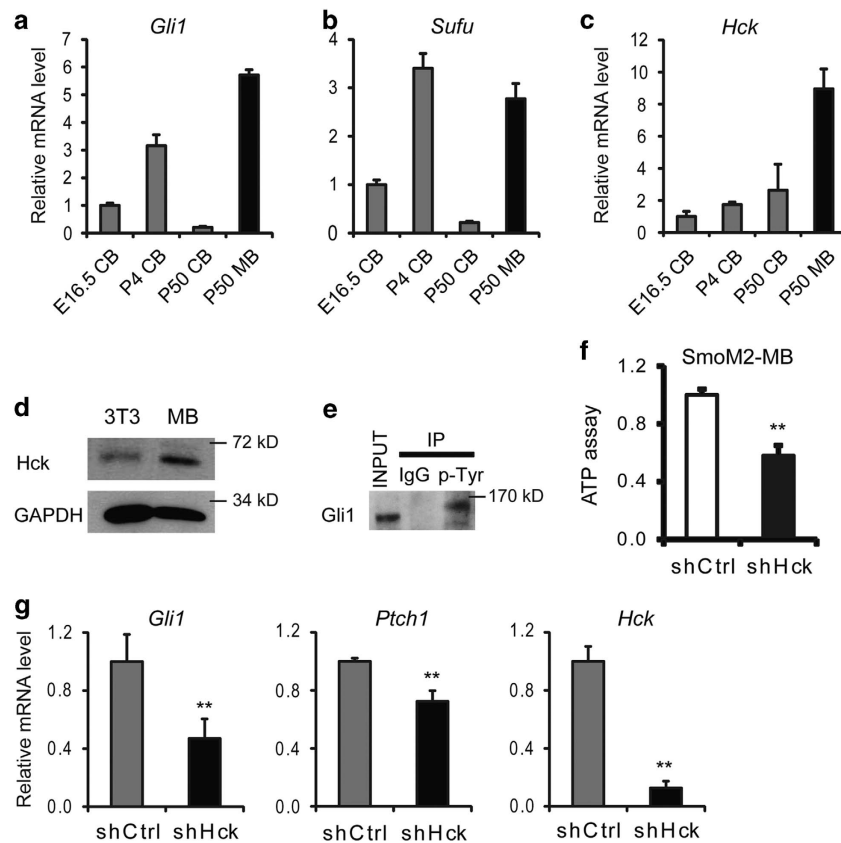


**Figure 6.** Hck is highly expressed in SmoM2-induced medulloblastoma cells and required for its growth. (a–c) Expression levels of (a) *Gli1*, (b) *Sufu* and (c) *Hck* in cerebellum (CB) during different developmental stages and in SmoM2-induced medulloblastoma (MB) are shown. (d) The levels of Hck protein in NIH3T3 cells and in SmoM2 medulloblastoma were determined by western blot. (e) Endogenous Gli1 protein in medulloblastoma is Tyr phosphorylated. SmoM2 medulloblastoma lysates were precipitated with 4G10 antibody against phospho-Tyr and probed by western blot using antibodies against Gli1. (f) Cultured SmoM2 medulloblastoma cells were infected with lentiviruses expressing control (scrambled shRNA) or shHck. The survival rates of Hck-deficient tumor cells relative to the control cultures were measured using an ATP cell viability assay. (g) RT-PCR analyses of the expression levels of *Gli1*, *Ptch1* and *Hck* in cultured SmoM2 medulloblastoma cells with *Hck* RNAi knockdown. Presented are means plus s.d.;  $n = 3$ . Significance was determined by Student's *t*-test; \*\* $P < 0.01$ .

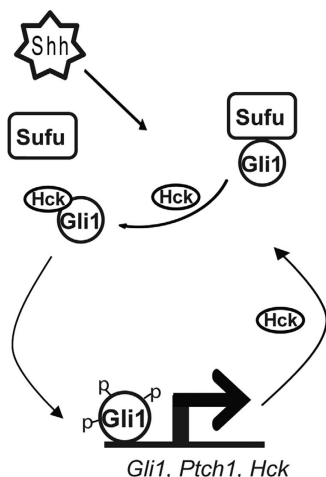


**Figure 7.** A model representing the positive feedback loop formed by Hck and Gli1 in activating Shh target genes. Active Gli1 in response to Shh signaling induces the expression of Shh target genes including *Hck*, which encodes a tyrosine kinase that could enhance Gli1 transcription activator functions. Hck disrupts the interaction between Gli1 and its inhibitor Sufu, possibly through Hck–Gli1 interactions. Hck could phosphorylate Gli1 and the Tyr phosphorylation of Gli1 further enhances the Gli1 activities. Thus the positive feedback loop formed by Hck and Gli1 amplifies Shh signaling outputs.

of highly active Shh signaling such as that observed in medulloblastoma. Our data support this hypothesis: (1) Hck transcriptional activation was much more sensitive to exogenous Gli1 than to Gli2 or Shh stimulation (Figure 1, 500-fold by Gli1 versus 50-fold by Gli2 and 5-fold by Shh). (2) Hck was highly expressed in Shh-type medulloblastoma where Gli1 was highly expressed and tyrosine phosphorylated. Hck levels in normal cerebellum and Shh-independent medulloblastoma were relatively low (Figures 6c, Supplementary Figure S5). (3) High levels of Hck interrupt Gli1–Sufu interactions and activate Gli1-mediated target gene activation. (4) Inhibition of *Hck* expression significantly inhibited Shh target gene expression and medulloblastoma growth (Figures 6f and g). Taken together, our results indicate that increased Hck expression in medulloblastoma induced by abnormally active Shh signaling enhances Gli1 oncogenic activities and contributes to tumor growth. As some of our experiments only examined the *Hck* RNA levels, an investigation of the Hck protein levels in medulloblastoma may further strengthen our conclusions.

As Hck is a novel enhancer for Gli1 oncogenic activities in medulloblastoma, Hck is a potential treatment target. A kinase study in medulloblastoma indicated high levels of Src family kinase (SFK) activities.<sup>51</sup> SFK inhibitors effectively inhibit medulloblastoma cell growth;<sup>52</sup> however, it is not clear whether these medulloblastoma cells are of the Shh subtype and little is known about how other SFKs regulate Shh signaling. Src has been shown to inhibit primary cilia growth<sup>53</sup> and is expressed at low levels in

Shh-type medulloblastoma (Supplementary Figure S5A), and thus may be an inhibitor of Shh signaling and Shh-type medulloblastoma growth. Thus SFKs may have opposing functions in Shh-induced tumors. As Hck may also enhance Gli1 activities with kinase-independent activities, specific inhibitors disrupting the Hck–Gli1 feedback loop would be more effective in inhibiting Shh-type medulloblastoma cancer progression than general kinase inhibitors.

In summary, our study identified the tyrosine kinase Hck as both a target of Gli1 and a regulator of Gli1 activation. The positive feedback loop formed by Gli1 and Hck amplifies Shh signaling output and contributes to medulloblastoma cell growth. Inhibiting Hck activities or disrupting the Hck–Gli1 feedback loop may be effective approaches for the treatment of Shh-type medulloblastoma and possibly other cancers with elevated Shh/Gli1 activities.

## MATERIALS AND METHODS

### Mice

The *SmoM2*<sup>45</sup> and *CAG-CreER*<sup>54</sup> transgenic mice were purchased from Jackson Laboratory. *SmoM2 CAG-CreER* mice develop medulloblastoma spontaneously at a frequency of 40%.<sup>45</sup> The mice were maintained on a mixed genetic background at UT Southwestern Medical Center Animal Facility.

### Cell line, primary CGNP and medulloblastoma cell cultures

NIH3T3 cells (an immortalized MEF cell line), immortalized *Kif3a*<sup>−/−</sup> MEF cells and *Sufu*<sup>−/−</sup> MEF cells were maintained in DMEM (Dulbecco's Modified Eagle's medium) containing 10% fetal bovine serum. The *Kif3a*<sup>−/−</sup> cells were provided by Dr PT Chuang.<sup>25</sup> *Sufu*<sup>−/−</sup> MEFs were kindly provided by Dr R Toftgard.<sup>44</sup> Primary CGNP cultures were derived from dissociated P4 mouse cerebella and cultured in DMEM/F12 media containing 25 mM KCl, N<sub>2</sub> and 10% fetal bovine serum, as previously described.<sup>27</sup> For Shh stimulation, Shh-conditioned medium produced from Shh-CM 293 T cells<sup>55</sup> was added at a 1:20 dilution to MEF and CGNP cultures. NIH3T3 cells were treated with Shh in low-serum media 24 h before harvesting. Primary tumor cells were derived from dissociated *SmoM2* medulloblastoma and cultured in the media containing DMEM/F12, B27, N<sub>2</sub>, EGF and FGF2. The ATP assay for cell viability analysis was carried out as described.<sup>39</sup>

### Luciferase reporter assay

Transient transfection and luciferase assays were done in NIH3T3 cells essentially as described.<sup>56</sup> Co-transfection of the vector pRL-TK Renilla (Promega, Fitchburg, WI, USA) allowed normalization of transfection efficiencies. The normalized data were expressed as multiples of the activity of the 1.7 kb Hck promoter reporter in pGL3basic.

### Plasmid construction, virus preparation and transfection/infection

The shRNA sequence targeting mouse *Hck* (5'-TACCATTGTGTCGCAC TGTA-3') was cloned into the PLKO lentiviral vector. The PLKO construct with a scrambled shRNA sequence was used as a negative control. Lentiviral vector pSin4-EF2-IRES-Puro was used to generate expression constructs for 3 × HA- or GFP-tagged human Gli1/2/3 and Hck. Lentiviruses were prepared according to a previously described procedure.<sup>27</sup> PolyJet (Signagen, Gaithersburg, MD, USA) was used for plasmid transfection of cultured cells. Attached cultured cells were infected at a multiplicity of infection of 5 for 24 h in media with 8 µg/ml polybrene.

### Immunoblotting

For immunoblotting, cells or tissues were lysed in RIPA buffer (50 mM Tris, pH 8, 150 mM NaCl, 0.05% SDS, 0.5% DOC, 1% NP-40), and cell lysates were separated on SDS–PAGE gels. Antibodies used for western blot recognized Hck (#06-833, Millipore, Billerica, MA, USA), HA (HA-7, Sigma-Aldrich, St Louis, MO, USA), anti-phospho-tyrosine (4G10, Millipore), Gli1 (#2643, Cell Signaling, Danvers, MA, USA), GFP (A11122, Life Technologies, Carlsbad, CA, USA) and GAPDH (G9545, Sigma-Aldrich). HRP-conjugated secondary antibodies were purchased from Jackson ImmunoResearch (West Grove, PA, USA). GAPDH was detected as a loading control.

### Mass spectrophotometry analyses of Gli1 Tyr phosphorylation

HA-Gli1 co-expressed with Hck in NIH3T3 cells were immunoprecipitated with anti-HA antibody and separated on SDS–PAGE gels. Coomassie Blue-stained Gli1 band was isolated and subjected for mass spectrophotometry analyses. Proteins from the gel slice were digested, extracted and analyzed by LC/MS/MS (UT Southwestern Medical Center Proteomic Core Facility, Dallas, TX, USA). Peptide identification was performed using the X!Tandem<sup>57</sup> and open MS search algorithm (OMSSA)<sup>58</sup> search engines against the mouse protein database from Uniprot, 23 Gli1 peptides were identified, which covers 26.3% of the Gli1 protein. Phosphorylation sites were localized using ModLS PTM Localization and confirmed by manual interpretation.

### Co-immunoprecipitation experiments

Experiments were performed essentially as described previously.<sup>27</sup> Antibodies were against the HA tag (ab9110, Abcam, Cambridge, UK), Flag-tag (F1802, Sigma), anti-phospho-tyrosine (4G10, Millipore) and GFP (A11122, Life Technologies). Shh-responsive NIH3T3 cells were transiently transfected with plasmids expressing HA- or GFP-tagged proteins using PolyJet (Signagen). Mock transfection was used as the negative control. Cells were collected 24–48 h after transfection and were lysed with co-IP Lysis Buffer (50 mM Tris, pH 8.0, 150 mM NaCl, 1 mM EDTA, 1% Triton X-100, with protease inhibitor freshly added). Cell lysates were snap-frozen in liquid nitrogen and then thawed on ice followed by sonication to facilitate cell lysis. After centrifugation, appropriate antibodies were added to pre-cleared cell lysate and incubated at 4°C overnight. Samples were incubated with protein A beads (GE Healthcare, Dallas, TX, USA) for 1 h; beads were washed with co-IP buffer four times. Precipitated proteins were eluted by boiling in 2 × Sample Buffer before SDS–PAGE and western blot analysis.

### ChIP assay

ChIP experiments were performed as described previously.<sup>27</sup> Dissociated cells were crosslinked with PFA, and DNA was sonicated to fragments (200–1000 bp). Antibody against HA (ab9110, Abcam) was used in the precipitation step. Rabbit IgG was used as a negative control. Precipitated DNA was purified and subjected to real-time PCR.

### Real-time quantitative PCR

RNA from cells or tissues was extracted with TRIzol (Invitrogen, Carlsbad, CA, USA). Complementary DNAs were synthesized by reverse transcription using Iscript (Bio-Rad, Hercules, CA, USA), followed by PCR or quantitative PCR analysis. A Bio-Rad real-time PCR system (C1000 Thermal Cycler) was used for quantitative PCR. Levels of *GAPDH* mRNA were used to normalize input RNA. Graphics shown are representative of experiments performed in triplicate. Sequences of PCR-primers used are listed in Supplementary Table S1.

### Statistical analysis

Data are expressed as means plus s.d. The error bars are standard deviations of three analyses of one representative experiment. Each experiment was repeated at least three times. Statistical analyses were performed using a two-tailed, unpaired Student's *t*-test.

## CONFLICT OF INTEREST

The authors declare no conflict of interest.

## ACKNOWLEDGEMENTS

We thank Qiu Wang for technical support, Drs J Jiang, PT Chuang, R Toftgard for reagents and Drs Xiaofeng Wu and Lawrence Lum for critical discussion and reagents. This work was supported by grants from March of Dimes Foundation (JW), American Cancer Society (JW) and Department of Defense Visionary postdoc fellowship (XS).

## REFERENCES

- Ingham PW, Placzek M. Orchestrating ontogenesis: variations on a theme by sonic hedgehog. *Nat Rev Genet* 2006; **7**: 841–850.
- Ingham PW, McMahon AP. Hedgehog signaling in animal development: paradigms and principles. *Genes Dev* 2001; **15**: 3059–3087.
- Jiang J, Hui C. Hedgehog signaling in development and cancer. *Dev Cell* 2008; **15**: 801–812.
- Altava A, Palma V, Dahmane N. Hedgehog-Gli signalling and the growth of the brain. *Nat Rev Neurosci* 2002; **3**: 24–33.

- 5 Fuccillo M, Joyner AL, Fishell G. Morphogen to mitogen: the multiple roles of hedgehog signalling in vertebrate neural development. *Nat Rev Neurosci* 2006; **7**: 772–783.
- 6 Briscoe J, Thérond PP. The mechanisms of Hedgehog signalling and its roles in development and disease. *Nat Rev Mol Cell Biol* 2013; **14**: 416–429.
- 7 Corrales JD, Rocco GL, Blaess S, Guo Q, Joyner AL. Spatial pattern of sonic hedgehog signalling through Gli genes during cerebellum development. *Development* 2004; **131**: 5581–5590.
- 8 Wang VY, Zoghbi HY. Genetic regulation of cerebellar development. *Nat Rev Neurosci* 2001; **2**: 484–491.
- 9 Dahmane N, Altaba A. Sonic hedgehog regulates the growth and patterning of the cerebellum. *Development* 1999; **126**: 3089–3100.
- 10 Wallace VA. Purkinje-cell-derived Sonic hedgehog regulates granule neuron precursor cell proliferation in the developing mouse cerebellum. *Curr Biol* 1999; **9**: 445–448.
- 11 Jones DT, Jager N, Kool M, Zichner T, Hutter B, Sultan M *et al*. Dissecting the genomic complexity underlying medulloblastoma. *Nature* 2012; **488**: 100–105.
- 12 Northcott PA, Korshunov A, Witt H, Hielscher T, Eberhart CG, Mack S *et al*. Medulloblastoma comprises four distinct molecular variants. *J Clin Oncol* 2011; **29**: 1408–1414.
- 13 Parsons DW, Li M, Zhang X, Jones S, Leary RJ, Lin JC *et al*. The genetic landscape of the childhood cancer medulloblastoma. *Science* 2011; **331**: 435–439.
- 14 Pugh TJ, Weeraratne SD, Archer TC, Pomeranz Krummel DA, Auclair D, Bochicchio J *et al*. Medulloblastoma exome sequencing uncovers subtype-specific somatic mutations. *Nature* 2012; **488**: 106–110.
- 15 Robinson G, Parker M, Kranenburg TA, Lu C, Chen X, Ding L *et al*. Novel mutations target distinct subgroups of medulloblastoma. *Nature* 2012; **488**: 43–48.
- 16 Ingham PW, Taylor AM, Nakano Y. Role of the *Drosophila* patched gene in positional signalling. *Nature* 1991; **353**: 184–187.
- 17 Stone DM, Hynes M, Armanini M, Swanson TA, Gu Q, Johnson RL *et al*. The tumour-suppressor gene patched encodes a candidate receptor for Sonic hedgehog. *Nature* 1996; **384**: 129–134.
- 18 Vaillant C, Monard D. SHH pathway and cerebellar development. *Cerebellum* 2009; **8**: 291–301.
- 19 Bai CB, Auerbach W, Lee JS, Stephen D, Joyner AL. Gli2, but not Gli1, is required for initial Shh signaling and ectopic activation of the Shh pathway. *Development* 2002; **129**: 4753–4761.
- 20 Bai CB, Joyner AL. Gli1 can rescue the *in vivo* function of Gli2. *Development* 2001; **128**: 5161–5172.
- 21 Matisse MP, Joyner AL. Gli genes in development and cancer. *Oncogene* 1999; **18**: 7852–7859.
- 22 Tukachinsky H, Lopez LV, Salic A. A mechanism for vertebrate Hedgehog signaling: recruitment to cilia and dissociation of SuFu-Gli protein complexes. *J Cell Biol* 2010; **191**: 415–428.
- 23 Stecca B, Ruiz IA. Context-dependent regulation of the Gli code in cancer by HEDGEHOG and non-HEDGEHOG signals. *J Mol Cell Biol* 2010; **2**: 84–95.
- 24 Lin C, Yao E, Wang K, Nozawa Y, Shimizu H, Johnson JR *et al*. Regulation of SuFu activity by p66beta and Mycbp provides new insight into vertebrate Hedgehog signaling. *Genes Dev* 2014; **28**: 2547–2563.
- 25 Chen MH, Wilson CW, Li YJ, Law KK, Lu CS, Gacayan R *et al*. Cilium-independent regulation of Gli protein function by SuFu in Hedgehog signaling is evolutionarily conserved. *Genes Dev* 2009; **23**: 1910–1928.
- 26 Hui CC, Angers S. Gli proteins in development and disease. *Annu Rev Cell Dev Biol* 2011; **27**: 513–537.
- 27 Zhan X, Shi X, Zhang Z, Chen Y, Wu JI. Dual role of Brg chromatin remodeling factor in Sonic hedgehog signaling during neural development. *Proc Natl Acad Sci USA* 2011; **108**: 12758–12763.
- 28 Canettieri G, Di ML, Greco A, Coni S, Antonucci L, Infante P *et al*. Histone deacetylase and Cullin3-REN(KCTD11) ubiquitin ligase interplay regulates Hedgehog signalling through Gli acetylation. *Nat Cell Biol* 2010; **12**: 132–142.
- 29 Atwood SX, Li MC, Lee A, Tang JY, Oro AE. Gli activation by atypical protein kinase C  $\iota$ /lambda regulates the growth of basal cell carcinomas. *Nature* 2013; **494**: 484–488.
- 30 Robinson DR, Wu YM, Lin SF. The protein tyrosine kinase family of the human genome. *Oncogene* 2000; **19**: 5548–5557.
- 31 Miller WT. Determinants of substrate recognition in nonreceptor tyrosine kinases. *Acc Chem Res* 2003; **36**: 393–400.
- 32 Ishizawa R, Parsons SJ. c-Src and cooperating partners in human cancer. *Cancer Cell* 2004; **6**: 209–214.
- 33 Parsons SJ, Parsons JT. Src family kinases, key regulators of signal transduction. *Oncogene* 2004; **23**: 7906–7909.
- 34 Rauch J, Volinsky N, Romano D, Kolch W. The secret life of kinases: functions beyond catalysis. *Cell Commun Signal* 2011; **9**: 23–29.
- 35 Paliwal P, Radha V, Swarup G. Regulation of p73 by Hck through kinase-dependent and independent mechanisms. *BMC Mol Biol* 2007; **8**: 45.
- 36 Ziegler SF, Marth JD, Lewis DB, Perlmutter RM. Novel protein-tyrosine kinase gene (hck) preferentially expressed in cells of hematopoietic origin. *Mol Cell Biol* 1987; **7**: 2276–2285.
- 37 Lowell CA, Niwa M, Soriano P, Varmus HE. Deficiency of the Hck and Src tyrosine kinases results in extreme levels of extramedullary hematopoiesis. *Blood* 1996; **87**: 1780–1792.
- 38 Lee EY, Ji H, Ouyang Z, Zhou B, Ma W, Vokes SA *et al*. Hedgehog pathway-regulated gene networks in cerebellum development and tumorigenesis. *Proc Natl Acad Sci USA* 2010; **107**: 9736–9741.
- 39 Shi X, Zhang Z, Zhan X, Cao M, Satoh T, Akira S *et al*. An epigenetic switch induced by Shh signalling regulates gene activation during development and medulloblastoma growth. *Nat Commun* 2014; **5**: 5425.
- 40 Briggs SD, Bryant SS, Jove R, Sanderson SD, Smithgall TE. The Ras GTPase-activating protein (GAP) is an SH3 domain-binding protein and substrate for the Src-related tyrosine kinase, Hck. *J Biol Chem* 1995; **270**: 14718–14724.
- 41 Johnson TM, Williamson NA, Scholz G, Jaworowski A, Wettenhall RE, Dunn AR *et al*. Modulation of the catalytic activity of the Src family tyrosine kinase Hck by autophosphorylation at a novel site in the unique domain. *J Biol Chem* 2000; **275**: 33353–33364.
- 42 Dunaeva M, Michelson P, Kogerman P, Toftgard R. Characterization of the physical interaction of Gli proteins with SUFU proteins. *J Biol Chem* 2003; **278**: 5116–5122.
- 43 Huangfu D, Liu A, Rakeman AS, Murcia NS, Niswander L, Anderson KV. Hedgehog signalling in the mouse requires intracellular transport proteins. *Nature* 2003; **426**: 83–87.
- 44 Svad J, Heby-Henricson K, Persson-Lek M, Rozell B, Lauth M, Bergström A *et al*. Genetic elimination of Suppressor of fused reveals an essential repressor function in the mammalian Hedgehog signaling pathway. *Dev Cell* 2006; **10**: 187–197.
- 45 Mao J, Ligon KL, Rakhlin EY, Thayer SP, Bronson RT, Rowitch D *et al*. A novel somatic mouse model to survey tumorigenic potential applied to the Hedgehog pathway. *Cancer Res* 2006; **66**: 10171–10178.
- 46 Zhang Y, Fu L, Qi X, Zhang Z, Xia Y, Jia J *et al*. Structural insight into the mutual recognition and regulation between Suppressor of Fused and Gli/Ci. *Nat Commun* 2013; **4**: 2608.
- 47 Cherry AL, Finta C, Karlstrom M, Jin Q, Schwend T, Astorga-Wells J *et al*. Structural basis of SUFU-Gli interaction in human Hedgehog signalling regulation. *Acta Crystallogr D Biol Crystallogr* 2013; **69**: 2563–2579.
- 48 Lowell CA, Soriano P, Varmus HE. Functional overlap in the src gene family: inactivation of hck and fgr impairs natural immunity. *Genes Dev* 1994; **8**: 387–398.
- 49 Park HL, Bai C, Platt KA, Matisse MP, Beeghly A, Hui CC *et al*. Mouse Gli1 mutants are viable but have defects in SHH signaling in combination with a Gli2 mutation. *Development* 2000; **127**: 1593–1605.
- 50 Kimura H, Stephen D, Joyner A, Curran T. Gli1 is important for medulloblastoma formation in Ptc1<sup>-/-</sup> mice. *Oncogene* 2005; **24**: 4026–4036.
- 51 Sikkema AH, Diks SH, den Dunnen WF, ter Elst A, Scherpen FJ, Hoving EW *et al*. Kinome profiling in pediatric brain tumors as a new approach for target discovery. *Cancer Res* 2009; **69**: 5987–5995.
- 52 Rossi A, Schenone S, Angelucci A, Cozzi M, Caracciolo V, Pentimalli F *et al*. New pyrazolo-[3,4-d]-pyrimidine derivative Src kinase inhibitors lead to cell cycle arrest and tumor growth reduction of human medulloblastoma cells. *FASEB J* 2010; **24**: 2881–2892.
- 53 Bershteyn M, Atwood SX, Woo WM, Li M, Oro AE. MIM and cortactin antagonism regulates ciliogenesis and hedgehog signaling. *Dev Cell* 2010; **19**: 270–283.
- 54 Hayashi S, McMahon AP. Efficient recombination in diverse tissues by a tamoxifen-inducible form of Cre: a tool for temporally regulated gene activation/inactivation in the mouse. *Dev Biol* 2002; **244**: 305–318.
- 55 Chen JK, Taipale J, Young KE, Maiti T, Beachy PA. Small molecule modulation of Smoothened activity. *Proc Natl Acad Sci USA* 2002; **99**: 14071–14076.
- 56 Shi X, Metges CC, Seyfert HM. Interaction of C/EBP-beta and NF-Y factors constrains activity levels of the nutritionally controlled promoter IA expressing the acetyl-CoA carboxylase-alpha gene in cattle. *BMC Mol Biol* 2012; **13**: 21.
- 57 Craig R, Beavis RC. TANDEM: matching proteins with tandem mass spectra. *Bioinformatics* 2004; **20**: 1466–1467.
- 58 Geer LY, Markey SP, Kowalak JA, Wagner L, Xu M, Maynard DM *et al*. Open mass spectrometry search algorithm. *J Proteome Res* 2004; **3**: 958–964.



Oncogenesis is an open-access journal published by Nature Publishing Group. This work is licensed under a Creative Commons Attribution 4.0 International License. The images or other third party material in this article are included in the article's Creative Commons license, unless indicated otherwise in the credit line; if the material is not included under the Creative Commons license, users will need to obtain permission from the license holder to reproduce the material. To view a copy of this license, visit <http://creativecommons.org/licenses/by/4.0/>

Supplementary Information accompanies this paper on the Oncogenesis website (<http://www.nature.com/oncsis>).



**Autism-Associated Chromatin Regulator Brg1/SmadA4 is Required  
for Synapse Development and MEF2-mediated Synapse Remodeling**

**AUTHORS:**

Zilai Zhang<sup>1#</sup>, Mou Cao<sup>1#</sup>, Chia-Wei Chang<sup>2</sup>, Cindy Wang<sup>1</sup>, Xuanming Shi<sup>1</sup>, Xiaoming Zhan<sup>1,3</sup>,  
Shari G. Birnbaum<sup>4</sup>, Ilya Bezprozvanny<sup>1</sup>, Kimberly Huber<sup>2</sup>, Jiang I. Wu<sup>1\*</sup>

**AFFILIATIONS:**

<sup>1</sup>Department of Physiology,

<sup>2</sup>Department of Neuroscience,

<sup>3</sup>Center for the Genetics of Host Defense,

<sup>4</sup>Department of Psychiatry,

University of Texas Southwestern Medical Center, Dallas, TX 75390, USA

# These authors contributed equally.

**CORRESPONDENCE:**

Jiang Wu

[jiang9.wu@utsouthwestern.edu](mailto:jiang9.wu@utsouthwestern.edu)

Department of Physiology and Developmental Biology

UT Southwestern Medical Center

5323 Harry Hines Blvd.

Dallas TX 75390-9133

Phone: 214-648-1824

Fax: 214-648-1960

**RUNNING TITLE:** Brg1 required for synapse development

**Conflict of interest:** The authors declare no conflict of interest.

**ABSTRACT**

Synapse development requires normal neuronal activities and the precise expression of synapse-related genes. Dysregulation of synaptic genes results in neurological diseases such as autism spectrum disorders (ASD). Mutations in genes encoding chromatin remodeling factor Brg1/SmarcA4 and its associated proteins are the genetic causes of several developmental diseases with neurological defects and autistic symptoms. Recent large-scale genomic studies predicted *Brg1/SmarcA4* as one of the key nodes of the ASD gene network. We report that *Brg1* deletion in early postnatal hippocampal neurons led to reduced dendritic spine density and maturation and impaired synapse activities. In developing mice, neuronal *Brg1* deletion caused severe neurological defects. Gene expression analyses indicated that Brg1 regulates a significant number of genes known to be involved in synapse function and implicated in ASD. We found that Brg1 is required for dendritic spine/synapse elimination mediated by the ASD-associated transcription factor MEF2 and that Brg1 regulates the activity-induced expression of a specific subset of genes that overlap significantly with the targets of MEF2. Our analyses showed that Brg1 interacts with MEF2 and that MEF2 is required for Brg1 recruitment to target genes in response to neuron activation. Thus, Brg1 plays important roles both in synapse development/maturation and in MEF2-mediated synapse remodeling. Our study reveals specific functions of the epigenetic regulator Brg1 in synapse development and provides insights into its role in neurological diseases such as ASD.

**KEYWORDS:** Brg1/SmarcA4, chromatin remodeling, autism spectrum disorders, synapse development, synapse elimination, MEF2

## INTRODUCTION

Synapses formed between axons and dendrites connect neurons and generate neural circuits that control brain functions (1). The dysregulation of synapse formation, maturation, or plasticity causes many neurodevelopmental diseases such as autism (2). Autism spectrum disorders (ASDs) are complex diseases characterized by a range of behavior abnormalities and regulated by genetic and epigenetic factors (3-5). In ASDs with various genetic or environmental causes, synaptic dysfunction is a central defect.

Many autism risk genes encode transcription factors and epigenetic regulators, which likely function to regulate the expression of synaptic genes (4, 6, 7). A gene network analysis predicted the core subunit of a SWI/SNF-like BAF ATP-dependent chromatin remodeling complex, Brg1/Smrca4, as one of the key nodes in autism pathogenesis (7). BAF complexes containing the ATPase Brg1 or Brm use energy derived from ATP hydrolysis to modulate chromatin structures and regulate transcription (8-10). Mutations in several BAF subunits are the genetic causes of Coffin-Siris syndrome and Nicolaides-Baraitser syndrome with autistic symptoms such as intellectual disability and delayed speech (11-15). In addition, *de novo* functional mutations of genes encoding several BAF subunits are identified repeatedly in autism patients (7, 16-18). Mutations in a gene encoding BAF-associated protein ADNP have been identified in 1.3% of autism patients, the most frequent of all autism risk-associated mutations identified so far (18). These data suggest that BAF complexes function in normal neural development and mutations cause autistic disorders. Previously we identified a neuron-specific BAF complex (nBAF) that regulates neuronal gene expression and is required for neural development (19-21). The BAF53b subunit of nBAF complexes is required for activity-dependent dendrite growth and learning and memory (19, 22). However, the functions of nBAF complexes in synapse development and in ASD remain unknown.

Neuronal activity regulates the expression of many ASD-associated genes and is critical in synapse maturation and plasticity (23, 24). Neuronal activity, which triggers  $\text{Ca}^{2+}$  influx, initiates multiple signaling pathways that transduce the signals into the nucleus to affect gene transcription. MEF2 family activity-responsive transcription factors are known to regulate ASD-associated genes important for neural development and synaptogenesis (25-27). Deletion of the key family member *MEF2C* in mouse brains increases synapse numbers and dendritic spines in

90 both cortical and hippocampal neurons, which may account for the learning and memory defects  
91 and autistic phenotypes observed (25, 28). Conversely, expression of a MEF2-VP16 super-  
92 active protein causes synapse elimination (25, 29). At the molecular level, MEF2 interacts with  
93 several transcription co-factors, and  $\text{Ca}^{2+}$  signaling-induced exchange from the co-repressor  
94 complex to co-activator complex is important for MEF2 transcription activities (30, 31). However,  
95 it is unclear how these cofactors coordinate with MEF2 to activate gene expression in response  
96 to neuronal activities.

97  
98 In this report, we specifically deleted *Brg1* in developing neurons and revealed essential  
99 functions of Brg1 in synapse formation, maturation, and remodeling. Brg1 specifically regulates  
100 a significant number of genes encoding synaptic proteins and proteins implicated in ASD. We  
101 found that Brg1 is required for dendritic spine/synapse elimination mediated by MEF2C and that  
102 Brg1 regulates the activity-induced expression of a number of MEF2 target genes. Our analysis  
103 showed that MEF2C is required for Brg1 recruitment to MEF2 targets upon neuronal activation.  
104 Thus, Brg1 regulates synapse formation, maturation and MEF2-mediated synapse remodeling.  
105 Our study revealed the specific mechanisms through which the epigenetic factor Brg1 regulates  
106 synapse development and provides insights into its role in neurological diseases.

107

## 108 MATERIALS AND METHODS

### 109 Mice

110 *Brg1<sup>F/F</sup>* mice (32), *Syn1-Cre* mice (33) and *MEF2C<sup>F/F</sup>* mice (34) were kindly provided by Drs.  
111 Pierre Chambon (IGBMC, France), Luis Parada (UTSW), and Eric Olson (UTSW), respectively.  
112 *BAF53b-Cre* mice were generated by transgenic injection of a BAC construct containing a *Cre*  
113 gene under the control of the neuron-specific *BAF53b* promoter and regulatory elements (35).  
114 These mice are maintained on a mixed genetic background at UT Southwestern Medical Center  
115 Animal Facility. All procedures were performed in accordance with the IACUC-approved  
116 protocols. In all animal experiments, both males and females were used and there is no  
117 significant difference found between genders.

### 119 Plasmid and constructs

120 The construct for expression of Cre is PMC-CreN (36). The MEF2 reporter construct MRE-Luc  
121 contains three MRE sequences upstream of the luciferase reporter. The MEF2C, MEF2-VP16,  
122 and MEF2Δ-VP16 expression constructs in the pCDNA3 vector and the GFP construct  
123 containing an expressing cassette for both GFP and myristoylated GFP were described  
124 previously (29) and were provided by Dr. Chris Cowan (Harvard). pSin-Brg1 (37) was used for  
125 expression of Brg1 in cultured cells.

### 127 Behavior tests

128 All experiments in this study were performed in the Behavior Core Facility and approved by the  
129 IACUC at UT Southwestern Medical Center. Mice were housed with food and water available *ad*  
130 *libitum* with a 12-h light/dark cycle, and all behavior testing occurring during the light cycle. For  
131 the Open Field Activity test, mice were placed in the periphery of a novel open field environment  
132 (44 cm x 44 cm, walls 30-cm high) in a dimly lit room and allowed to explore for 15 min. The  
133 animals were monitored from above by a video camera connected to a computer running video  
134 tracking software (Ethovision 3.0, Noldus) to determine the time, distance moved, and number  
135 of entries into two areas: the periphery (5 cm from the walls) and the center (14 cm x 14 cm).  
136 The open field arenas were wiped and allowed to dry between mice.

### 138 Immunofluorescent staining

139 Immunostaining experiments were performed on paraffin sections (7  $\mu$ m) or vibratome thick  
140 sections (50  $\mu$ m) of brain tissues and on cultured hippocampal slices and neurons cultured on  
141 cover glasses. Antibodies used were against Brg1 (G7 or H88, Santa Cruz Biotechnology),  
142 NeuN (Abcam), GFP (Molecular Probes), and HuC/D (Molecular Probes). The images were  
143 visualized using an Olympus BX50 microscope.

144

145 **Dendritic spine analyses of dentate gyrus granule neurons with lucifer yellow injection**

146 *Brg1<sup>F/F</sup>* or *Syn1-Cre Brg1<sup>F/F</sup>* mice at P21 were intracardially perfused with 1.5%  
147 paraformaldehyde (PFA) solution, and brains were post-fixed in 1.5% PFA solutions for 6 h and  
148 then sectioned into 300- $\mu$ m thick slices. Lucifer yellow injection into single DG neurons was  
149 performed with a microelectrode amplifier (Multiclamp 700B, Molecular Devices). Neurons in the  
150 DG granule cell layer were selected visually under the microscope and patched with the  
151 electrodes filled with lucifer yellow solution (L-12926, Invitrogen). Secondary dendrites (50-200  
152  $\mu$ m from the cell body) were imaged using a Zeiss LSM780 two-photon microscope (40x water  
153 immersion lens). Spine density was measured with the NeuronStudio software package with  
154 default settings (38). Z-stack confocal images of dendrite segments were reconstructed and  
155 analyzed in Neuronstudio for dendritic spine identification and classification as mushroom-,  
156 stubby-, or thin-shaped spines. In classification of spine shapes we used the following cutoff  
157 values: aspect ratio for thin spines, 2.5; head to neck ratio, 1.3; and head diameter, 0.45  $\mu$ m.  
158 Two segments (50-100  $\mu$ m) per neuron (n=16-22 neurons in each condition) were chosen for  
159 quantitative analysis. Dendritic spine volume was further analyzed with the Imaris software (39).

160

161 **Hippocampal slice culture, biolistic transfection, and dendritic spine analyses**

162 Organotypic hippocampal slice cultures were prepared from P6 *Brg1<sup>F/F</sup>* mice (29). Hippocampi  
163 were dissected and sliced to 300  $\mu$ m with a tissue slicer. Hippocampal slices were cultured on a  
164 membrane at the interface between the medium and the air. The culture media include MEM  
165 with horse serum, L-glutamine, CaCl<sub>2</sub>, MgSO<sub>4</sub>, dextrose, NaHCO<sub>3</sub>, HEPES (pH 7.2), and insulin.  
166 Gold bullet preparation and biolistic DNA transfection to 1 div hippocampal slices was  
167 performed with the Helios Gene Gun system (Bio-Rad) according to the manufacturer's  
168 protocols. Five days after transfection, dendritic spines were imaged and analyzed as described  
169 above.

170

171 **Electrophysiological measurement of synapse activities**

172 Organotypic hippocampal slice cultures were prepared from P6 wild-type or *Brg1<sup>F/F</sup>* mice.  
173 Cultures were biolistically transfected with plasmids for expression of GFP and Cre or control  
174 plasmids at 3 div. Ten days later, simultaneous whole-cell recordings were obtained from CA1  
175 pyramidal neurons in slice cultures visualized using IR-DIC and GFP fluorescence to identify  
176 transfected and non-transfected neurons. Recordings were made at 32 °C in a submersion  
177 chamber perfused with artificial cerebrospinal fluid (ACSF) containing 119 mM NaCl, 2.5 mM  
178 KCl, 26 mM NaHCO<sub>3</sub>, 1 mM NaH<sub>2</sub>PO<sub>4</sub>, 11 mM D-glucose, 3 mM CaCl<sub>2</sub>, 2 mM MgCl<sub>2</sub>, 0.1 mM  
179 picrotoxin, 0.002 mM 2-chloro-adenosine, 0.1% DMSO at pH 7.28 at 305 mOsm and saturated  
180 with 95% O<sub>2</sub>/5% CO<sub>2</sub>. Neurons were voltage clamped at -60 mV through whole cell recording  
181 pipettes (~4-6 MΩ) filled with an intracellular solution containing 0.2 mM EGTA, 130 mM K-  
182 gluconate, 6 mM KCl, 3 mM NaCl, 10 mM HEPES, 2 mM QX-314, 4 mM ATP-Mg, 0.4 mM GTP-  
183 Na, 14 mM phosphocreatine-Tris, pH 7.2, adjusted using KOH; 285 mOsm.

184  
185 For mEPSC measurements, the ACSF was supplemented with 1 μM TTX. Series and input  
186 resistance were measured in voltage clamp with a 400-ms, 10-mV step from a -60 mV holding  
187 potential (filtered at 30 kHz, sampled at 50 kHz). Cells were only used for analysis if the starting  
188 series resistance was less than 30 MΩ and was stable throughout the experiment. Input  
189 resistance ranged from 50-900 MΩ. Data were not corrected for junction potential. No significant  
190 difference was observed between transfected and untransfected neurons in resting membrane  
191 potential, indicating that overall neuronal health was unaffected by expression of Cre. Synaptic  
192 currents were filtered at 3 kHz, acquired and digitized at 10 kHz using custom software  
193 (Labview; National Instruments). mEPSCs were filtered at 1 kHz and detected off-line using an  
194 automatic detection program (MiniAnalysis; Synaptosoft Inc.) with a detection threshold set at a  
195 value greater than at least 5 fold of the root mean square noise levels, followed by a subsequent  
196 round of visual confirmation. Significance of differences between transfected and untransfected  
197 neurons was determined using a paired t-test.

198

199 **Cortical and hippocampal neuron culture and transfection**

200 E18.5 hippocampal and E16.5-E18.5 cortical cells were cultured as previously described (Wu et  
201 al., 2007). Dissociated cells were plated on poly-L-ornithine- and fibronectin-coated coverslips.  
202 Culture media contained DMEM/F12 with putrescine, 2-mercaptoethanol, transferrin, insulin,

203 selenium, progesterone, MEM vitamin additive, and 5% FBS. At 7 div, hippocampal cultures  
204 were transfected with GFP and MEF2 expression constructs using Lipofectamine 2000.  
205 Cultures were fixed and imaged on 14 div for dendritic spine analyses as described above.  
206 Cortical cultures were transfected with reporter and MEF2 constructs on 5 div and analyzed at 6  
207 div. For depolarization, 50 mM KCl was added to the cultures for 1 to 6 h as described (25).  
208 Luciferase reporter assays were performed using the Dual-Luciferase Assay kit (Promega). The  
209 mating to produce *BAF53b-Cre Brg1<sup>F/F</sup>* mutant embryos for primary neuron cultures was  
210 between *BAF53b-Cre Brg1<sup>F/+</sup>* and *Brg1<sup>F/F</sup>*. Neurons from *Brg1<sup>F/+</sup>*, *Brg1<sup>F/F</sup>*, or *BAF53b-Cre*  
211 *Brg1<sup>F/+</sup>* heterozygous littermates displayed no significant differences from each other in all  
212 experiments and were used as controls.

213

#### 214 **RT-PCR and q-PCR**

215 RNA from cells or ground tissues was extracted with TRIZOL (Invitrogen). cDNAs were  
216 synthesized by reverse transcription using Iscript (Bio-Rad), followed by PCR or quantitative  
217 PCR analysis. A Bio-Rad real-time PCR system (C1000 Thermal Cycler) was used for  
218 quantitative PCR. Levels of *GAPDH* mRNA were used to normalize input RNA. Graphics shown  
219 are representative of experiments performed in triplicate. The experiments were repeated at  
220 least three times. Standard errors were calculated according to a previously described method  
221 (37). The sequences of all the primers are listed in Table S3.

222

#### 223 **RNA-seq and data analyses**

224 DG of P13 or P21 *Brg1<sup>F/F</sup>* and *Syn1-Cre Brg1<sup>F/F</sup>* mice were used for RNA-seq analyses. One  
225 pair of P13 and P21 control and mutant samples were used; each sample was pooled from two  
226 mice. In addition, cultured *BAF53b-Cre Brg1<sup>F/F</sup>* and control cortical neurons with or without KCl  
227 stimulation (each sample was pooled from three mice) were subjected to RNA-seq analyses.  
228 Total RNAs were extracted, and RNA-seq libraries prepared using the Illumina RNA-Seq  
229 Preparation Kit were sequenced on a HiSeq 2500 sequencer at UT Southwestern Sequencing  
230 Core Facility. RNA-seq reads were mapped using TopHat with default settings  
231 (<http://tophat.cbcb.umd.edu>). The mapped reads with the Phred quality score < 20 were filtered  
232 out, whereas the duplicates were marked but not removed using SAMTOOLS (40) and PICARD  
233 (<http://picard.sourceforge.net>). Transcript assembly and transcript abundance quantification  
234 were carried out using CUFFLINKS, and then differential expression analysis between control



235 and *Brg1* mutants was performed using CUFFDIFF (41). The differentially expressed genes with  
236 fold change larger than 1.5 and  $p < 0.05$  were selected as *Brg1*-regulated genes. Gene ontology  
237 analysis was performed using DAVID (<http://david.abcc.ncifcrf.gov/>). Fisher's exact test was  
238 used to determine the significance of overlapping datasets.

239

#### 240 **ChIP experiments**

241 ChIP experiments were performed as described previously (37, 42). Dounced tissue or  
242 dissociated cells were crosslinked with PFA and sonicated to fragments (200-500 bp).  
243 Antibodies used were against *Brg1*/*Brm* (J1) (43) or rabbit IgG control. J1 antibody has been  
244 used previously for *Brg1* ChIP-seq analyses (44, 45). Precipitated DNA was purified and  
245 subjected to real-time PCR. Percentage of input or fold of enrichment over IgG ChIP was  
246 measured.

247

#### 248 **Immunoprecipitation and western blot**

249 Cultured cortical neurons were treated with or without KCl at 7 div for 1 hour. Cells were  
250 harvested and lysed with Co-IP buffer (50 mM Tris, pH 8.0, 150 mM NaCl, 1 mM EDTA, 1%  
251 Triton X-100, with protease inhibitor freshly added). After centrifugation, rabbit polyclonal  
252 antibodies against *Brg1*/*Brm* (J1) were added to pre-cleared cell extracts, and samples were  
253 incubated at 4 °C overnight. Samples were incubated with protein A beads (GE Healthcare) for  
254 1 h; beads were washed with Co-IP buffer four times. Precipitated proteins were eluted by  
255 boiling in 2X Sample Buffer (Bio-Rad) before SDS-PAGE and western blot analysis. For  
256 immunoblotting, cell lysates or immunoprecipitation were separated on SDS-PAGE gels.  
257 Antibodies used were against *Brg1* (G7, Santa Cruz Biotechnology), MEF2C (Cell Signaling)  
258 and MEF2D (BD Biosciences). HRP-conjugated secondary antibodies were purchased from  
259 Jackson Immunology.

260

## 261 RESULTS

262

### 263 **Deleting *Brg1* in hippocampal neurons impairs synapse formation and maturation.**

264 The association of *Brg1* with ASD prompted us to evaluate synapse development in *Brg1*  
265 mutant neurons. To determine the cell-autonomous functions of *Brg1* in synapse formation, we  
266 deleted *Brg1* in individual hippocampal neurons and determined the effects on excitatory  
267 synapse activities. Using a Gene Gun biolistic particle delivery system, we introduced plasmids  
268 expressing Cre or control empty vector into cultured postnatal day 6 (P6) *Brg1<sup>F/F</sup>* (32)  
269 hippocampal slices. The co-transfection efficiency using this method is more than 95% and we  
270 observed Cre-mediated *Brg1* deletion in GFP<sup>+</sup> neurons (Figure 1A). Since very few neurons can  
271 be transfected with this method, any effects of *Brg1* deletion on postsynaptic development  
272 should be cell-autonomous. We focused on CA1 pyramidal neurons as their stereotypical  
273 position and morphology make them easily identifiable in the hippocampal cultures. Ten days  
274 after transfection, miniature excitatory postsynaptic currents (mEPSCs) were measured from  
275 simultaneous recordings of transfected GFP<sup>+</sup> and neighboring untransfected CA1 neurons.  
276 *Brg1*-deleted neurons displayed decreased mEPSC frequency relative to untransfected  
277 neurons, whereas mEPSC amplitudes were unchanged (Figure 1B, 1C). The reduction of  
278 mEPSC frequency was not caused by Cre expression, but by *Brg1* deletion, because  
279 transfection of CA1 neurons from wild-type hippocampal slice cultures with the vector for  
280 expression of Cre had no effect on mEPSCs (Figure 1D). mEPSC frequency is correlated with  
281 synapse number (Pfeiffer et al., 2010), whereas mEPSC amplitude represents the strength of  
282 individual synapses. These data indicate that *Brg1* is required for the development of functional  
283 excitatory synapse.

284

285 Most excitatory synapses are built on dendritic spines that contain the postsynaptic signaling  
286 machinery and receive synaptic inputs. Spine densities and morphologies faithfully reflect  
287 synapse numbers and levels of maturations (46-48). Mushroom-shaped and stubby spines with  
288 larger volume usually indicate mature synapses, whereas long and thin spines with small  
289 volume indicate no or immature synapses. To assess the role of *Brg1* in development of  
290 dendritic spine, we measured spine densities, volumes and shapes from CA1 neurons of  
291 cultured P6 *Brg1<sup>F/F</sup>* hippocampal slices biolistically transfected with constructs for expression of  
292 Cre or control and membrane-targeted GFP. Six days after transfection, two photon confocal

293 microscopy images of GFP<sup>+</sup> dendritic spines were taken and analyzed with Neuronstudio  
294 software for quantification and spine classification (38, 49). We observed a significant decrease  
295 of dendritic spine densities in *Brg1*<sup>F/F</sup> CA1 neurons expressing Cre relative to neurons  
296 transfected with empty vectors (Figure 1E, 1F), indicating impaired synapse formation in the  
297 absence of Brg1. Analyses of the spine shapes showed a significant reduction in mushroom-  
298 shaped spines and an increase in thin spines in *Brg1*-deleted neurons compared to control  
299 neurons (Figure 1G). Consistently, there was a significant decrease in spine volumes in *Brg1*-  
300 deleted neurons compared to control neurons (Figure 1H). These data demonstrate that Brg1 is  
301 required for dendritic spine/synapse formation and maturation in postsynaptic neurons and  
302 indicate that Brg1 promotes synapse formation and maturation in a cell-autonomous manner.

303

#### 304 **Brg1 deletion in neurons led to neurological defects in mouse.**

305 To determine the function of Brg1 in synapse development *in vivo*, we crossed *Brg1* conditional  
306 knockout mice (32) with several neuron-specific Cre transgenes. A widely used *Camk2a-Cre*  
307 line (50) mediated Brg1 deletion in forebrain neurons led to hydrocephalus, mainly due to non-  
308 cell autonomous effects (51). A newly developed *BAF53b-Cre* line (35) deleted Brg1 in all  
309 developing neurons, which caused lethality at birth due to respiratory defects (data not shown).  
310 Therefore these mice cannot be used to study postnatal synaptogenesis. *Synapsin1-Cre* (*Syn1*-  
311 *Cre*) transgene (33) is expressed exclusively in neurons beginning in the late embryonic stage,  
312 but its expression pattern is mosaic in most brain areas. *Syn1-Cre Brg1*<sup>F/F</sup> mice survive, which  
313 enable us to study Brg1 function in synapse development *in vivo*. In hippocampus, *Syn1-Cre* is  
314 not expressed in the CA1 region, but has a strong expression in the dentate gyrus (DG) and  
315 CA3 regions (Figure 2A and (33)). In *Syn1-Cre Brg1*<sup>F/F</sup> mice, *Brg1* deletion from the NeuN<sup>+</sup> DG  
316 granule neurons was detected at P7; at P14 and P21, *Brg1* deletion was clearly observed in  
317 neurons in the DG and CA3 regions (Figure 2A). Control and Brg1-deleted dentate gyrus  
318 showed similar morphology (Figure 2A). The gross examination of *Syn1-Cre Brg1*<sup>F/F</sup> brain at  
319 different ages did not reveal obvious structural defects (Figure 2B). The brain weights of these  
320 mice were also normal (Figure 2C).

321

322 Although born with normal weight, *Syn1-Cre Brg1*<sup>F/F</sup> mutant mice were smaller during  
323 development than control mice (Figure 2D). *Brg1*-mutants displayed locomotor and behavior  
324 abnormalities beginning in the early postnatal stage. They exhibited significantly increased

hindlimb clasp frequency compared to *Brg1*<sup>F/F</sup> controls that was more severe prior to weaning than after (Figure 2E). At young age, *Brg1*-mutant pups were overactive and unbalanced. At P7, in the righting reflex test none of the *Brg1*-mutant pups righted after one minute, whereas all control mice righted within 30 seconds (Figure 2F and data not shown). These severe behavioral abnormalities at young age suggest that *Brg1* deletion affects neuronal and synapse development. Adult *Syn1-Cre Brg1*<sup>F/F</sup> mice had significantly increased hindlimb clasp (Figure 2E) but had largely recovered from locomotor abnormalities and displayed normal activity/anxiety levels in the open field activity test in the first 5 minutes (data not shown) or in the full 15 minutes (Figure 2G). During a foot shock test, we observed that adult *Brg1*-mutant mice had significantly increased sensitivity to the foot shock stimulation as indicated by the significantly decreased jump threshold compared to that of control *Brg1*<sup>F/F</sup> mice (Figure 2H). These neurological defects indicate that *Brg1* deletion in developing neurons impairs neuronal development and function.

### Neuronal *Brg1* deletion impairs synapse maturation *in vivo*.

To evaluate the dendritic spine morphology in *Brg1*-mutant neurons *in vivo*, we injected a fluorescent dye, lucifer yellow, into individual DG granule neurons in fixed hippocampal slices from P21 *Brg1*<sup>F/F</sup> control and *Syn1-Cre Brg1*<sup>F/F</sup> mice to visualize the dendritic spines. We chose P21 DG because in *Syn1-Cre Brg1*<sup>F/F</sup> hippocampus, *Brg1* was not deleted in CA1 neurons but was completely deleted in DG granule neurons at this development stage (Figure 2A). Analyses of two photon confocal microscopy images of dendritic spines showed that although *Brg1*-mutant granule neurons displayed similar spine densities (Figure 3A, 3B), there was a significant increase of thin spines in *Brg1*-mutant neurons (Figure 3C), which indicates impaired synapse maturation. Similar to the individual *Brg1*-deleted CA1 neurons, these *Brg1*-deleted DG granule neurons also displayed significantly reduced dendritic spine volumes (Figure 3D). Since spine volume correlates well with synapse maturation and activities, the synapse defects in both *Brg1* deleted CA1 pyramidal neurons in hippocampal slice cultures and in DG granule neurons *in vivo* indicate that *Brg1* is likely required for synapse development and maturation in general.

### *Brg1* regulates synaptic genes in developing hippocampus.

The identification of many transcription factors and epigenetic regulators as autism risk genes suggest that the regulation of synaptic gene network is a key step to control synaptogenesis in

357 normal development and in diseases. To determine how Brg1 regulates synapse development,  
358 we performed RNA-seq to compare the gene expression profiles in control and *Syn1-Cre*  
359 *Brg1<sup>F/F</sup>* neurons (Figure 4, Table S1). We analyzed P13 and P21 DG because Brg1 is  
360 completely deleted in the *Syn1-Cre Brg1<sup>F/F</sup>* granule neurons at these stages (Figure 2A). From  
361 P13 DG, we identified 1383 differentially expressed genes (DEGs) with 868 downregulated and  
362 515 upregulated in *Brg1* mutants compared to controls (fold change >1.5,  $p < 0.05$ ). From P21  
363 DG, we identified 1623 DEGs: 1187 were upregulated and 446 were downregulated in *Brg1*-  
364 deleted DG compared to controls. The intersection of P13 and P21 DEGs identified 120  
365 commonly downregulated and 148 commonly upregulated genes, which are high confidence  
366 Brg1 regulated genes (Figure 4A). These common Brg1-regulated genes include many genes  
367 known to encode proteins that function in neuron-specific features such as neuron projections  
368 and channels and in neurotransmitter release and synaptogenesis (Figure 4B). Brg1 likely  
369 directly activates or represses a significant number of these genes since the ChIP-qPCR  
370 experiments indicate that Brg1 occupancy was enriched in the regulatory regions of these  
371 neuronal genes in P13 and P21 DG compared to IgG controls and a negative Brg1 binding  
372 region (Figure 4C). Thus, Brg1 may coordinate the expression of a transcription program that is  
373 important for synapse formation and maturation.

374  
375 Gene ontology analysis of the Brg1-regulated genes in both P13 and P21 DG revealed that the  
376 most enriched group of genes encode extracellular matrix-associated proteins ( $p = 5.9 \times 10^{-8}$ )  
377 (Figure 4D). High enrichment was also observed in genes encoding growth factor binding  
378 proteins, cell adhesion proteins, cytoskeleton regulators, plasma membrane proteins, and  
379 calcium signaling pathway components (Figure 4D), which are all closely related to synapse  
380 development. The enrichment of the target genes in these synapse-associated pathways  
381 indicate that neuronal Brg1 and nBAF complexes specifically regulate genes involved in  
382 synapse formation, maturation, and plasticity. To further understand the molecular functions of  
383 Brg1 in synaptic gene regulation, we compared the Brg1-regulated genes in developing DG with  
384 known synaptic genes (52) and with human genes linked to autism as shown in the SFARI  
385 Gene Database ([www.sfari.org](http://www.sfari.org)). P13 DEG dataset was also used for comparison, as this is a  
386 stage when synaptic and neurological defects are apparent in *Brg1*-mutant mice. There are  
387 significant overlaps between Brg1-regulated genes and synaptic and autism genes (Figure 4E).

388 Thus Brg1 specifically regulates synaptic genes in developing neurons; the abnormal  
389 expression of these genes may contribute to autism pathogenesis.

390

391 ***BAF53b-Cre-mediated pan-neuronal Brg1 deletion in cultures.***

392 Many synaptic genes are regulated by neuronal activities that help convert transient stimuli into  
393 long-term changes in neuronal morphology and synapse activities. Neuronal BAF complexes  
394 regulate activity-dependent dendrite growth, suggesting a signaling pathway from  $\text{Ca}^{2+}$  influx to  
395 chromatin regulation (19). Brg1 was found to repress the basal expression of the *c-fos* gene  
396 (57). However, activity-induced nBAF target genes are not known, and it is not clear how nBAF  
397 complexes regulate gene activation in response to neuronal activities. To understand the  
398 function of Brg1 and nBAF complexes in activity-dependent gene regulation, we deleted *Brg1* in  
399 cultured neurons. The mosaic expression pattern of *Syn1-Cre* in the cortex and hippocampus  
400 prevented us to use this line for neuronal culture studies. Therefore, we took advantage of the  
401 newly generated pan-neuron-specific *BAF53b-Cre* transgene (35) to delete *Brg1* in all neurons  
402 in the culture (Figure 5). The BAF53b subunit of the nBAF complexes is expressed exclusively  
403 in neurons and in all neurons examined (19). *BAF53b-Cre* BAC transgene activities were  
404 detected in all neurons by E18.5. *BAF53b-Cre Brg1<sup>F/F</sup>* mice die at birth due to respiratory failure.  
405 However, Brg1 proteins were not completely deleted from cortical and hippocampal neurons at  
406 birth (Figure 5, 1div). We cultured mixed cortical/hippocampal neurons from E18.5 control or  
407 *BAF53b-Cre Brg1<sup>F/F</sup>* mice. Using a *Rosa-YFP Cre* reporter (58), we observed a complete  
408 overlap between YFP<sup>+</sup> cells and the neuronal marker HuC/D staining in *BAF53b-Cre Rosa-YFP*  
409 cultures (Figure 5, bottom panel), confirming that BAF53b-Cre is pan-neuron-specific. In  
410 *BAF53b-Cre Brg1<sup>F/F</sup> Rosa-YFP* cultures, Brg1 proteins became undetectable in YFP<sup>+</sup> neurons  
411 after 5 to 7 days in culture (Figure 5, 7div and 14 div). Brg1 was detected in all non-neuronal  
412 cells. *Brg1*-mutant (*BAF53b-Cre Brg1<sup>F/F</sup>*) and control neurons had similar viability and cell  
413 numbers, indicating that Brg1 is not required for neuron survival in general. We therefore used  
414 this culture system to study Brg1 function in neuronal activity-dependent gene regulation and  
415 synapse plasticity.

416

417 ***Brg1 is required for MEF2-mediated gene activation.***

418 To determine the function of Brg1 in neuronal activity-induced gene activation, we measured  
419 gene expression profiles in the cultured control and *Brg1*-mutant neurons under the basal and

420 depolarized conditions. Cultured cortical neurons were used to identify Brg1 regulated neuronal  
421 activity-induced genes because these cultures have a high content of neurons (>80%) and are  
422 suitable for molecular and biochemical experiments. Many previous studies and publicly  
423 available data of activity-induced gene regulation were performed using the similar culture  
424 conditions (19, 26, 57). The target genes and regulatory mechanisms identified here could be  
425 applied to many other experimental systems.

426

427 *BAF53b-Cre Brg1<sup>FF</sup>* mutant or control cortical cultures at 7 div were treated with KCl for 6 hours  
428 to trigger depolarization-induced gene expression. RNA-seq experiments were performed to  
429 determine the effect of *Brg1* deletion on activity-induced gene transcription. By comparing  
430 transcription profiles under basal and depolarized conditions in control neurons, we identified  
431 1943 DEGs (fold change>1.5,  $p<0.05$ ), of which 1254 were increased by neuron depolarization  
432 (Table S2). By comparing the RNA signals from depolarized control and *Brg1*-mutant neuron  
433 cultures, we found that 219 genes were downregulated after *Brg1* deletion. The intersection with  
434 the activity-induced genes yielded 76 Brg1-regulated activity-induced genes (Figure 6A). Of  
435 these 76 genes, 74 were not regulated by Brg1 under basal conditions but only at the activity-  
436 induced level. Interestingly, 15 of the 74 Brg1-regulated activity-induced genes are also target  
437 genes of MEF2 family of transcription factors (Figure 6A). Previously, MEF2 target genes were  
438 identified from neurons cultured in the similar conditions (26). By comparing the MEF2 target  
439 genes with our activity-induced neuronal gene list, we obtained 57 activity-induced MEF2  
440 targets; of these 15 are also regulated by Brg1 (Figure 6A). The overlap rate is significantly  
441 higher than the overlap between two groups of 74 and 57 genes randomly selected from the  
442 1254 activity-induced gene pool ( $p=2.5\times 10^{-7}$ ). The common Brg1/MEF2 target genes include  
443 genes known to be important for synapse structure and plasticity such as *BDNF*, *Kcna1*,  
444 *Homer1*, *Nr4a1* (*Nur77*), and *PCDH17* (24). We confirmed the impaired induction of several  
445 Brg1/MEF2 target genes by neuronal depolarization in *Brg1*-mutant cortical neuron cultures  
446 (Figure 6B). *Junb*, a gene that is not a MEF2 target, was used as a control. *Brg1* deletion did not  
447 significantly change the activity-induced *Junb* expression. Moreover, the fact that Brg1 only  
448 regulated the activity-dependent expression of 74 genes (<10% of all activity-induced genes)  
449 (Figure 6A) indicates that Brg1 is required for neither the activation of the upstream  $Ca^{2+}$   
450 signaling nor the activity-induced gene expression in general. Brg1 deletion in neurons did not  
451 impair the protein levels or activation of MEF2 proteins by dephosphorylation as indicated by



western blot of MEF2C and MEF2D (Figure 6C). Thus Brg1 is specifically required for gene activation mediated by certain transcription factors such as MEF2.

The MEF2 family of transcription factors contains four members that have high homology in their DNA binding domains. MEF2C is the major form expressed in the cortex and has been shown to play a predominant role in neuronal synapse development and function (59). A fusion of the MEF2C DNA-binding and dimerization domain with the VP16 activation domain serves as an activator of MEF2 target genes and bypasses the need for MEF2-specific co-activators (25). To determine whether Brg1 is required for MEF2-mediated transcription activation, we examined the effect of *Brg1* deletion on the expression of a MEF2-activated reporter gene. Although the reporters are different from endogenous genes, plasmids could incorporate nucleosomes and have been used successfully to test the transcription regulator functions of Brg1 (57). A luciferase reporter with three MEF2 response elements (MRE-Luc) (25) was co-transfected with plasmids for expression of MEF2C or MEF2-VP16 or a control plasmid into cultured *BAF53b-Cre Brg1<sup>F/F</sup>* or control neurons. As expected, in control neurons, MRE-Luc was minimally expressed in the resting stage but was induced by either depolarization or co-expression of MEF2C or MEF-VP16 (Figure 6D). In *Brg1*-mutant neurons, both depolarization-induced and MEF2C-induced reporter expression was significantly impaired. Interestingly MEF2-VP16 activated MRE-Luc to the same degree in the presence and absence of Brg1 (Figure 6D). The different requirements for Brg1 in activation of MRE-Luc by exogenous MEF2C and MEF2-VP16 suggest that Brg1 functions as a co-activator of MEF2C and that this requirement is bypassed by MEF2-VP16. Importantly, defective depolarization-induced expression of endogenous MEF2 targets such as *Kcna1* caused by Brg1-deletion could be rescued by expression of MEF2-VP16 (Figure 6E). Therefore, Brg1 is required for MEF2-mediated gene activation.

#### **MEF2C is required for the activity-dependent recruitment of Brg1 to target genes.**

MEF2 regulates activity-dependent target genes by exchanging co-factors from co-repressors to co-activators upon neuron activation. Since Brg1 is a potential co-activator for MEF2-activated gene expression, we examined the dynamic binding of Brg1 to MEF2 targets. Cultured cortical neurons at 7 div were depolarized by a 1-hour KCl treatment. Brg1 ChIP was performed, and the signals in the regulatory regions of activity-dependent MEF2 target genes in resting and



484 depolarized neurons were compared. Depolarization of the neurons significantly induced the  
485 binding of Brg1 to these genes (Figure 7A). *GAP43* is a neuronal Brg1-target gene that is not  
486 induced by neuronal activities and is not a MEF2 target; Brg1 was not further recruited to the  
487 *GAP43* promoter upon depolarization. Since Brg1 is required for the depolarization-induced  
488 activation of these MEF2 target genes, the activity-dependent recruitment of Brg1 likely  
489 coordinates with MEF2 to direct the activation of these genes in response to neuronal  
490 depolarization.

491

492 To determine whether MEF2 is required for the activity-dependent recruitment of Brg1 to the  
493 target genes, we performed Brg1 ChIP in control (*MEF2C<sup>F/F</sup>*) (34) and *MEF2C* mutant (*Emx1-  
494 Cre MEF2C<sup>F/F</sup>*) cortical neuron cultures in resting and depolarized conditions. Loss of *MEF2C*  
495 significantly diminished the activity-induced Brg1 binding to the regulatory regions of the target  
496 genes examined (Figure 7A). Thus, MEF2C is required for the activity-induced Brg1 binding to  
497 target genes. In cultured cortical neurons, endogenous MEF2C co-immunoprecipitated with  
498 Brg1 in basal and KCl-depolarized conditions; depolarization led to an increase in the MEF2C-  
499 Brg1 co-immunoprecipitation efficiency (Figure 7B). This suggests that MEF2C interacts with  
500 Brg1 or other tightly associated BAF subunits to facilitate the recruitment of nBAF complexes to  
501 target genes in response to neuronal activities; nBAF then directs the activation of these genes.  
502

### 503 **Brg1 is required for MEF2-mediated dendritic spine elimination.**

504 The function of MEF2 in synapse remodeling and plasticity is most clearly demonstrated by data  
505 indicating that MEF2 activator overexpression in neurons reduces synapse and dendritic spine  
506 densities (25, 29). To determine whether Brg1 is required for MEF2-mediated dendritic  
507 spine/synapse elimination, we transfected plasmids for expression of MEF2C, MEF2-VP16, or a  
508 control MEF2-VP16 mutant without DNA-binding ability (MEF2Δ-VP16) together with GFP into  
509 *BAF53b-Cre Brg1<sup>F/F</sup>* or control hippocampal neuron cultures. In control neurons, both MEF2-  
510 VP16 and MEF2C significantly reduced dendritic spine densities compared to MEF2Δ-VP16  
511 (Figure 8A, 8B). In *Brg1*-mutant neurons, MEF2-VP16 reduced the dendritic spine densities, but  
512 the ability of MEF2C to eliminate dendritic spines was impaired (Figure 8A, 8B), indicating that  
513 Brg1 is required for MEF2C-mediated synapse elimination in dissociated neuron cultures.

514

515 To exclude the potential for non-cell-autonomous effects of *Brg1* deletion, we overexpressed  
516 MEF2C in individual *Brg1* deleted CA1 neurons in cultured hippocampal slices. In cultured  
517 *Brg1<sup>F/F</sup>* hippocampal slices, plasmids for expression of GFP and MEF2C and/or Cre and  
518 corresponding controls were co-transfected using the biolistic delivery system. GFP-labeled  
519 CA1 pyramidal neurons were imaged after 5 days for dendritic spine analyses. In control  
520 neurons, MEF2C expression significantly reduced dendritic spine densities. In CA1 neurons  
521 where *Brg1* was deleted by Cre-induction, dendritic spine densities were significantly lower than  
522 in control neurons; moreover, MEF2C failed to further reduce spine densities in the *Brg1*-mutant  
523 neurons (Figure 8C, 8D). The expression of MEF2C did not significantly change the ratio  
524 between the thin and mushroom-shaped or stubby spines in either control or *Brg1*-deleted  
525 neurons (Figure 8E). These experiments indicate that *Brg1* is required for MEF2C-mediated  
526 dendritic spine/synapse elimination in hippocampal neurons in both dissociated and slice  
527 cultures.  
528  
529

530 **DISCUSSION**

531 In this study, using different Cre systems that are most suitable for the required studies, we  
532 found that the ASD-associated chromatin remodeler Brg1 regulates expression of genes  
533 involved in synapse development and plasticity during development and in response to neuronal  
534 activities. During neuronal development, Brg1 is required for synapse formation and maturation  
535 in several types of neurons. In response to neuronal activities, Brg1 is recruited to MEF2 target  
536 genes to control synapse elimination (Figure 8F). *Brg1* deletion in neurons of mice led to severe  
537 behavioral defects especially during development. Our studies thus identified potential  
538 molecular and cellular mechanisms underlying Brg1 functions in neurological diseases such as  
539 autism.

540

541 **Brg1 is critical for synaptic gene regulation and synapse development.**

542 Brg1 and BAF complexes regulate gene activation or repression by modulating chromatin  
543 structures either directly by ATP-dependent chromatin remodeling or indirectly by recruiting  
544 other epigenetic regulators (8-10). The recruitment of BAF complexes to target genes mostly  
545 requires sequence-specific transcription factors. Functional studies of BAF subunits in different  
546 developmental tissues at different stages revealed distinct cell-type-specific functions of BAF  
547 complexes. The diverse subunit compositions of BAF complex in different cell types may  
548 provide interactions with tissue specific transcription factors to target the complex to loci that are  
549 required for specific developmental programs. Previous studies have shown that BAF  
550 complexes in embryonic stem cells, neural progenitors, and neurons have distinct functions in  
551 each cell type (19, 20, 60). There are few overlapping target loci of Brg1/BAF in different tissues  
552 (44, 61).

553

554 In this study, we showed that synaptic genes are specific Brg1 targets in developing neurons. A  
555 large number of Brg1 regulated genes have known functions in neuronal and synapse  
556 development. We speculate that Brg1 support a transcription program that coordinates synapse  
557 formation and maturation. However, it is not clear which transcription factors are involved in  
558 activating or repressing these genes. Our observation that Brg1 is a MEF2 co-activator enables  
559 us to speculate that MEF2 is one of the transcription factors that mediate Brg1 functions in  
560 synaptic gene regulation and in synapse maturation during development. Interestingly, We  
561 observed that Brg1 regulates both synapse formation and MEF2C mediated synapse

elimination. Although it seems that Brg1 regulates synapse number in two directions, it reflects the diverse functions of Brg1 in neuron development and the dynamic synapse developmental processes. At early postnatal stage, synapse/dendritic spines are actively formed and eliminated. Synapse formation peaks around the second week postnatally in mouse brain, whereas synapse elimination peaks as neurons mature in the third week after birth, partially due to the increased activities of MEF2 family transcription factors (62-65). Therefore proteins that play diverse functions during synapse development may appear to cause opposite effects on synapse numbers depending on the developmental stages when the genes are altered and MEF2 activities at the specific time point. For example, it has been reported that the autism-associated FMRP protein bidirectionally regulates synaptogenesis as a function of developmental age and MEF2 activity(64). Therefore, we propose that Brg1 is required for synapse formation and maturation by regulating synaptic structural genes. In addition, it also regulates MEF2C mediated activity-induced gene expression and synapse elimination. The two scenarios described in the proposed model about nBAF functions during development and in activated neurons are not mutually exclusive and reflect diverse functions of Brg1 during different synapse developmental stages (Figure 8F).

In addition to synaptic genes, Brg1 deletion in dentate gyrus also led to the increased expression of several growth factors such as *Igf1* and *Igf2* (data not shown), which may compensate for the impaired synapse formation. Therefore, the relative subtle defects in synaptic spine densities in *Syn1-Cre Brg1<sup>F/F</sup>* DG neuron in vivo (Figure 3) than in Cre expressing individual CA1 neurons in hippocampal cultures (Figure 1) could be due to the non-cell autonomous compensatory mechanisms. Alternatively, it could be caused by the different developmental stages of the neurons examined. However, we could not exclude the possibility that it is due to the regional differences between dentate gyrus granule neurons and CA1 neurons. Nevertheless, our experiments clearly demonstrated that Brg1 is required for synapse maturation for both neuron types and it is required cell autonomously for synapse formation in CA1 neurons.

#### **nBAF complexes function in activity-dependent gene activation.**

The ability of neurons to convert transient stimuli into long-term changes in brain function underlies long-lasting neural plasticity; activity-dependent gene expression plays a central role

594 in this process. Much evidence suggests that the cooperation between transcription factors and  
595 chromatin regulators controls the rapid response of neurons to stimuli as well as long-lasting  
596 changes in neuron function (24, 66, 67). Despite the understanding that chromatin regulation is  
597 important in neuronal plasticity, the biochemical and molecular mechanisms remain largely  
598 unclear.

599

600 Analyses of *BAF53b*-knockout neurons demonstrated that nBAF complexes regulate activity-  
601 dependent dendrite growth, suggesting that signaling resulting from  $\text{Ca}^{2+}$  influx leads to  
602 chromatin regulation (19). In this study, by deleting *Brg1* specifically in neurons and by  
603 comparing the Brg1-regulated genes under basal and depolarized conditions, we identified a  
604 specific group of genes that are regulated by Brg1 during activation of neurons. These genes  
605 significantly overlap with activity-dependent MEF2 targets. We demonstrated the requirement of  
606 Brg1 for the expression of MEF2C targets and the requirement of MEF2C for Brg1 recruitment  
607 in response to neuronal depolarization. These results indicate that Brg1 functions as an  
608 essential co-activator of MEF2C-mediated transcription. This regulation is consistent with our  
609 observation that Brg1 is essential for MEF2C-mediated synapse elimination, which may also  
610 contribute to nBAF complex functions in neurodevelopmental diseases. However, in addition to  
611 MEF2, Brg1 may regulate additional transcription factors or pathways that are important for  
612 synapse development. *Brg1* mutant mice display early defects in synapse formation and  
613 maturation whereas *MEF2C* mutant neurons have defects in synapse elimination, which is a  
614 relatively late stage in synapse development. Deleting Brg1 using inducible Cre lines in  
615 neurons at later developmental stages after synapse formation may reveal its requirement for  
616 synapse elimination *in vivo* and additional functions in mature neurons.

617

618 One remaining question is how nBAF complexes, including Brg1 and its 10 tightly associated  
619 subunits, are recruited to MEF2 targets in response to  $\text{Ca}^{2+}$  signaling activation. Several  
620 modifications to MEF2 lead to exchange of co-repressors for co-activators (30, 31). One  
621 possibility is that  $\text{Ca}^{2+}$  signaling induces MEF2 modification changes that facilitate the  
622 recruitment of Brg1. This is supported by our observation of an increase of MEF2C-Brg1 co-  
623 immunoprecipitation efficiency in neurons in response to KCl treatment. However, the  
624 interaction between MEF2C and Brg1 is moderate. Therefore, additional mechanisms may also  
625 contribute to the recruitment of Brg1 in response to neuronal activation. It is possible that

626 changes of local chromatin environment induced by MEF2 activation could help recruit nBAF  
627 complexes by interacting with several histone modification binding domains existed in various  
628 BAF subunits (8).

629

630 In this study we found that the core BAF subunit Brg1 is critical for synapse development,  
631 maturation, and plasticity. The close functional connections of Brg1 to the ASD-associated  
632 MEF2 proteins discovered here provide molecular and cellular mechanisms for the role of BAF  
633 complexes in neurodevelopmental diseases. In *Brg1*-mutant mice, the mutant phenotypes are  
634 most severe during development and become less severe in adults. It is possible that mice  
635 develop compensating mechanisms that enable recovery from the defects. Interestingly, in adult  
636 neurons, Brg1 homolog Brm is highly expressed, and this might compensate for *Brg1* deletion.  
637 Mutations in *Brm*, but not in *Brg1*, have been linked to schizophrenia (68). Thus during different  
638 developmental stages, specific BAF complexes may be required for different aspects of  
639 neuronal development and function. The understanding of the functions and mechanisms of  
640 epigenetic regulators in ASD and other neurological disorders may provide new treatment  
641 strategies for these diseases.

642

643 **ACKNOWLEDGEMENTS**

644 We thank Qiu Wang for technical support and mouse colony maintenance. We are grateful to  
645 Andrew Yoo, Lei Chen, and Gerald Crabtree (Stanford University) for generating the *BAF53b-*  
646 *Cre* transgenic mouse. We thank Drs. Pierre Chambon (IGBMC, France), Luis Parada (UTSW),  
647 and Eric Olson (UTSW) for providing transgenic or knockout mice, and Kacey Rajkovich, Dr.  
648 Makoto Taniguchi, and Dr. Christopher Cowan for providing reagents. The behavior tests were  
649 performed in the Behavior Core Facility in UTSW. The RNA-seq experiments with the basic  
650 analyses were performed in the UTSW Sequencing Facility. This work was supported by grants  
651 from March of Dimes Foundation, American Cancer Society, and NIMH (R21MH102820) to J.  
652 Wu.  
653

## 654 REFERENCES

- 655 1. **Choquet D, Triller A.** 2013. The dynamic synapse. *Neuron* **80**:691-703.
- 656 2. **Zoghbi HY.** 2003. Postnatal neurodevelopmental disorders: meeting at the synapse?  
657 *Science* **302**:826-830.
- 658 3. **Spooren W, Lindemann L, Ghosh A, Santarelli L.** 2012. Synapse dysfunction in  
659 autism: a molecular medicine approach to drug discovery in neurodevelopmental  
660 disorders. *Trends Pharmacol Sci* **33**:669-684.
- 661 4. **van Bokhoven H.** 2011. Genetic and epigenetic networks in intellectual disabilities.  
662 *Annu Rev Genet* **45**:81-104.
- 663 5. **Lichtenstein P, Carlstrom E, Rastam M, Gillberg C, Anckarsater H.** 2010. The  
664 genetics of autism spectrum disorders and related neuropsychiatric disorders in  
665 childhood. *Am J Psychiatry* **167**:1357-1363.
- 666 6. **Ben-David E, Shifman S.** 2013. Combined analysis of exome sequencing points toward  
667 a major role for transcription regulation during brain development in autism. *Mol*  
668 *Psychiatry* **18**:1054-1056.
- 669 7. **De Rubeis S, He X, Goldberg AP, Poultney CS, Samocha K, Cicek AE, Kou Y, Liu**  
670 **L, Fromer M, Walker S, Singh T, Klei L, Kosmicki J, Shih-Chen F, Aleksic B,**  
671 **Biscaldi M, Bolton PF, Brownfeld JM, Cai J, Campbell NG, Carracedo A, Chahrour**  
672 **MH, Chiocchetti AG, Coon H, Crawford EL, Curran SR, Dawson G, Duketis E,**  
673 **Fernandez BA, Gallagher L, Geller E, Guter SJ, Hill RS, Ionita-Laza J, Jimenez**  
674 **Gonzalez P, Kilpinen H, Klauck SM, Klevzon A, Lee I, Lei I, Lei J, Lehtimaki T, Lin**  
675 **CF, Ma'ayan A, Marshall CR, McInnes AL, Neale B, Owen MJ, Ozaki N, Parellada M,**  
676 **et al.** 2014. Synaptic, transcriptional and chromatin genes disrupted in autism. *Nature*  
677 **515**:209-215.
- 678 8. **Wu JI, Lessard J, Crabtree GR.** 2009. Understanding the words of chromatin  
679 regulation. *Cell* **136**:200-206.
- 680 9. **Cairns BR.** 2007. Chromatin remodeling: insights and intrigue from single-molecule  
681 studies. *Nat Struct Mol Biol* **14**:989-996.
- 682 10. **Wu JI.** 2012. Diverse functions of ATP-dependent chromatin remodeling complexes in  
683 development and cancer. *Acta Biochim Biophys Sin (Shanghai)* **44**:54-69.
- 684 11. **Santen GW, Aten E, Sun Y, Almomani R, Gilissen C, Nielsen M, Kant SG, Snoeck**  
685 **IN, Peeters EA, Hilhorst-Hofstee Y, Wessels MW, den Hollander NS, Ruivenkamp**



- 686 **CA, van Ommen GJ, Breuning MH, den Dunnen JT, van Haeringen A, Kriek M.**  
687 2012. Mutations in SWI/SNF chromatin remodeling complex gene ARID1B cause Coffin-  
688 Siris syndrome. *Nat Genet* **44**:379-380.
- 689 12. **Tsurusaki Y, Okamoto N, Ohashi H, Kosho T, Imai Y, Hibi-Ko Y, Kaname T,**  
690 **Naritomi K, Kawame H, Wakui K, Fukushima Y, Homma T, Kato M, Hiraki Y,**  
691 **Yamagata T, Yano S, Mizuno S, Sakazume S, Ishii T, Nagai T, Shiina M, Ogata K,**  
692 **Ohta T, Niikawa N, Miyatake S, Okada I, Mizuguchi T, Doi H, Saitsu H, Miyake N,**  
693 **Matsumoto N.** 2012. Mutations affecting components of the SWI/SNF complex cause  
694 Coffin-Siris syndrome. *Nat Genet* **44**:376-378.
- 695 13. **Van Houdt JK, Nowakowska BA, Sousa SB, van Schaik BD, Seuntjens E, Avonce**  
696 **N, Sifrim A, Abdul-Rahman OA, van den Boogaard MJ, Bottani A, Castori M,**  
697 **Cormier-Daire V, Deardorff MA, Filges I, Fryer A, Fryns JP, Gana S, Garavelli L,**  
698 **Gillessen-Kaesbach G, Hall BD, Horn D, Huylebroeck D, Klapcecki J, Krajewska-**  
699 **Walasek M, Kuechler A, Lines MA, Maas S, Macdermot KD, McKee S, Magee A, de**  
700 **Man SA, Moreau Y, Morice-Picard F, Obersztyn E, Pilch J, Rosser E, Shannon N,**  
701 **Stolte-Dijkstra I, Van Dijck P, Vilain C, Vogels A, Wakeling E, Wieczorek D, Wilson**  
702 **L, Zuffardi O, van Kampen AH, Devriendt K, Hennekam R, Vermeesch JR.** 2012.  
703 Heterozygous missense mutations in SMARCA2 cause Nicolaides-Baraitser syndrome.  
704 *Nat Genet* **44**:445-449, S441.
- 705 14. **Hersh JH, Bloom AS, Weisskopf B.** 1982. Childhood Autism in a female with Coffin  
706 Siris Syndrome. *J Dev Behav Pediatr* **3**:249-252.
- 707 15. **Gana S, Panizzon M, Fongaro D, Selicorni A, Memo L, Scandurra V, Vannucci C,**  
708 **Bigozzi M, Scordo MR.** 2011. Nicolaides-Baraitser syndrome: two new cases with  
709 autism spectrum disorder. *Clin Dysmorphol* **20**:38-41.
- 710 16. **Neale BM, Kou Y, Liu L, Ma'ayan A, Samocha KE, Sabo A, Lin CF, Stevens C,**  
711 **Wang LS, Makarov V, Polak P, Yoon S, Maguire J, Crawford EL, Campbell NG,**  
712 **Geller ET, Valladares O, Schafer C, Liu H, Zhao T, Cai G, Lihm J, Dannenfelser R,**  
713 **Jabado O, Peralta Z, Nagaswamy U, Muzny D, Reid JG, Newsham I, Wu Y, Lewis L,**  
714 **Han Y, Voight BF, Lim E, Rossin E, Kirby A, Flannick J, Fromer M, Shakir K,**  
715 **Fennell T, Garimella K, Banks E, Poplin R, Gabriel S, DePristo M, Wimbish JR,**  
716 **Boone BE, Levy SE, Betancur C, Sunyaev S, et al.** 2012. Patterns and rates of exonic  
717 de novo mutations in autism spectrum disorders. *Nature* **485**:242-245.
- 718 17. **Halgren C, Kjaergaard S, Bak M, Hansen C, El-Schich Z, Anderson CM, Henriksen**  
719 **KF, Hjalgrim H, Kirchhoff M, Bijlsma EK, Nielsen M, den Hollander NS,**

- 720 **Ruivenkamp CA, Isidor B, Le Caignec C, Zannolli R, Mucciolo M, Renieri A, Mari F,**  
721 **Anderlid BM, Andrieux J, Dieux A, Tommerup N, Bache I.** 2012. Corpus callosum  
722 abnormalities, intellectual disability, speech impairment, and autism in patients with  
723 haploinsufficiency of ARID1B. *Clin Genet* **82**:248-255.
- 724 18. **Helsmoortel C, Vulto-van Silfhout AT, Coe BP, Vandeweyer G, Rooms L, van den**  
725 **Ende J, Schuurs-Hoeijmakers JH, Marcelis CL, Willemsen MH, Vissers LE, Yntema**  
726 **HG, Bakshi M, Wilson M, Witherspoon KT, Malmgren H, Nordgren A, Anneren G,**  
727 **Fichera M, Bosco P, Romano C, de Vries BB, Kleefstra T, Kooy RF, Eichler EE, Van**  
728 **der Aa N.** 2014. A SWI/SNF-related autism syndrome caused by de novo mutations in  
729 ADNP. *Nat Genet* **46**:380-384.
- 730 19. **Wu JI, Lessard J, Olave IA, Qiu Z, Ghosh A, Graef IA, Crabtree GR.** 2007.  
731 Regulation of dendritic development by neuron-specific chromatin remodeling  
732 complexes. *Neuron* **56**:94-108.
- 733 20. **Lessard J, Wu JI, Ranish JA, Wan M, Winslow MM, Staahl BT, Wu H, Aebersold R,**  
734 **Graef IA, Crabtree GR.** 2007. An Essential Switch in Subunit Composition of a  
735 Chromatin Remodeling Complex during Neural Development. *Neuron* **55**:201-215.
- 736 21. **Son EY, Crabtree GR.** 2014. The role of BAF (mSWI/SNF) complexes in mammalian  
737 neural development. *Am J Med Genet C Semin Med Genet* **166C**:333-349.
- 738 22. **Vogel-Ciernia A, Matheos DP, Barrett RM, Kramar EA, Azzawi S, Chen Y, Magnan**  
739 **CN, Zeller M, Sylvain A, Haettig J, Jia Y, Tran A, Dang R, Post RJ, Chabrier M,**  
740 **Babayan AH, Wu JI, Crabtree GR, Baldi P, Baram TZ, Lynch G, Wood MA.** 2013.  
741 The neuron-specific chromatin regulatory subunit BAF53b is necessary for synaptic  
742 plasticity and memory. *Nat Neurosci* **16**:552-561.
- 743 23. **West AE, Greenberg ME.** 2011. Neuronal activity-regulated gene transcription in  
744 synapse development and cognitive function. *Cold Spring Harb Perspect Biol* **3**.
- 745 24. **Ebert DH, Greenberg ME.** 2013. Activity-dependent neuronal signalling and autism  
746 spectrum disorder. *Nature* **493**:327-337.
- 747 25. **Flavell SW, Cowan CW, Kim TK, Greer PL, Lin Y, Paradis S, Griffith EC, Hu LS,**  
748 **Chen C, Greenberg ME.** 2006. Activity-dependent regulation of MEF2 transcription  
749 factors suppresses excitatory synapse number. *Science* **311**:1008-1012.
- 750 26. **Flavell SW, Kim TK, Gray JM, Harmin DA, Hemberg M, Hong EJ, Markenscoff-**  
751 **Papadimitriou E, Bear DM, Greenberg ME.** 2008. Genome-wide analysis of MEF2

- transcriptional program reveals synaptic target genes and neuronal activity-dependent polyadenylation site selection. *Neuron* **60**:1022-1038.
27. **Shalizi A, Gaudilliere B, Yuan Z, Stegmuller J, Shirogane T, Ge Q, Tan Y, Schulman B, Harper JW, Bonni A.** 2006. A calcium-regulated MEF2 sumoylation switch controls postsynaptic differentiation. *Science* **311**:1012-1017.
28. **Barbosa AC, Kim MS, Ertunc M, Adachi M, Nelson ED, McAnally J, Richardson JA, Kavalali ET, Monteggia LM, Bassel-Duby R, Olson EN.** 2008. MEF2C, a transcription factor that facilitates learning and memory by negative regulation of synapse numbers and function. *Proc Natl Acad Sci U S A* **105**:9391-9396.
29. **Pfeiffer BE, Zang T, Wilkerson JR, Taniguchi M, Maksimova MA, Smith LN, Cowan CW, Huber KM.** 2010. Fragile X mental retardation protein is required for synapse elimination by the activity-dependent transcription factor MEF2. *Neuron* **66**:191-197.
30. **Potthoff MJ, Olson EN.** 2007. MEF2: a central regulator of diverse developmental programs. *Development* **134**:4131-4140.
31. **Guasconi V, Puri PL.** 2009. Chromatin: the interface between extrinsic cues and the epigenetic regulation of muscle regeneration. *Trends Cell Biol* **19**:286-294.
32. **Sumi-Ichinose C, Ichinose H, Metzger D, Chambon P.** 1997. SNF2beta-BRG1 is essential for the viability of F9 murine embryonal carcinoma cells. *Mol Cell Biol* **17**:5976-5986.
33. **Zhu Y, Romero MI, Ghosh P, Ye Z, Charnay P, Rushing EJ, Marth JD, Parada LF.** 2001. Ablation of NF1 function in neurons induces abnormal development of cerebral cortex and reactive gliosis in the brain. *Genes Dev* **15**:859-876.
34. **Arnold MA, Kim Y, Czubyrt MP, Phan D, McAnally J, Qi X, Shelton JM, Richardson JA, Bassel-Duby R, Olson EN.** 2007. MEF2C transcription factor controls chondrocyte hypertrophy and bone development. *Dev Cell* **12**:377-389.
35. **Zhan X, Cao M, Yoo AS, Zhang Z, Chen L, Crabtree GR, Wu JI.** 2015. Generation of BAF53b-Cre transgenic mice with pan-neuronal Cre activities. *Genesis* **53**:440-448.
36. **Achatz G, Nitschke L, Lamers MC.** 1997. Effect of transmembrane and cytoplasmic domains of IgE on the IgE response. *Science* **276**:409-411.
37. **Zhan X, Shi X, Zhang Z, Chen Y, Wu JI.** 2011. Dual role of Brg chromatin remodeling factor in Sonic hedgehog signaling during neural development. *Proc Natl Acad Sci U S A* **108**:12758-12763.

- 784 38. **Rodriguez A, Ehlenberger DB, Dickstein DL, Hof PR, Wearne SL.** 2008. Automated  
785 three-dimensional detection and shape classification of dendritic spines from  
786 fluorescence microscopy images. *PLoS One* **3**:e1997.
- 787 39. **Swanger SA, Yao X, Gross C, Bassell GJ.** 2011. Automated 4D analysis of dendritic  
788 spine morphology: applications to stimulus-induced spine remodeling and  
789 pharmacological rescue in a disease model. *Mol Brain* **4**:38.
- 790 40. **Li H, Handsaker B, Wysoker A, Fennell T, Ruan J, Homer N, Marth G, Abecasis G,**  
791 **Durbin R.** 2009. The Sequence Alignment/Map format and SAMtools. *Bioinformatics*  
792 **25**:2078-2079.
- 793 41. **Trapnell C, Williams BA, Pertea G, Mortazavi A, Kwan G, van Baren MJ, Salzberg**  
794 **SL, Wold BJ, Pachter L.** 2010. Transcript assembly and quantification by RNA-Seq  
795 reveals unannotated transcripts and isoform switching during cell differentiation. *Nat*  
796 *Biotechnol* **28**:511-515.
- 797 42. **Shi X, Zhang Z, Zhan X, Cao M, Satoh T, Akira S, Shpargel K, Magnuson T, Li Q,**  
798 **Wang R, Wang C, Ge K, Wu J.** 2014. An epigenetic switch induced by Shh signalling  
799 regulates gene activation during development and medulloblastoma growth. *Nat*  
800 *Commun* **5**:5425.
- 801 43. **Khavari PA, Peterson CL, Tamkun JW, Mendel DB, Crabtree GR.** 1993. BRG1  
802 contains a conserved domain of the SWI2/SNF2 family necessary for normal mitotic  
803 growth and transcription. *Nature* **366**:170-174.
- 804 44. **Ho L, Jothi R, Ronan JL, Cui K, Zhao K, Crabtree GR.** 2009. An embryonic stem cell  
805 chromatin remodeling complex, esBAF, is an essential component of the core  
806 pluripotency transcriptional network. *Proc Natl Acad Sci U S A* **106**:5187-5191.
- 807 45. **Yu Y, Chen Y, Kim B, Wang H, Zhao C, He X, Liu L, Liu W, Wu LM, Mao M, Chan**  
808 **JR, Wu J, Lu QR.** 2013. Olig2 targets chromatin remodelers to enhancers to initiate  
809 oligodendrocyte differentiation. *Cell* **152**:248-261.
- 810 46. **Bhatt DH, Zhang S, Gan WB.** 2009. Dendritic spine dynamics. *Annu Rev Physiol*  
811 **71**:261-282.
- 812 47. **Nimchinsky EA, Sabatini BL, Svoboda K.** 2002. Structure and function of dendritic  
813 spines. *Annu Rev Physiol* **64**:313-353.
- 814 48. **Star EN, Kwiatkowski DJ, Murthy VN.** 2002. Rapid turnover of actin in dendritic spines  
815 and its regulation by activity. *Nat Neurosci* **5**:239-246.

- 816 49. **Sun S, Zhang H, Liu J, Popugaeva E, Xu NJ, Feske S, White CL, 3rd, Bezprozvanny**  
817 **I.** 2014. Reduced synaptic STIM2 expression and impaired store-operated calcium entry  
818 cause destabilization of mature spines in mutant presenilin mice. *Neuron* **82**:79-93.
- 819 50. **Minichiello L, Korte M, Wolfer D, Kuhn R, Unsicker K, Cestari V, Rossi-Arnaud C,**  
820 **Lipp HP, Bonhoeffer T, Klein R.** 1999. Essential role for TrkB receptors in  
821 hippocampus-mediated learning. *Neuron* **24**:401-414.
- 822 51. **Cao M, Wu JI.** 2015. Camk2a-Cre-mediated conditional deletion of chromatin remodeler  
823 Brg1 causes perinatal hydrocephalus. *Neurosci Lett* **597**:71-76.
- 824 52. **von Eichborn J, Dunkel M, Gohlke BO, Preissner SC, Hoffmann MF, Bauer JM,**  
825 **Armstrong JD, Schaefer MH, Andrade-Navarro MA, Le Novere N, Croning MD,**  
826 **Grant SG, van Nierop P, Smit AB, Preissner R.** 2013. SynSysNet: integration of  
827 experimental data on synaptic protein-protein interactions with drug-target relations.  
828 *Nucleic Acids Res* **41**:D834-840.
- 829 53. **Darnell JC, Van Driesche SJ, Zhang C, Hung KY, Mele A, Fraser CE, Stone EF,**  
830 **Chen C, Fak JJ, Chi SW, Licatalosi DD, Richter JD, Darnell RB.** 2011. FMRP stalls  
831 ribosomal translocation on mRNAs linked to synaptic function and autism. *Cell* **146**:247-  
832 261.
- 833 54. **Bhakar AL, Dolen G, Bear MF.** 2012. The pathophysiology of fragile X (and what it  
834 teaches us about synapses). *Annu Rev Neurosci* **35**:417-443.
- 835 55. **Wang MW, Huber KM.** 2009. Protein translation in synaptic plasticity: mGluR-LTD,  
836 Fragile X. *Curr Opin Neurobiol* **19**:319-326.
- 837 56. **Darnell JC, Klann E.** 2013. The translation of translational control by FMRP: therapeutic  
838 targets for FXS. *Nat Neurosci* **16**:1530-1536.
- 839 57. **Qiu Z, Ghosh A.** 2008. A calcium-dependent switch in a CREST-BRG1 complex  
840 regulates activity-dependent gene expression. *Neuron* **60**:775-787.
- 841 58. **Srinivas S, Watanabe T, Lin CS, Williams CM, Tanabe Y, Jessell TM, Costantini F.**  
842 2001. Cre reporter strains produced by targeted insertion of EYFP and ECFP into the  
843 ROSA26 locus. *BMC Dev Biol* **1**:4.
- 844 59. **Akhtar MW, Kim MS, Adachi M, Morris MJ, Qi X, Richardson JA, Bassel-Duby R,**  
845 **Olson EN, Kavalali ET, Monteggia LM.** 2012. In vivo analysis of MEF2 transcription  
846 factors in synapse regulation and neuronal survival. *PLoS One* **7**:e34863.

- 847 60. **Ho L, Ronan JL, Wu J, Staahl BT, Chen L, Kuo A, Lessard J, Nesvizhskii AI,**  
848 **Ranish J, Crabtree GR.** 2009. An embryonic stem cell chromatin remodeling complex,  
849 esBAF, is essential for embryonic stem cell self-renewal and pluripotency. *Proc Natl*  
850 *Acad Sci U S A* **106**:5181-5186.
- 851 61. **Attanasio C, Nord AS, Zhu Y, Blow MJ, Biddie SC, Mendenhall EM, Dixon J, Wright**  
852 **C, Hosseini R, Akiyama JA, Holt A, Plajzer-Frick I, Shoukry M, Afzal V, Ren B,**  
853 **Bernstein BE, Rubin EM, Visel A, Pennacchio LA.** 2014. Tissue-specific SMARCA4  
854 binding at active and repressed regulatory elements during embryogenesis. *Genome*  
855 *Res* **24**:920-929.
- 856 62. **Holtmaat A, Svoboda K.** 2009. Experience-dependent structural synaptic plasticity in  
857 the mammalian brain. *Nat Rev Neurosci* **10**:647-658.
- 858 63. **Hua JY, Smith SJ.** 2004. Neural activity and the dynamics of central nervous system  
859 development. *Nat Neurosci* **7**:327-332.
- 860 64. **Zang T, Maksimova MA, Cowan CW, Bassel-Duby R, Olson EN, Huber KM.** 2013.  
861 Postsynaptic FMRP bidirectionally regulates excitatory synapses as a function of  
862 developmental age and MEF2 activity. *Mol Cell Neurosci* **56**:39-49.
- 863 65. **Zuo Y, Yang G, Kwon E, Gan WB.** 2005. Long-term sensory deprivation prevents  
864 dendritic spine loss in primary somatosensory cortex. *Nature* **436**:261-265.
- 865 66. **Borrelli E, Nestler EJ, Allis CD, Sassone-Corsi P.** 2008. Decoding the epigenetic  
866 language of neuronal plasticity. *Neuron* **60**:961-974.
- 867 67. **Hsieh J, Gage FH.** 2005. Chromatin remodeling in neural development and plasticity.  
868 *Curr Opin Cell Biol* **17**:664-671.
- 869 68. **Koga M, Ishiguro H, Yazaki S, Horiuchi Y, Arai M, Niizato K, Iritani S, Itokawa M,**  
870 **Inada T, Iwata N, Ozaki N, Ujike H, Kunugi H, Sasaki T, Takahashi M, Watanabe Y,**  
871 **Someya T, Kakita A, Takahashi H, Nawa H, Muchardt C, Yaniv M, Arinami T.** 2009.  
872 Involvement of SMARCA2/BRM in the SWI/SNF chromatin-remodeling complex in  
873 schizophrenia. *Hum Mol Genet* **18**:2483-2494.
- 874
- 875



**FIGURE LEGENDS****Figure 1. Deleting *Brg1* in hippocampal neurons impairs synapse/dendritic spine formation and maturation.**

**A.** Organotypic hippocampal slice cultures from P6 wild-type or *Brg1*<sup>F/F</sup> mice were biolistically transfected with Cre expressing plasmids or empty vector controls together with GFP. Immunostaining showed Brg1 deletion in Cre expressing GFP labeled cells but not in the control cells 5 days after transfection (arrows). **B-D.** In the organotypic hippocampal slice culture system, synaptic function was measured using whole-cell patch clamp recordings of Cre-transfected CA1 pyramidal neurons or neighboring untransfected neurons. **(B)** Representative traces of mEPSCs. **(C)** Average mEPSC frequency and mEPSC amplitude from Cre-expressing (n=21) or untransfected (n=21) *Brg1*<sup>F/F</sup> CA1 neurons and **(D)** Cre-expressing (n=18) or untransfected (n=18) wild-type neurons. **E-H.** Organotypic hippocampal slice cultures from P6 *Brg1*<sup>F/F</sup> mice were biolistically transfected with GFP and Cre expressing plasmids or with vector control. **(E)** Representative pictures of dendritic spines of CA1 pyramidal neurons. Scale bar: 5  $\mu$ m. **(F)** Average dendritic spine densities, **(G)** classifications, and **(H)** spine volumes of control (n=16) and *Brg1*-deleted (n=20) CA1 neurons. The graphs are shown as Avg+SE. \*\* p< 0.01, \* p< 0.05, Student's t-test.

**Figure 2. *Syn1*-Cre-mediated *Brg1* deletion in neurons led to neurological defects in mouse.**

**A.** *Syn1*-Cre-mediated *Brg1* deletion occurs in hippocampal neurons as indicated by co-staining of Brg1 and neuronal marker NeuN. Brg1 was present in all cells in *Brg1*<sup>F/F</sup> sections, whereas images from representative *Syn1*-Cre *Brg1*<sup>F/F</sup> mice show that Brg1 is not observed in NeuN+ DG granule neurons at P7 or in DG and CA3 regions at P14 and P21. Brg1 was intact in CA1 neurons. Scale bars: 100  $\mu$ m. **B.** H&E staining of coronal sections of *Brg1*<sup>F/F</sup> and *Syn1*-Cre *Brg1*<sup>F/F</sup> brains at different ages. Scale bars: 500  $\mu$ m. **C.** Brain weights of *Brg1*<sup>F/F</sup> and *Syn1*-Cre *Brg1*<sup>F/F</sup> mice during development (n=3 in each group). **D.** Body weights of *Brg1*<sup>F/F</sup> and *Syn1*-Cre *Brg1*<sup>F/F</sup> mice during development (n=6, with matching number of male and females). **E.** Hindlimb clasp scores of *Brg1*<sup>F/F</sup> and *Syn1*-Cre *Brg1*<sup>F/F</sup> mice during development (n=6). Scoring: 0, both hindlimbs consistently splayed outward; 1, one hindlimb partially retracted; 2, both hindlimbs partially retracted; 3, both hindlimbs entirely retracted. The graphs in D and E are shown as

908 Avg+SE. Student's t-test, \* $p < 0.01$ . **F.** Representative photograph of *Brg1<sup>F/F</sup>* and *Syn1-Cre*  
909 *Brg1<sup>F/F</sup>* pups at P7. The *Brg1* mutant mouse displays a posture typical of the mutant pups  
910 indicative of difficulties righting to the face-down position. **G.** Open field activity tests were  
911 performed on adult *Brg1<sup>F/F</sup>* (n=13) and *Syn1-Cre Brg1<sup>F/F</sup>* (n=11) mice. No significant differences  
912 were found in either the distance moved or the preference for the open field areas in the full 15  
913 minutes tested. **H.** Foot shock test to determine the response threshold of *Brg1<sup>F/F</sup>* (n=13) and  
914 *Syn1-Cre Brg1<sup>F/F</sup>* (n=11) adult mice. The graphs in G and H are shown as Avg+SE. Student's t-  
915 test, \*\* $p < 0.01$ .

916

917 **Figure 3. Syn1-Cre mediated Brg1 deletion in neurons impairs synapse maturation in**  
918 **vivo.**

919 **A-D.** Individual DG granule neurons in fixed P21 *Brg1<sup>F/F</sup>* and *Syn1-Cre Brg1<sup>F/F</sup>* hippocampal  
920 slices were injected with Lucifer yellow to enable visualization. **(A)** Representative two-photon  
921 confocal microscopy images of dendritic spines. Scale bar: 5  $\mu$ m. **(B)** Average spine densities,  
922 **(C)** classifications of spines and **(D)** Average spine volumes from *Brg1<sup>F/F</sup>* (n=18) and *Syn1-Cre*  
923 *Brg1<sup>F/F</sup>* (n=20) neurons. The graphs are shown as Avg+SE. \*  $p < 0.05$ , Student's t-test.

924

925 **Figure 4. Brg1 regulates synaptic genes in developing neurons.**

926 **A.** Brg1-regulated genes in P13 and P21 DG identified with RNA-seq were compared. The Venn  
927 diagrams show the number of common genes activated or repressed by Brg1 in each  
928 developmental stage. **B.** Examples of neuronal genes activated and repressed by Brg1 in both  
929 P13 and P21 DG. **C.** Brg1 ChIP-qPCR experiments were performed using P13 and P21 DG.  
930 Enrichment of Brg1 binding to the regulatory regions of the indicated target genes compared to  
931 IgG ChIP was observed. A region in the *CD4* gene was used as a Brg1 binding negative control.  
932 The graph is shown as Avg+SE (n=3). **D.** List of the most enriched Brg1-regulated biological  
933 processes identified by DAVID gene ontology analysis of the RNA-seq dataset obtained from  
934 both P13 and P21 DG. **E.** Significant overlap between Brg1-regulated genes in developing DG  
935 and synaptic genes (52) and autism genes (SFARI Gene database). Fisher's exact test was  
936 used to calculate p values.

937

938 **Figure 5. BAF53b-Cre-mediated Brg1 deletion in cultured cortical/hippocampal neurons.**



939 **A.** *BAF53b-Cre* was used to mediate *Brg1* deletion in cultured neurons. Mixed cortical and  
940 hippocampal neurons cultured from E18.5 embryos with the indicated genotypes at 1 div, 7 div  
941 and 14 div were stained with antibodies against Brg1, YFP reporter, and neuronal marker  
942 HuC/D. Note that at 1 div, Brg1 was not completely deleted in YFP-labeled neurons in *Brg1*-  
943 mutant culture, whereas at 7 div and 14 div, Brg1 was completely deleted in YFP+ *Brg1*-mutant  
944 neurons. At 14 div, the YFP reporter completely co-stained with all HuC/D positive cells,  
945 confirming the pan-neuron specific feature of *BAF53b-Cre* transgene.

946

947

948 **Figure 6. Brg1 is required for MEF2-mediated gene activation.**

949 **A.** Analyses of Brg1-regulated activity-dependent gene expression using RNA-seq datasets  
950 obtained from *BAF53b-Cre Brg1<sup>F/F</sup>* *Brg1*-mutant and control cultured cortical neurons at 7 div  
951 were treated with or without KCl for 6 hours. The Venn diagrams show the intersections of Brg1-  
952 activated genes and activity-induced genes (left panel) and the significant overlap between  
953 Brg1-regulated and MEF2-regulated activity-induced genes (right panel). **B.** Impaired  
954 expression of activity-induced MEF2 target genes in *Brg1*-mutant neuronal cultures as indicated  
955 by RT-qPCR analyses. *Junb* was used as a non-MEF2 target gene control. **C.** Western blot  
956 showing MEF2 proteins in control and *Brg1*-mutant neuron cultures in the absence and  
957 presence of KCl treatment for 1 hour. **D.** Brg1 is required for MEF2C-mediated reporter gene  
958 activation. MRE-Luc and plasmids expressing MEF2C, MEF2-VP16, or vector control were co-  
959 transfected into cultured cortical neurons at 5 div. Luciferase assays were performed 24 hour  
960 later. KCl was added to a group of cells 6 hours before harvesting. **E.** MEF2-VP16 or vector  
961 control were transfected into cultured control or *Brg1*-mutant cortical neurons at 5 div. KCl was  
962 added at 7 div for 6 hours. MEF2-VP16 rescued impaired MEF2 target gene *Kcna1* expression  
963 in *Brg1*-mutant cultures in response to KCl depolarization as indicated by RT-qPCR  
964 measurement. The graphs are shown as Avg+SE. Significance was determined using t-test or  
965 ANOVA with post hoc t-test. n=3, \*\* p< 0.01.

966

967 **Figure 7. MEF2 is required for the activity-induced recruitment of Brg1 to target genes.**

968 **A.** Brg1 ChIP-qPCR experiments were performed using cultured *MEF2C<sup>F/F</sup>* control and *Emx1*-  
969 *Cre MEF2C<sup>F/F</sup>* cortical neurons treated with or without KCl for 1 hour. Significant increases in  
970 Brg1 binding to the regulatory regions of all the activity-induced MEF2 target genes were

971 observed. *Gap43* was used as a non-activity-dependent gene control. Induction was  
972 significantly diminished in *MEF2C* mutant cortical cultures. \*\*  $p < 0.01$ , ANOVA post hoc t-test.

973 **B.** Interactions between endogenous MEF2C and Brg1 were evaluated in cell lysates from  
974 cultured cortical neurons treated with or without KCl for 1 hour. Samples were  
975 immunoprecipitated with Brg1 antibody or IgG control. MEF2C and Brg1 were detected by  
976 western blot.

977

978 **Figure 8. Brg1 is required for MEF2C-induced dendritic spine elimination.**

979 **A-B.** Brg1 is required for MEF2C-mediated dendritic spine elimination in cultured hippocampal  
980 neurons. *BAF53b-Cre Brg1<sup>F/F</sup>* mutant and control hippocampal neuron cultures were transfected  
981 with plasmids expressing GFP and MEF2C, MEF2-VP16, or control MEF2Δ-VP16 at 7 div. **(A)**  
982 GFP-labeled neurons were imaged at 14 div and **(B)** dendritic spine densities were measured  
983 and compared. **C-E.** Organotypic hippocampal slice cultures from P6 *Brg1<sup>F/F</sup>* mice were  
984 biolistically transfected with plasmids for expression of Cre, GFP, and MEF2C or control at 1  
985 div. **(C)** GFP-labeled CA1 neurons were imaged after 5 days and **(D)** the dendritic spine  
986 densities and **(E)** classifications were analyzed. Scale bar: 5  $\mu\text{m}$ . The graphs are shown as  
987 Avg+SE. ANOVA post hoc t-test, \*\*  $p < 0.01$ , \*  $p < 0.05$ . The numbers of neurons examined in  
988 each group are shown in the bar graph. **F.** A model illustrating the function of Brg1 in synapse  
989 development and plasticity. During synaptic development, nBAF complexes are recruited by  
990 specific transcription factors to regulate expression of a significant number of genes required for  
991 synapse formation and maturation (left panel). In response to neuronal activity-triggered  $\text{Ca}^{2+}$   
992 signaling, activated MEF2 proteins recruit nBAF complexes to MEF2 targets and regulate the  
993 activity-induced genes required for synapse elimination and plasticity (right panel). These two  
994 scenarios are not mutually exclusive and may reflect the different developmental stages of  
995 neurons.

996

997

998

Figure 1. Deleting Brg1 in hippocampal neurons impairs synapse/dendritic spine formation and maturation.

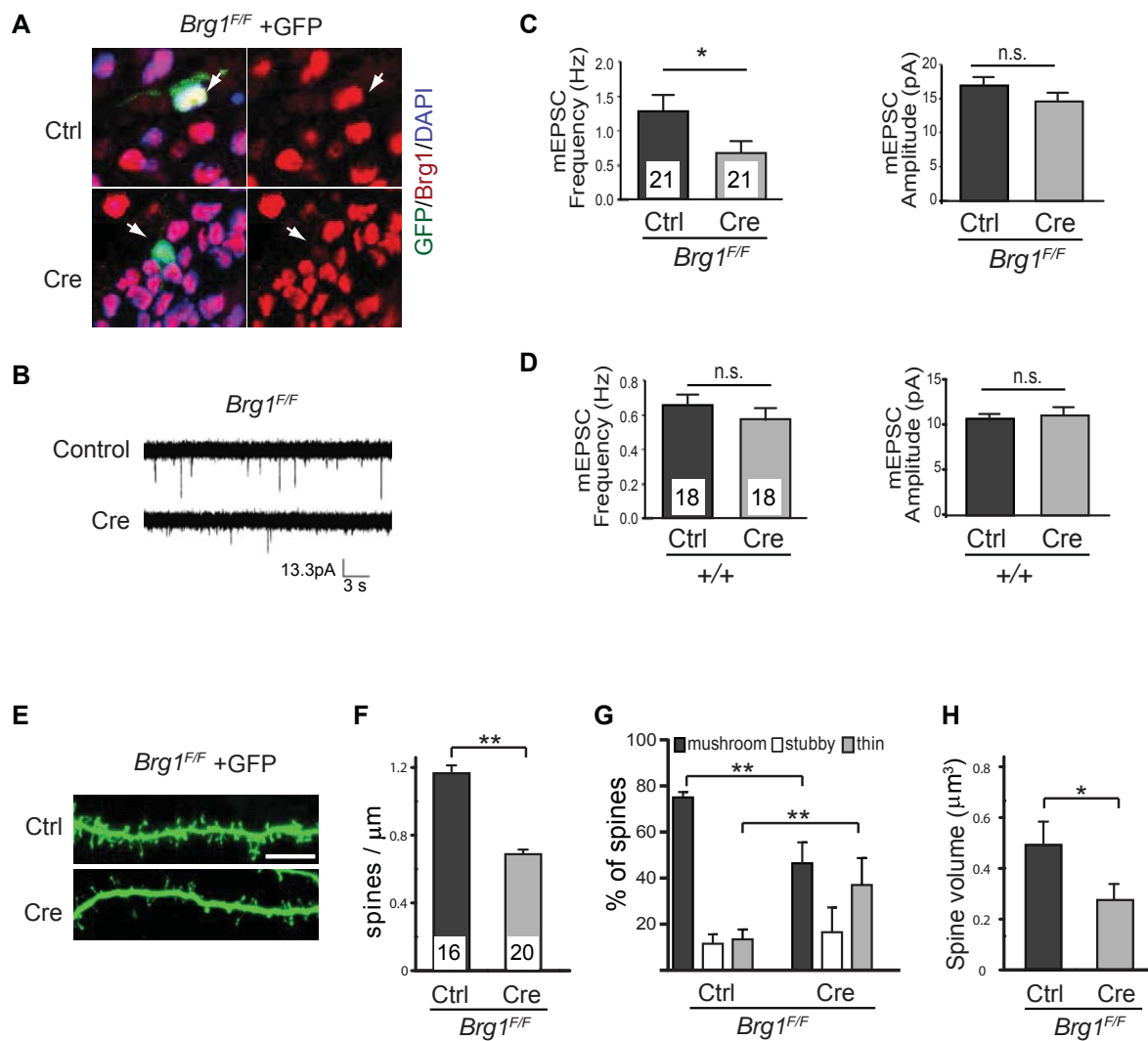


Figure 2. *Syn1-Cre*-mediated *Brg1* deletion in neurons led to neurological defects in mouse.

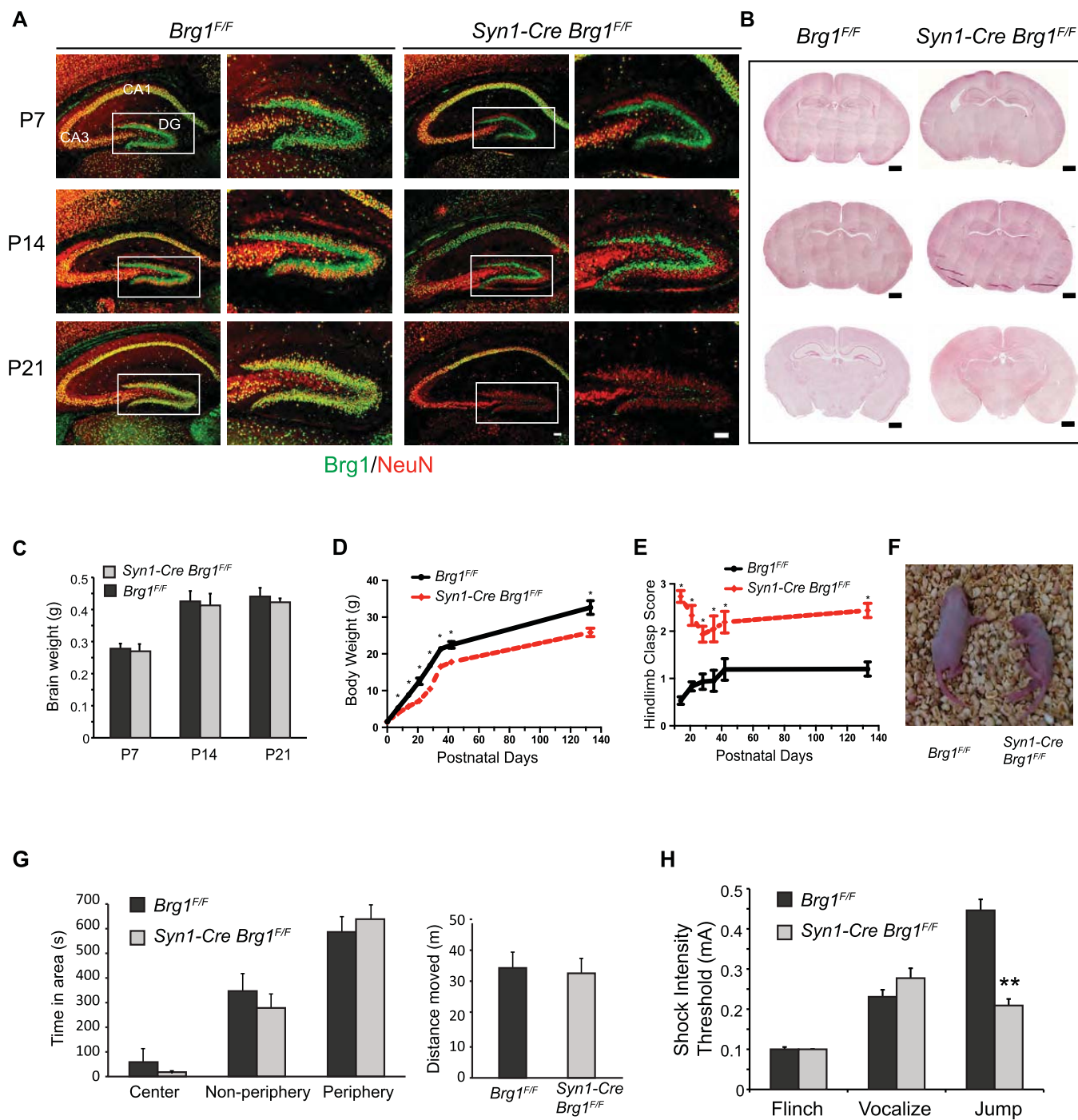


Figure 3. *Syn1-Cre*-mediated *Brg1* deletion in neurons impairs synapse maturation in vivo.

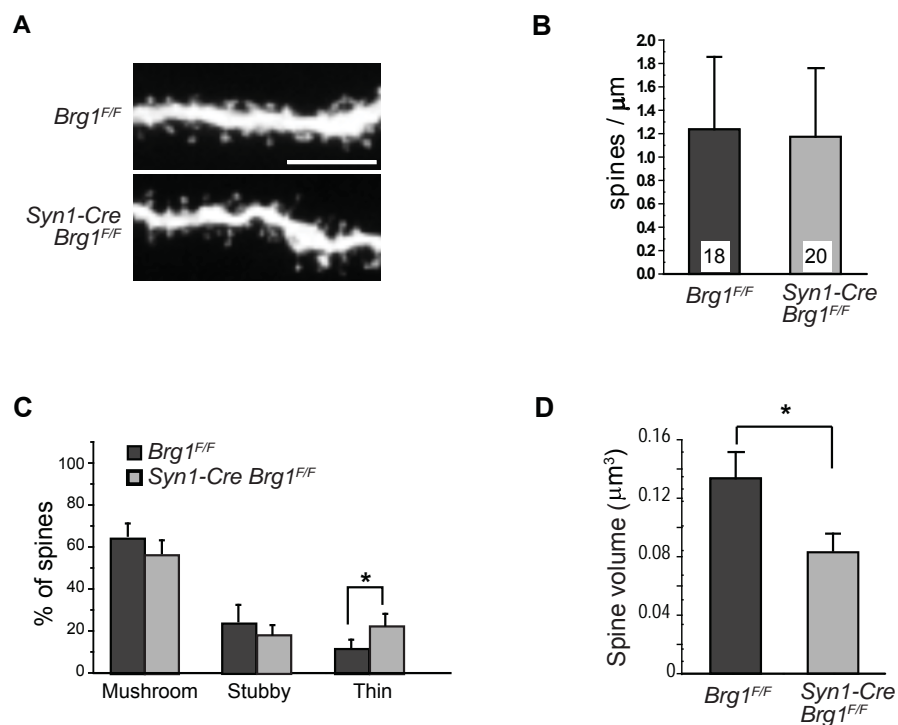


Figure 4. Brg1 Regulates synaptic genes in developing neurons.

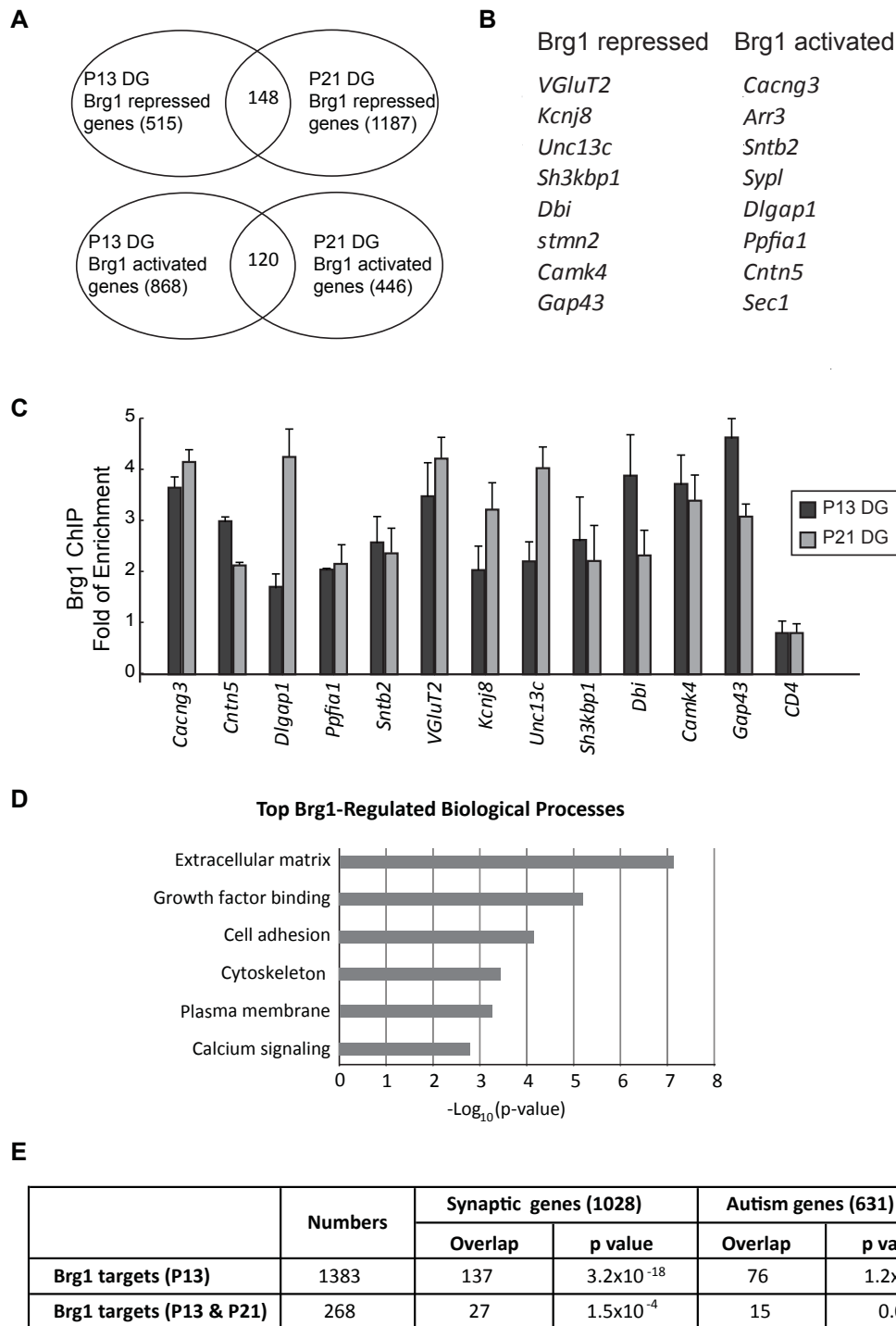


Figure 5. *BAF53b*-Cre-mediated Brg1 deletion in cultured cortical/hippocampal neurons.

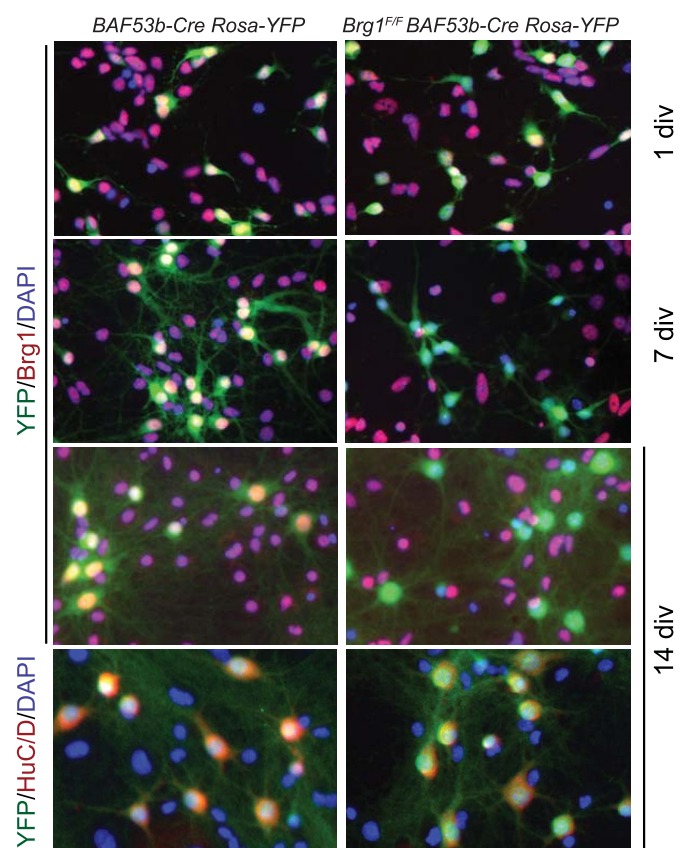




Figure 6. Brg1 is required for MEF2-mediated gene activation.

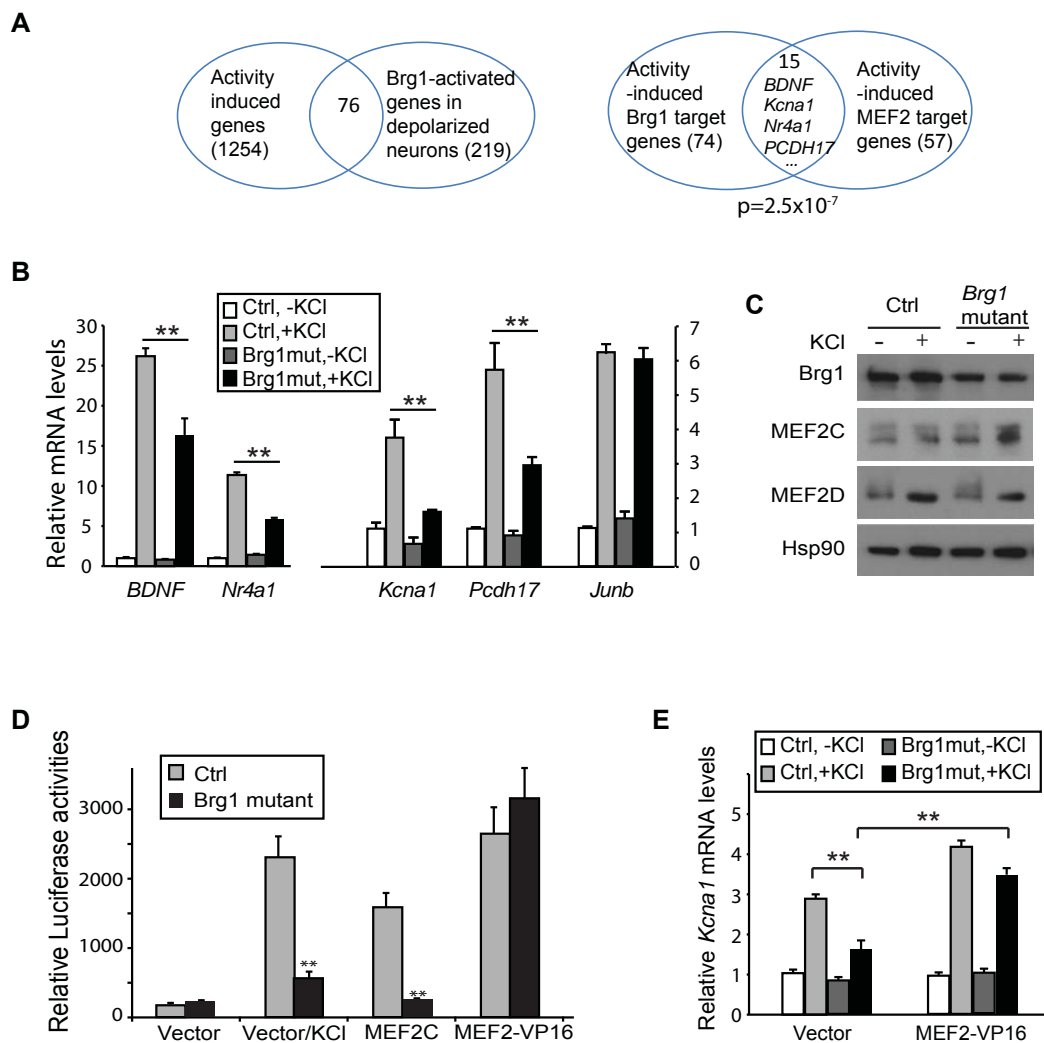




Figure 7. MEF2 is required for the activity-dependent recruitment of Brg1 to target genes.

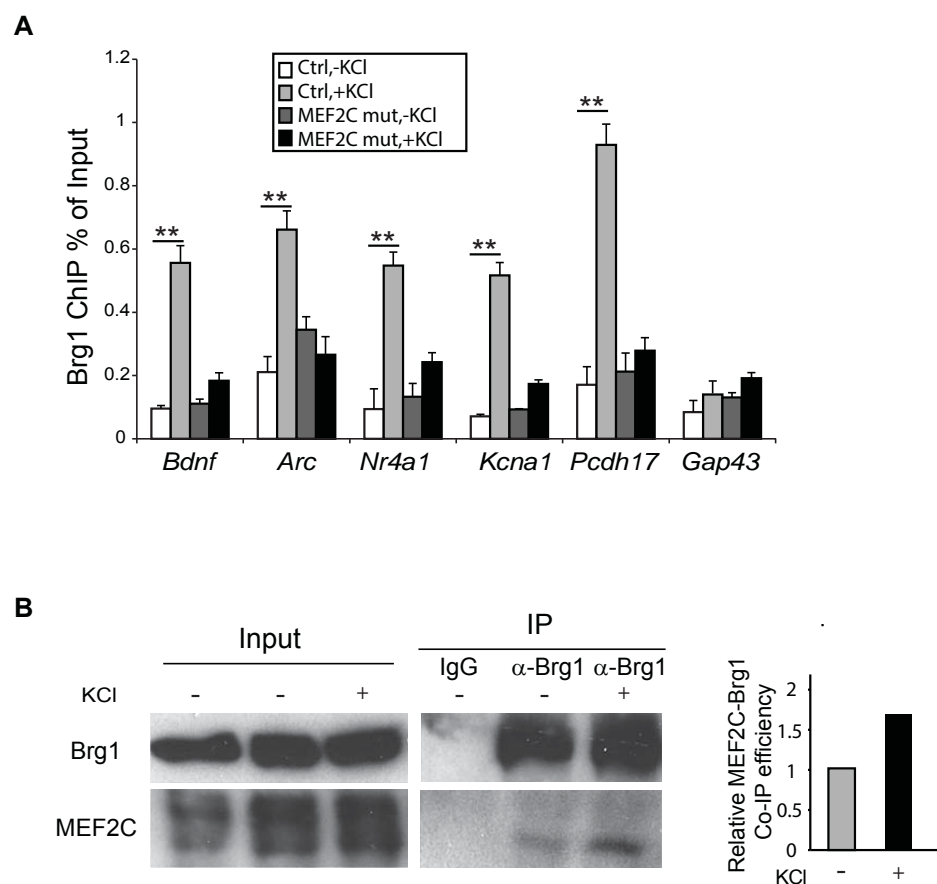
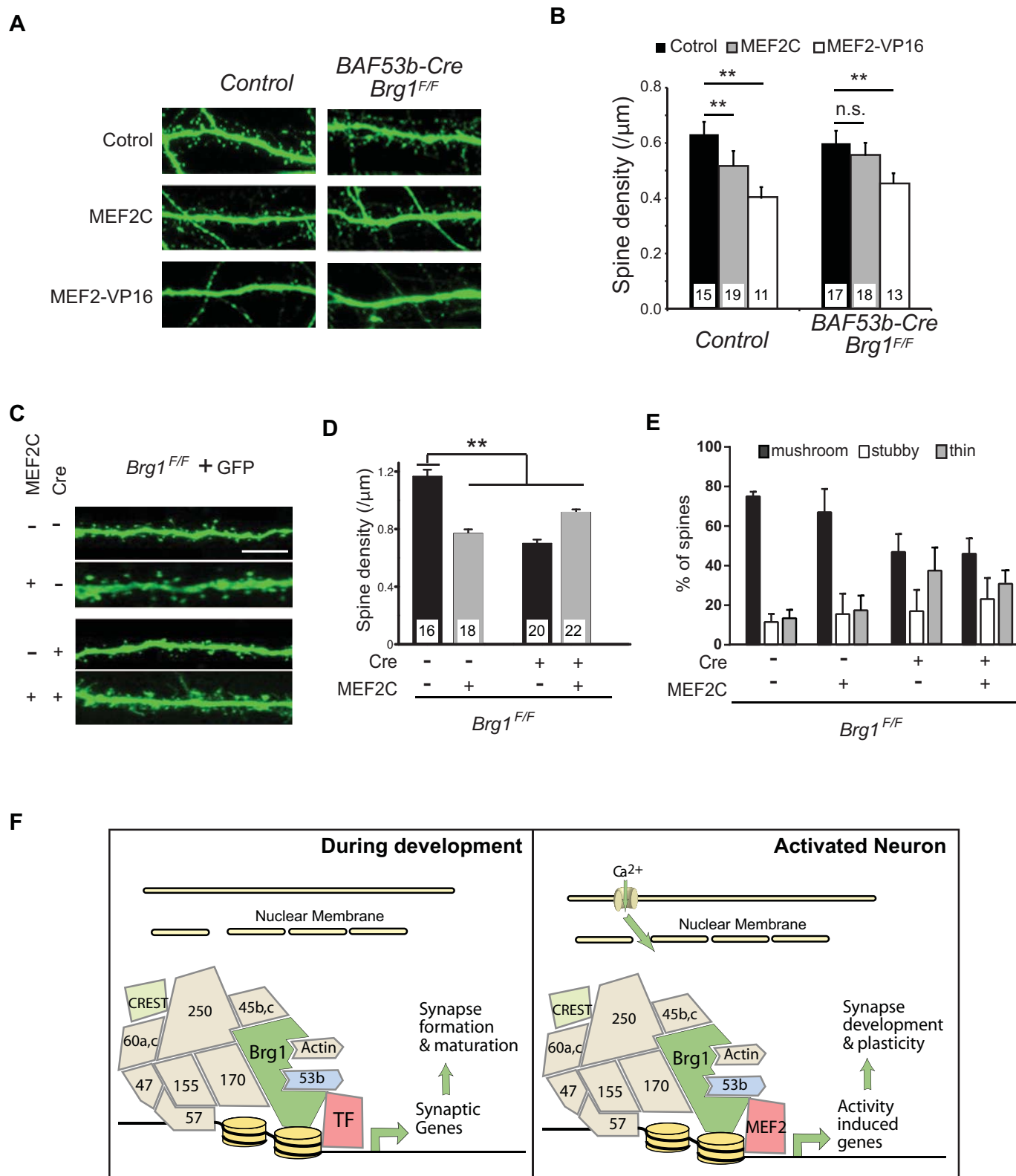


Figure 8. Brg1 is required for MEF2C-induced dendritic spine elimination.



## ARTICLE

Received 11 May 2014 | Accepted 30 Sep 2014 | Published 5 Nov 2014

DOI: 10.1038/ncomms6425

# An epigenetic switch induced by Shh signalling regulates gene activation during development and medulloblastoma growth

Xuanming Shi<sup>1</sup>, Zilai Zhang<sup>1</sup>, Xiaoming Zhan<sup>1</sup>, Mou Cao<sup>1</sup>, Takashi Satoh<sup>2</sup>, Shizuo Akira<sup>2</sup>, Karl Shpargel<sup>3</sup>, Terry Magnuson<sup>3</sup>, Qingtian Li<sup>4</sup>, Rongfu Wang<sup>4</sup>, Chaochen Wang<sup>5</sup>, Kai Ge<sup>5</sup> & Jiang Wu<sup>1</sup>

The Sonic hedgehog (Shh) signalling pathway plays important roles during development and in cancer. Here we report a Shh-induced epigenetic switch that cooperates with Gli to control transcription outcomes. Before induction, poised Shh target genes are marked by a bivalent chromatin domain containing a repressive histone H3K27me3 mark and an active H3K4me3 mark. Shh activation induces a local switch of epigenetic cofactors from the H3K27 methyltransferase polycomb repressive complex 2 (PRC2) to an H3K27me3 demethylase Jmjd3/Kdm6b-centred coactivator complex. We also find that non-enzymatic activities of Jmjd3 are important and that Jmjd3 recruits the Set1/MLL H3K4 methyltransferase complexes in a Shh-dependent manner to resolve the bivalent domain. *In vivo*, changes of the bivalent domain accompanied Shh-activated cerebellar progenitor proliferation. Overall, our results reveal a regulatory mechanism that underlies the activation of Shh target genes and provides insight into the causes of various diseases and cancers exhibiting altered Shh signalling.

<sup>1</sup>Department of Physiology and Developmental Biology, University of Texas Southwestern Medical Center, Dallas, Texas 75390, USA. <sup>2</sup>Laboratory of Host Defense, World Premier Institute Immunology Frontier Research Center and Department of Host Defense, RIMD, Osaka University, Osaka, Japan.

<sup>3</sup>Department of Genetics, University of North Carolina School of Medicine, Chapel Hill, North Carolina 27599, USA. <sup>4</sup>Center for Inflammation and Epigenetics, The Methodist Hospital Research Institute, Houston, Texas 77030, USA. <sup>5</sup>NIDDK, NIH, Bethesda, Maryland 20892, USA. Correspondence and requests for materials should be addressed to J.W. (email: jiang9.wu@utsouthwestern.edu).

**S**onic hedgehog (Shh) signalling, mediated by Patched and Smoothened, functions as a morphogen or a mitogen during many developmental processes<sup>1–3</sup>. Mutations in the Shh pathway components lead to developmental diseases and cancers<sup>4,5</sup>. Shh signalling produces specific transcriptional outcomes by differentially regulating the activities of Gli family transcription factors<sup>1,2</sup>. Under basal conditions, Gli3, and to a lesser extent Gli2, is processed to generate a truncated Gli repressor (GliR) that represses basal expression of Shh target genes. Shh signalling de-represses and activates target genes by inhibiting Gli3 processing, inducing Gli3 degradation and activating Gli2/Gli1 transcription activators (GliA). The morphogen activity of Shh (for example, in neural tube patterning) is largely dependent on its role as an antagonist of GliR function. GliA-mediated transcription activation in response to Shh is critical for neural tube progenitor specification in the most ventral areas<sup>6,7</sup>. The mitogenic effects of Shh in many normal and cancer cell types also require the GliA activities<sup>1,2</sup>. For example, Shh/GliA signalling plays a predominant role in the proliferation of early postnatal cerebellum granule neuron precursors (CGNPs)<sup>8–11</sup>. Mutations that result in constitutively active Shh signalling cause CGNP overproliferation and are the leading genetic causes of the childhood brain tumour medulloblastoma<sup>4,5</sup>. Recent studies suggest a link between active Shh pathways and other cancers, and it appears that the oncogenic functions of the Shh pathway require GliA-mediated transcription activation<sup>1,4</sup>.

Despite extensive studies of Hedgehog signalling in multiple organisms, one fundamental question remains to be answered: how do Gli proteins de-repress and activate target gene expression in response to Shh? Epigenetic factors play critical roles in determining transcription outcomes by regulating chromatin structures and accessibilities of DNA to transcription machineries. Recently, we identified a Brg1-containing chromatin remodelling complex that represses basal expression and activates Shh signalling-induced target gene expression<sup>12</sup>. Interestingly, our results suggest that Brg1 mainly functions as a docking site for other chromatin regulators. Brg1 deletion leads to changes in histone modifications in the regulatory regions of Shh target genes. Thus, additional histone modifiers may regulate Shh signalling, and it is likely that Shh signalling-induced transcription factor exchange from GliR to GliA is accompanied by changes of associated epigenetic cofactor complexes to produce specific chromatin environments and transcription outcomes.

Bivalent chromatin domains containing both a repressive H3K27me3 and an active H3K4me3 mark are found in the regulatory regions of many developmental genes in stem cells; these bivalent domains keep gene expression repressed but poised for induction<sup>13–16</sup>. During development, the resolution of the bivalent domain accompanies the activation or silencing of the poised genes. The PRC2 complex catalyses the addition of H3K27me3 ref. 17, whereas the H3K27me3-specific demethylases UTX/Kdm6a and Jmjd3/Kdm6b remove it<sup>18–22</sup>. UTX is also a subunit of H3K4 methyltransferase MLL2/3 complexes<sup>20,23</sup>, which may coordinately activate bivalent genes by removing H3K27me3 and increasing levels of H3K4me3. The Jmjd3 catalytic domain shares homology with UTX; however, genetic analyses indicate that they play distinct roles during development<sup>24–27</sup>. Although Jmjd3 does not appear to be a subunit of Set1/MLL complexes, it is able to interact with Set1/MLL complexes<sup>21</sup>. The interaction is not strong, and it is not clear whether this interaction plays a role in resolving bivalent domains during bivalent gene activation. How bivalent domains are regulated coordinately by epigenetic factors in response to specific developing signals has not been well understood.

In this study, we identified a bivalent domain at the regulatory regions of poised Shh target genes. Shh signalling induces an epigenetic switch to resolve bivalent domains and activates gene expression. PRC2 complexes repress Shh target genes by maintaining the repressive H3K27me3 levels, whereas Shh-induced recruitment of Jmjd3 activates target genes by displacing PRC2, enzymatically removing H3K27me3 and recruiting Set1/MLL complex. The central role of Jmjd3 in regulating Shh-activated gene expression was demonstrated *in vivo* in Shh activation-dependent development and medulloblastoma growth. Our study reveals an important epigenetic mechanism underlying the gene activation in response to Shh and identifies a potential target to disrupt the mitogenic effect of Shh signalling during tumour progression.

## Results

### Poised Shh-responsive genes are marked by a bivalent domain.

To understand the chromatin environment of poised Shh target genes, we analysed the publicly available histone modification data obtained from Shh-responsive mouse embryonic fibroblast (MEF) cells (Geo data sets GSE21271 (ref. 28)). MEFs as well as NIH3T3 mouse fibroblasts express both Gli repressors and activators and are widely used in studies of Shh signalling<sup>29</sup>. Several universal Gli target genes, such as *Gli1*, *Ptch1* and *Hhip*, are relatively restricted to the Shh pathway, and their expression reflects Shh/Gli signalling activities. In this screen, we identified an H3K27me3/H3K4me3 bivalent domain in the regulatory regions of these Shh target genes (Fig. 1a). The H3K27me3 marks are close to the previously identified Gli-binding regions<sup>30,31</sup>. These regions are close to the promoters and may represent proximal enhancers. In contrast, the Shh-independent *Gli3* gene was only marked with H3K4me3, whereas a silenced neural-specific target gene *Olig2* was only marked with H3K27me3 (Fig. 1a). We performed an RNA-seq analysis to compare expression profiles in wild-type MEFs cultured with or without Shh; expression of 25 genes was significantly induced by Shh treatment ( $P < 0.05$ ). Eighteen of these contain the bivalent chromatin domain (Supplementary Table 1). Other typical repressive marks, such as H3K9me3 and the PRC1-mediated ubiquitinated H2AK119 (refs 32,33), were not present. Thus, the poised Shh target genes may be specifically marked by the bivalent chromatin domain.

Using *Gli1* as a representative Shh target gene, we examined whether the marks in the bivalent domain changed with Shh induction. Using chromatin immunoprecipitation (ChIP), we found that H3K27me3 was present in the regulatory region of *Gli1* gene, and levels were significantly reduced on Shh treatment (Fig. 1b). H3K4me3 levels in the *Gli1* promoter were significantly increased in Shh-treated MEFs (Fig. 1b). Similar changes were observed when *Gli1* and other Shh target genes were de-repressed in *Gli3*<sup>−/−</sup> MEFs or further activated in Shh-treated *Gli3*<sup>−/−</sup> MEFs (Supplementary Figs 1 and 2). Thus, Gli-mediated Shh target gene de-repression and activation are accompanied with the removal of H3K27me3 and increase in levels of H3K4me3.

### PRC2 and Jmjd3 are important for Shh target gene expression.

To determine whether H3K27me3 reduction is a causal factor in the Shh-mediated gene activation, we manipulated the enzymes that add or erase H3K27me3 marks. The PRC2 complex, which methylates H3K27, contains three essential subunits, EZH2, SUZ12 and EED<sup>13</sup>. RNAi inhibition of *SUZ12* expression led to decreased local H3K27me3 levels and increased *Gli1* basal expression (Fig. 1c). In *EZH2*<sup>−/−</sup> MEFs<sup>34,35</sup>, global H3K27me3 levels were decreased and basal expression of Shh target genes such as *Gli1* and *Ptch1* was increased compared with those in

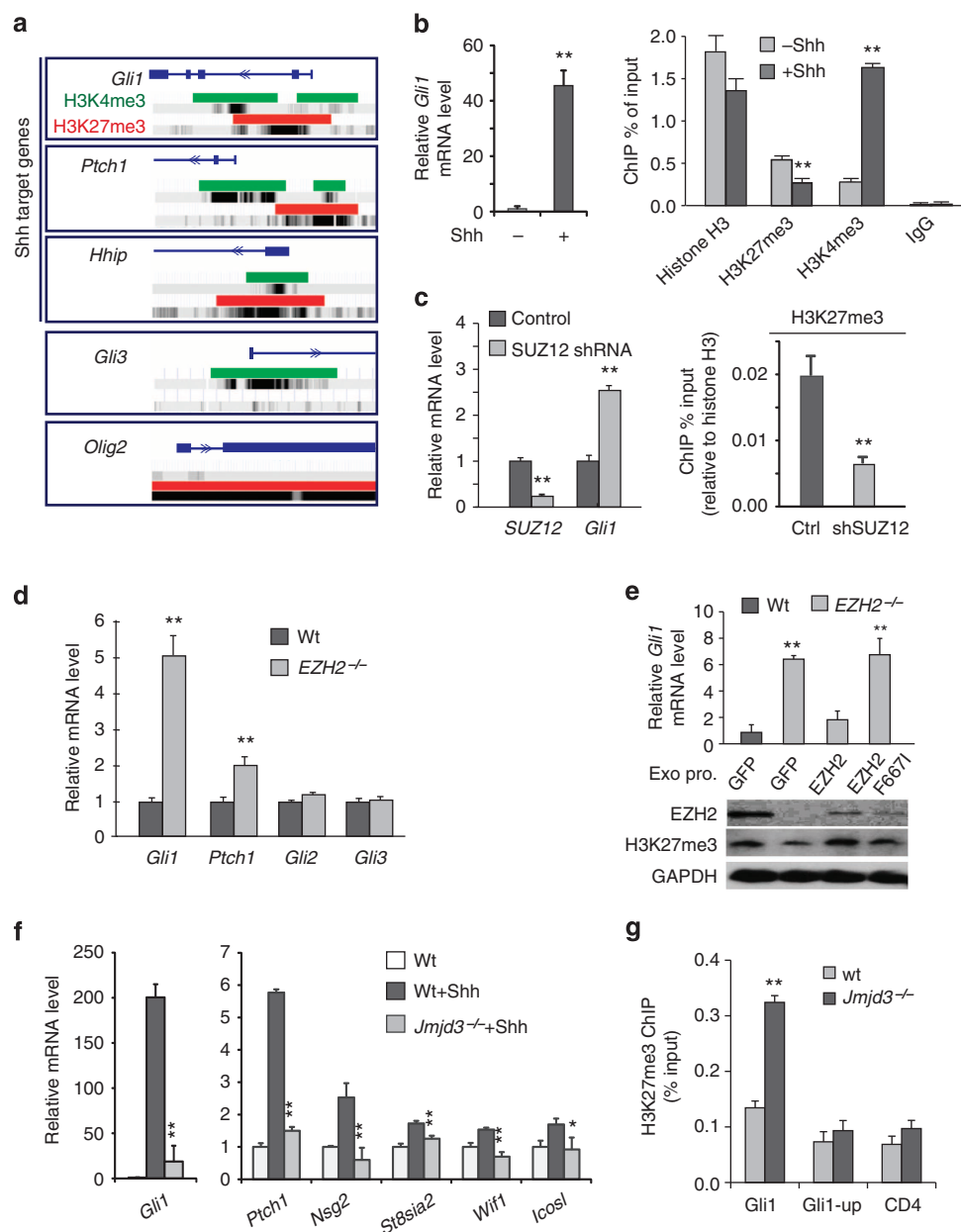


**Figure 1 | PRC2 and Jmjd3 regulate Shh target gene expression by modulating the bivalent domains.** (a) Analyses of ChIP-seq data (Geo datasets GSE21271) showed bivalent domains close to transcription start sites of Shh target genes in MEFs. Red and green bars represent the chromatin regions enriched for H3K27me3 and H3K4me3, respectively. The 5' regions of the genes are shown as blue lines. *Gli3* is not a Shh target gene; *Olig2* is a neural-specific Shh target gene not expressed in MEFs. (b) Activation of *Gli1* by addition of Shh to MEF cultures was associated with decreased H3K27me3 and increased H3K4me3 levels in the *Gli1* regulatory region. The mRNA levels were measured by RT-qPCR, and the ChIP results were analysed by ChIP-qPCR. Histone H3 and IgG ChIP were used as histone and antibody controls, respectively (means  $\pm$  s.d.,  $n = 3$ ). (c) Reducing SUZ12 levels in MEFs by shRNA treatment led to decreased local H3K27me3 levels and increased *Gli1* expression as shown by RT-qPCR. Histone H3 ChIP was used for ChIP normalization (means  $\pm$  s.d.,  $n = 3$ ). (d) Deletion of *EZH2* led to increased basal expression of *Gli1* and *Ptch1*, but not *Gli2/3*, as shown by RT-qPCR (means  $\pm$  s.d.,  $n = 3$ ). (e) Upper panel: exogenous wild-type EZH2, but not the F667I mutant, rescued *Gli1* expression defects in *EZH2*<sup>-/-</sup> MEFs as analysed by RT-qPCR. Lower panel: western blots show the expression of EZH2 and global H3K27me3 in wild-type and *EZH2*<sup>-/-</sup> MEFs (means  $\pm$  s.d.,  $n = 3$ ). (f) Wild-type and *Jmjd3*<sup>-/-</sup> MEFs were treated with Shh. RT-qPCR analyses of *Gli1*, *Ptch1* and other Shh-responsive genes are shown (means  $\pm$  s.d.,  $n = 3$ ). (g) *Jmjd3* deletion led to higher H3K27me3 levels in the *Gli1* regulatory region in Shh-treated MEFs as shown by ChIP-qPCR. A region upstream of *Gli1* and the *CD4* gene were negative controls. Significance was determined using *t*-test or ANOVA with *post hoc t*-test (means  $\pm$  s.d.,  $n = 3$ ). \*\* indicates  $P < 0.01$  and \* indicates  $P < 0.05$ .

wild-type cells (Fig. 1d). Neither *Gli2* nor *Gli3* expression was affected and *Olig2* was not de-repressed by *EZH2* deletion (Fig. 1d). Only the wild type but not an enzymatically inactive mutant EZH2 (F667I)<sup>35</sup> rescued the *Gli1* expression defect (Fig. 1e). These experiments suggest that the PRC2 complex

represses basal Shh target gene expression by maintaining the H3K27me3 mark. This mechanism also provides a possible explanation for the recent findings that *EZH2* deletion leads to a de-repression of Shh target genes in developing limbs and dorsal hindbrains<sup>36,37</sup>.

In MEFs lacking Jmjd3 ref. 25, an H3K27me3 demethylase, we observed defects in Shh-induced gene activation. The activation of several bivalent Shh-responsive genes identified in RNA-seq experiments (Supplementary Table 1) was significantly impaired in *Jmjd3*<sup>-/-</sup> MEFs (Fig. 1f). *Jmjd3* deletion resulted in higher local H3K27me3 levels in the *Gli1* gene in the presence of Shh (Fig. 1g) but not in higher global H3K27me3 levels (Supplementary Fig. 3), suggesting that Jmjd3 plays a specific role in Shh target gene activation. RNAi inhibition of *Jmjd3* expression in MEFs phenocopied the *Jmjd3*<sup>-/-</sup> defects in Shh-induced *Gli1* expression and local H3K27me3 reduction (Supplementary Fig. 4). Notably, lack of another H3K27me3 demethylase, UTX<sup>27</sup>, did not produce significant effects on Shh-induced target gene expression in MEFs (Supplementary Fig. 5). These results indicate that H3K27me3 and PRC2 are required for the repression of Shh target gene basal expression and that erasure of the mark by Jmjd3 in response to Shh is required for gene activation.

**Shh induces a local epigenetic switch from PRC2 to Jmjd3.** We next monitored the dynamic binding of PRC2 and Jmjd3 in response to Shh signalling. In the *Gli1* gene, a cluster of Gli-binding sites<sup>30,31</sup> overlaps the H3K27me3-enriched region (Supplementary Fig. 6A). Using ChIP, we demonstrated that endogenous SUZ12 and, by inference, PRC2, binds to *Gli1*; binding decreased on Shh treatment (Fig. 2a). Conversely, ChIP with a Jmjd3 antibody indicated increased binding of Jmjd3 to the *Gli1* regulatory region on Shh induction (Fig. 2b). A ChIP experiment performed in NIH3T3 cells expressing FLAG-tagged

Jmjd3 or HA-tagged EZH2 confirmed the binding dynamics: Shh treatment reduced EZH2 binding and increased Jmjd3 binding to *Gli1* (Supplementary Fig. S6). In MEFs, levels of EZH2, SUZ12 and Jmjd3 were similar with or without Shh treatment (Fig. 2c,d). Thus, the Shh-induced switch from PRC2 to Jmjd3 in these regulatory regions was not due to changes in the global levels of these factors but was likely caused by an active recruitment of Jmjd3 to replace PRC2 on Shh stimulation. Indeed, in the absence of Jmjd3, a significant amount of SUZ12 remained bound to *Gli1* in Shh-treated cells (Fig. 2a), suggesting that Jmjd3 is required for removal of PRC2 from Shh target genes.

Shh-induced *Gli1/2* activation and binding to target genes may mediate Jmjd3 recruitment. *Gli2* and Shh-induced *Gli1* both can co-immunoprecipitate with Jmjd3 (Fig. 2e,f, Supplementary Fig. 7). The exogenous tagged Jmjd3 proteins are expressed in NIH3T3 cells at relatively low levels, as it is difficult to detect the full-length Jmjd3 proteins with standard western blot. Importantly, RNAi inhibition of *Gli1/2* in Shh-treated MEF cultures (Fig. 2g) reduced Jmjd3 binding to the *Gli1* regulatory region (Fig. 2h) and increased local H3K27me3 levels (Fig. 2i), suggesting that *Gli1/2* are required for Jmjd3 binding to Shh target genes. In contrast, *Gli1/2* binding to Shh target genes was not affected by *Jmjd3* deletion (Supplementary Fig. 8). Thus, *Gli1/2* activators are required for the recruitment of Jmjd3 and possibly other coactivators to displace PRC2 and activate target gene expression. To further confirm that Jmjd3 directly regulates Gli-mediated transcription, we expressed HA-*Gli1* in MEFs and observed that the activation of endogenous Gli target genes by HA-*Gli1* was significantly impaired in *Jmjd3*<sup>-/-</sup> MEFs compared with that in wild-type cells (Fig. 2j).

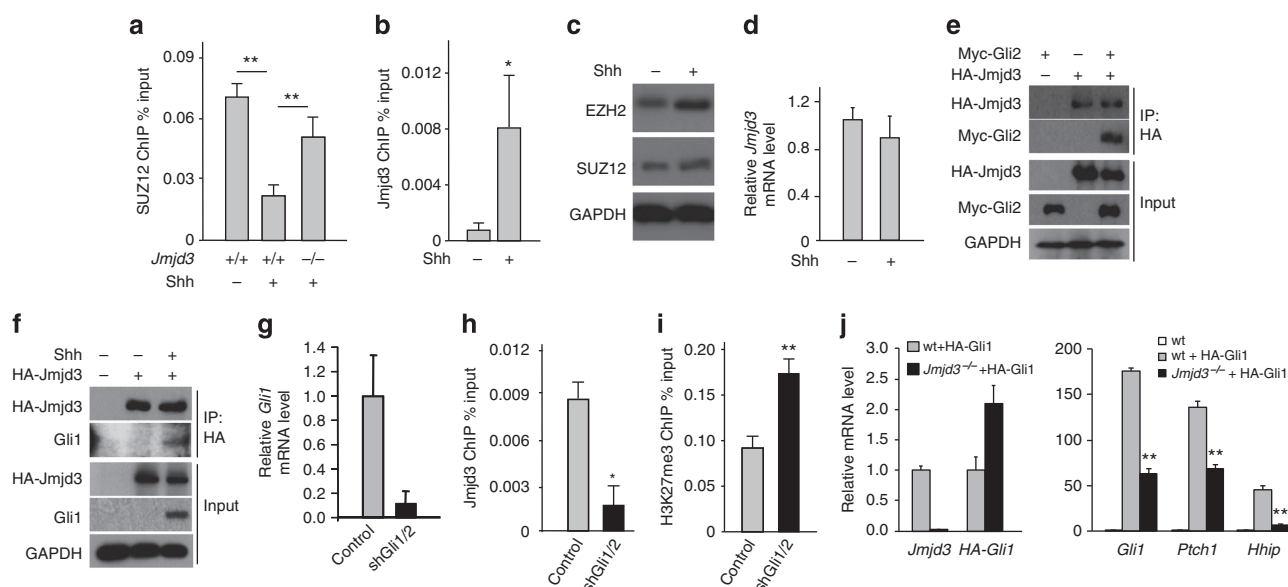


**Figure 2 | Shh induces a Gli-dependent local epigenetic switch from PRC2 to Jmjd3.** (a) ChIP-qPCR indicates the dynamic binding of endogenous SUZ12 to the *Gli1* regulatory region in wild-type and *Jmjd3*<sup>-/-</sup> MEF cells on Shh induction. (means  $\pm$  s.d.,  $n = 3$ ). (b) Increased Jmjd3 binding to *Gli1* gene on Shh treatment was shown by ChIP-qPCR (means  $\pm$  s.d.,  $n = 3$ ). (c) Shh treatment did not reduce levels of PRC2 subunits as shown by EZH2 and SUZ12 western blot. (d) *Jmjd3* expression level was not significantly changed in MEFs by Shh treatment as analysed by RT-qPCR (means  $\pm$  s.d.,  $n = 3$ ). (e) Jmjd3 co-immunoprecipitates with Gli2. Lysates of NIH3T3 cells transiently transfected with plasmids expressing HA-Jmjd3 and Myc-Gli2 were immunoprecipitated with anti-HA antibodies and blotted with antibodies against HA and Myc. (f) Jmjd3 co-immunoprecipitates with endogenous Gli1. Cell lysates of Shh-treated NIH3T3 cells expressing HA-Jmjd3 were immunoprecipitated with anti-HA antibodies and blotted with antibodies against HA and Gli1. (g) RNAi-induced inhibition of *Gli1* and *Gli2* in Shh-treated MEFs led to (h) decreased Jmjd3 binding and (i) increased H3K27me3 levels in the *Gli1* regulatory region (means  $\pm$  s.d.,  $n = 3$ ). (j) Deletion of *Jmjd3* in MEFs led to impaired endogenous Shh target gene (*Gli1*, *Ptch1*, *Hhip*) expression induced by lentiviral expressed HA-*Gli1* as shown by RT-qPCR. Expressions of endogenous *Gli1* and exogenous HA-*Gli1* were measured using primers specific for the 5'-UTR and the HA tag region, respectively. Significance was determined using *t*-test or ANOVA with *post hoc t*-test (means  $\pm$  s.d.,  $n = 3$ ). \*\* indicates  $P < 0.01$  and \* indicates  $P < 0.05$ .



**Shh-induced switch is essential for target gene expression.** To determine whether the Shh-induced, Gli-mediated PRC2 to Jmjd3 switch is required for proper target gene expression, we manipulated local PRC2 and Jmjd3 levels to perturb the epigenetic switch, either by increasing local PRC2 levels after Shh treatment or introducing Jmjd3 onto the *Gli1* gene before Shh stimulation. All three Gli proteins contain five conserved zinc-fingers that are sufficient to bind specifically to the Gli consensus sequence<sup>38</sup>. We fused the Gli3 DNA binding domain (GliDBD) to HA-tagged EZH2 and expressed this fusion in either NIH3T3 cells or MEF cells (Fig. 3a, Supplementary Fig. 9A). GliDBD-EZH2 interacted with endogenous SUZ12 as the two proteins were co-immunoprecipitated (Fig. 3b), suggesting that these proteins form a functional PRC2 complex. In the presence of Shh, GliDBD-EZH2 can bind *Gli1* and increase local H3K27me3 levels as shown by ChIP (Fig. 3c,d, Supplementary Fig. 9B,C). Both GliDBD-EZH2 and exogenous EZH2 reduced Shh-activated *Gli1* expression (Fig. 3e, Supplementary Fig. 9D). GliDBD-EZH2 repressed *Gli1* more effectively and specifically than EZH2; EZH2 also repressed another Shh-independent target gene *HoxA10* (Fig. 3e, Supplementary Fig. 9D). Thus, increasing the local PRC2 concentration in Shh-stimulated conditions effectively repressed *Gli1* expression, indicating that PRC2 must be removed to activate gene expression. Using similar approaches, we found that

GliDBD-Jmjd3 expressed in NIH3T3 cells (Fig. 3f) bound to the Shh target gene regulatory regions under basal conditions (Fig. 3g) and decreased local H3K27me3 (Fig. 3h). GliDBD-Jmjd3 activated Shh target genes even in the absence of Shh stimulation (Fig. 3i). Thus, recruitment of Jmjd3 is sufficient to increase Gli target gene expression before Shh stimulation. These data indicate that the presence of PRC2 represses the expression of Shh target genes, whereas the removal of PRC2 and the recruitment of Jmjd3 on Shh stimulation activate gene expression. Thus, the Shh-induced epigenetic switch from PRC2 to Jmjd3 is essential for target gene activation.

### Coordinated target gene activation by Jmjd3 and Set1/MLL.

Our results indicate that Jmjd3 is required for the removal of H3K27me3 and activation of Shh target genes. It is not clear whether its demethylase activity is essential and/or sufficient for this function. The C-terminal fragment of Jmjd3, encompassing the JmjdC domain, is sufficient to catalyse H3K27me3 demethylation and rescues several Jmjd3-deficient phenotypes<sup>21,25</sup>. The expression of the C-terminal fragment (aa 1,141–1,641) fused with GliDBD (GliDBD-JmjdC) was sufficient to reduce local H3K27me3 levels at *Gli1* locus (Fig. 3g,h), but it did not activate Shh target gene basal expression (Fig. 3i). Thus, the Jmjd3

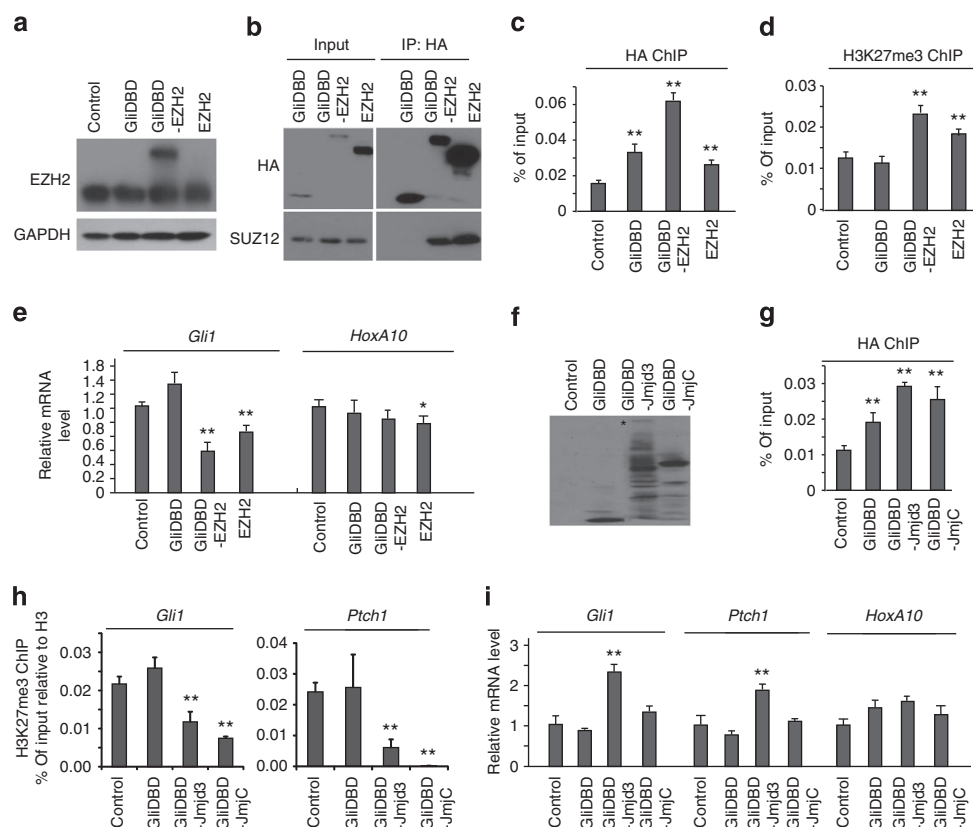


**Figure 3 | The Shh-induced local PRC2 to Jmjd3 switch is essential for proper target gene expression.** (a) Total EZH2 levels in NIH3T3 cells expressing the indicated exogenous proteins as shown by western blot with anti-EZH2 antibodies. (b) Exogenous EZH2 and GliDBD-EZH2, but not GliDBD, expressed in NIH3T3 cells interact with endogenous SUZ12 as indicated by IP with an HA antibody and western blot with SUZ12 antibody. All exogenous proteins contain an HA tag. (c) GliDBD-EZH2 proteins are recruited to *Gli1* regulatory region as indicated by ChIP-qPCR with anti-HA antibodies (means  $\pm$  s.d.,  $n = 3$ ). (d) Local H3K27me3 levels at *Gli1* regulatory region as measured by ChIP-qPCR in Shh-treated NIH3T3 cells expressing exogenous proteins (means  $\pm$  s.d.,  $n = 3$ ). (e) RT-qPCR analyses of *Gli1* and *HoxA10* in Shh-treated NIH3T3 cells expressing the indicated exogenous proteins (means  $\pm$  s.d.,  $n = 3$ ). (f) Expression of fused Jmjd3 proteins in transfected NIH3T3 cells detected by western blot using anti-HA antibodies. The full-length GliDBD-Jmjd3 protein band is marked with a star. (g) Binding of HA-tagged GliDBD fusion Jmjd3 proteins and (h) local H3K27me3 levels at *Gli1* and *Ptch1* loci as shown by ChIP-qPCR. Histone H3 ChIP was used for normalization (means  $\pm$  s.d.,  $n = 3$ ). (i) RT-qPCR analyses of *Gli1*, *Ptch1* and *HoxA10* in NIH3T3 cells expressing the indicated exogenous Jmjd3 proteins in basal conditions (means  $\pm$  s.d.,  $n = 3$ ). Significance was determined using *t*-test or ANOVA with *post hoc t*-test; \*\* indicates  $P < 0.01$  and \* indicates  $P < 0.05$ . The comparisons are all against the control samples.

enzymatic activity alone is not sufficient to activate Shh target genes. We performed rescue experiments in NIH3T3 cells co-expressing an shRNA targeting *Jmjd3* and exogenous RNAi-resistant genes encoding *Jmjd3*, the JmjC domain, or the *Jmjd3*-H1388A enzymatically inactive proteins<sup>21</sup>. The cultures were co-transfected with plasmids expressing GFP-Gli1 to activate the endogenous Shh target genes (Fig. 4a,b). Although each of these *Jmjd3* proteins bound to the *Gli1* regulatory region (Fig. 4c), only wild-type full-length *Jmjd3* rescued the defective Gli1-induced gene expression in *Jmjd3*-knockdown cells (Fig. 4a), indicating that the demethylase activity is necessary but not sufficient for activation of Gli target genes. The non-enzymatic activity of *Jmjd3* may serve to recruit other epigenetic regulators.

Activation of bivalent genes is accompanied by coordinated changes in levels of both H3K27me3 and H3K4me3. Thus, it is likely that *Jmjd3* and the Set1/MLL family of H3K4me3 methyltransferase complexes function cooperatively to regulate Shh-induced gene activation. Ash2L, RbBP5, DPY30 and WDR5 are essential subunits for all Set1/MLL family complexes<sup>39</sup>. RNAi inhibition of expression of individual subunits significantly impaired *Gli1* expression in Shh-treated NIH3T3 cells (Fig. 4d). To determine whether Shh signalling regulates Set1/MLL complex binding to Shh target genes, we performed ChIP with WDR5 antibodies. Consistent with the Shh-induced increase of local H3K4me3, the binding of endogenous WDR5 to *Gli1* and *Ptch1* regulatory regions was significantly increased on Shh treatment (Fig. 4e). Importantly, in cells deficient in *Jmjd3*, Shh-induced WDR5 binding to target genes and local H3K4me3 increases were significantly impaired (Fig. 4e). Consistent with this result, local levels of H3K4me3 in the *Gli1* gene in the presence of Shh were significantly lower in *Jmjd3*<sup>-/-</sup> MEFs than in wild-type cells (Supplementary Fig. 10). Thus, *Jmjd3* is required for Set1/MLL complexes recruitment to target genes in response to Shh stimulation.

It is not clear whether the interaction between *Jmjd3* and Set1/MLL complexes<sup>21</sup> plays a role in resolving bivalent domains; however, our co-immunoprecipitation analyses showed that interactions between *Jmjd3* and Set1/MLL subunits, WDR5 and ASH2L, were significantly enhanced by Shh stimulation (Fig. 4f, Supplementary Fig. 11). The Shh-induced *Jmjd3*-MLL interaction is potentially phosphorylation-dependent, as treating the lysate with  $\lambda$ -phosphatase reduced the interaction to the basal level (Supplementary Fig. 11). This result suggests that Shh signalling directly modulates epigenetic complexes required for target gene activation. Thus, in addition to the PRC2 to *Jmjd3* switch, Shh signalling also induces the formation of an epigenetic coactivator complex containing at least *Jmjd3* and Set1/MLL, which regulates target gene activation coordinately by modulating the bivalent domains.

### ***Jmjd3*<sup>-/-</sup> mice display Shh-dependent developmental defects.**

As *Jmjd3* is a key factor in Shh-induced epigenetic switch and gene activation, we examined its function in Shh-activation-dependent developmental processes. As shown by analysis of *Gli2*<sup>-/-</sup> mice, Gli2-mediated Shh activation is required for multiple developmental processes such as hair follicle development, ventral neural tube patterning and cerebellum progenitor proliferation<sup>8,40–42</sup>. Like *Gli2*<sup>-/-</sup> mice, *Jmjd3*<sup>-/-</sup> mice die at birth due to respiratory failure<sup>24,25,43</sup>. Interestingly, *Jmjd3*<sup>-/-</sup> mice display multiple defects similar to *Gli2*<sup>-/-</sup> mice in Shh/Gli2-dependent developmental processes.

As a morphogen, Shh is important for neural tube patterning and neural progenitor specification. During neural tube development, Shh mainly functions to antagonize GliR activity, whereas GliA is only required for the formation of the floor plate and

specification of the most ventral neural progenitors<sup>6,7</sup>. *Gli2*<sup>-/-</sup> neural tubes display reduced expression of markers for floor plate and V3 interneuron progenitors<sup>40,41</sup>. *Jmjd3* is expressed in the ventral neural tube but not in the floor plate<sup>44</sup>. In E10.5 *Jmjd3*<sup>-/-</sup> neural tubes, V3 interneuron progenitor marker *Nkx2.2* levels were significantly reduced (Supplementary Fig. 12A,A',C,C',F) and Olig2-expressing motor neuron progenitor regions were expanded (Supplementary Fig. 12B,B',C,C',F). These defects are similar to those observed in *Gli2*<sup>-/-</sup> embryos<sup>40</sup>. We also observed a reduction of FoxA2 expression in *Jmjd3*<sup>-/-</sup> neural tubes but not in the floor plate (Supplementary Fig. 12D,D'), possibly due to the absence of *Jmjd3* in the floor plate or the usage of alternative activation mechanisms. The enriched expression of *Ptch1* in the most ventral neural tubes was also reduced in *Jmjd3*<sup>-/-</sup> embryos (Supplementary Fig. 12E,E'). Thus, these results are consistent with a function of *Jmjd3* in GliA-dependent target gene expression and ventral neural tube development.

Shh-dependent Gli2 activation is essential for embryonic hair follicle development. *Gli2*<sup>-/-</sup> embryos exhibit an arrest in hair follicle development with reduced cell proliferation<sup>42</sup>. When hair follicles in the sections of E18.5 *Jmjd3*<sup>-/-</sup> skin were analysed, we observed similarly delayed development of hair follicles. Although both control (wild type and *Jmjd3*<sup>+/-</sup>) and *Jmjd3*<sup>-/-</sup> skins contain hair follicles from all stages<sup>45</sup> (stage 1 to 5, Supplementary Fig. 13A–D), *Jmjd3*<sup>-/-</sup> hair follicles were arrested at earlier developmental stages with a peak at stage 2 (Supplementary Fig. 13E). Control hair follicles grew deeper and had more mature morphologies with a peak at stage 3 (Supplementary Fig. 13E). This defect in Shh/GliA-dependent hair follicle development further corroborates the importance of *Jmjd3* in Shh signalling activation.

### ***Jmjd3* is required for Shh-dependent CGNP proliferation.**

During cerebellum development from late embryonic to the early postnatal stage (E18.5–P14), CGNPs in the external granule layer (EGL) undergo significant expansion and differentiation into granule neurons, the most abundant neuron type in the nervous system. Multiple signalling pathways and transcription factors coordinate to regulate this process, and Shh-mediated Gli activation is necessary for CGNP proliferation<sup>9–11</sup>. Interestingly, during the period from E16.5 to P5, there is a global decrease of H3K27me3 and increase of H3K4me3 and H3K27Ac in the cerebellum (Fig. 5a). The decrease of global H3K27me3 levels was apparent in EGL CGNPs (Fig. 5b) and correlated with the expression of a large amount of genes required for rapid expansion and differentiation of CGNPs at P5. Specifically, at Shh target genes, the activation of *Gli1* expression at P5 was accompanied by a decrease of H3K27me3 and an increase of H3K4me3 (Fig. 5c), which is similar to the signalling-induced resolution of the bivalent domain in MEFs. These data suggest that the Shh-induced epigenetic switch also occurs in the developing cerebellum to modulate the bivalent domain and activate target genes, which contributes to the global change of H3K27me3 levels.

Despite the low global level of H3K27me3, EZH2 protein levels remained high in P5 CGNPs (Fig. 5b), suggesting that a high level of H3K27me3 demethylase activity is present. We observed that *Jmjd3* expression was increased during cerebellar development from E16.5 to P4 (Fig. 5d). In P5 cerebellum, *Jmjd3* was enriched in EGL (Fig. 5e). Interestingly, at E18.5, *Jmjd3*<sup>-/-</sup> mice displayed decreased cerebellum size and lack of foliation (Fig. 5f), which are similar to the defects observed in the *Gli2*<sup>-/-</sup> cerebellum<sup>8</sup> and are likely caused by impaired CGNP proliferation. To directly determine the function of *Jmjd3* in



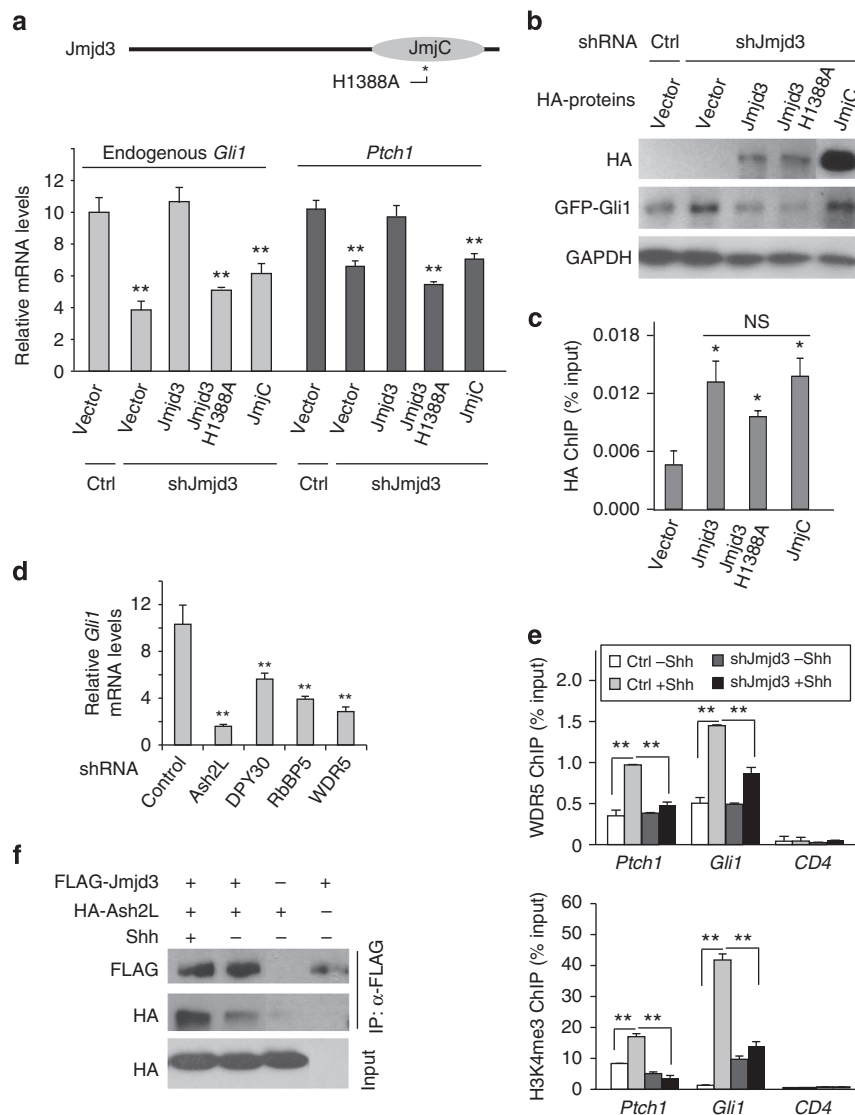


**Figure 4 | Coordinated functions of Jmjd3 and Set1/MLL regulate Shh-activated gene transcription.** (a) Both the enzymatic and non-enzymatic activities of Jmjd3 are required for its function in Shh-induced gene activation. NIH3T3 cells infected with *Jmjd3* shRNA or vector control were transfected with plasmids co-expressing GFP-Gli1 and indicated Jmjd3 proteins or vector controls. Levels of endogenous *Gli1* and *Ptch1* were determined by RT-qPCR (means  $\pm$  s.d.,  $n = 3$ ). (b) Expression of HA-tagged Jmjd3 proteins and exogenous GFP-Gli1 levels in transfected cells as detected by western blot. (c) Binding of Jmjd3 and mutants to *Gli1* regulatory region was determined by HA ChIP-qPCR. 'NS' indicates not significant (means  $\pm$  s.d.,  $n = 3$ ). (d) Set1/MLL complexes are important for Shh-induced target gene activation. RNAi-mediated inhibition of expression of individual Set1/MLL subunits Ash2L, DPY30, RbBP5 and WDR5 significantly impaired *Gli1* expression in the presence of Shh as measured by RT-qPCR (means  $\pm$  s.d.,  $n = 3$ ). (e) Shh-induced binding of WDR5 to Shh target genes requires the presence of Jmjd3. Shown are ChIP-qPCR analyses with antibodies against endogenous WDR5 and H3K4me3 in NIH3T3 cells expressing shRNA targeting *Jmjd3* or scrambled shRNA in the basal or Shh-treated conditions. *CD4* was the negative control (means  $\pm$  s.d.,  $n = 3$ ). (f) Shh enhances the interactions between Jmjd3 and Set1/MLL subunits. NIH3T3 cells co-transfected with plasmids expressing FLAG-Jmjd3 and HA-Ash2L were treated with or without Shh. An anti-FLAG antibody was used for immunoprecipitation, and antibodies against FLAG or HA were used for western blot. Significance was determined using *t*-test or ANOVA with *post hoc t*-test; \*\* indicates  $P < 0.01$  and \* indicates  $P < 0.05$ . The comparisons are all against the control samples.

CGNP proliferation, we inactivated Jmjd3 using RNAi in Shh-treated P4 CGNP cultures. Reduction of *Jmjd3* levels in CGNPs significantly impaired the expression of Shh-induced genes such as *Gli1* and mitogenic *Ccnd1* but not other genes such as *Brg1* and the CGNP marker *Math1* (Fig. 5g). The proliferation of CGNPs in which *Jmjd3* expression was inhibited was significantly impaired as shown by the lower BrdU incorporation rates compared with control cultures (Fig. 5h). Although neither Shh treatment nor *Jmjd3* inhibition in CGNPs led to global changes of histone modifications, we observed altered H3K27me3 as well as H3K4me3 and H3K27Ac levels at *Gli1* regulatory

regions in Shh-treated *Jmjd3*-deficient cultures compared with the controls (Fig. 5i-k). A Cre-induced *Jmjd3* conditional deletion<sup>46</sup> in CGNP cultures displayed similar defects in Shh target gene expression and altered histone modifications (Supplementary Fig. 14). Thus, Jmjd3 regulates Shh-activated gene expression and CGNP proliferation by modulating the chromatin environment.

**Inhibition of Jmjd3 impairs medulloblastoma cell growth.** Mutations leading to constitutively active Shh signalling cause Shh-subtype medulloblastoma, the progression of which also

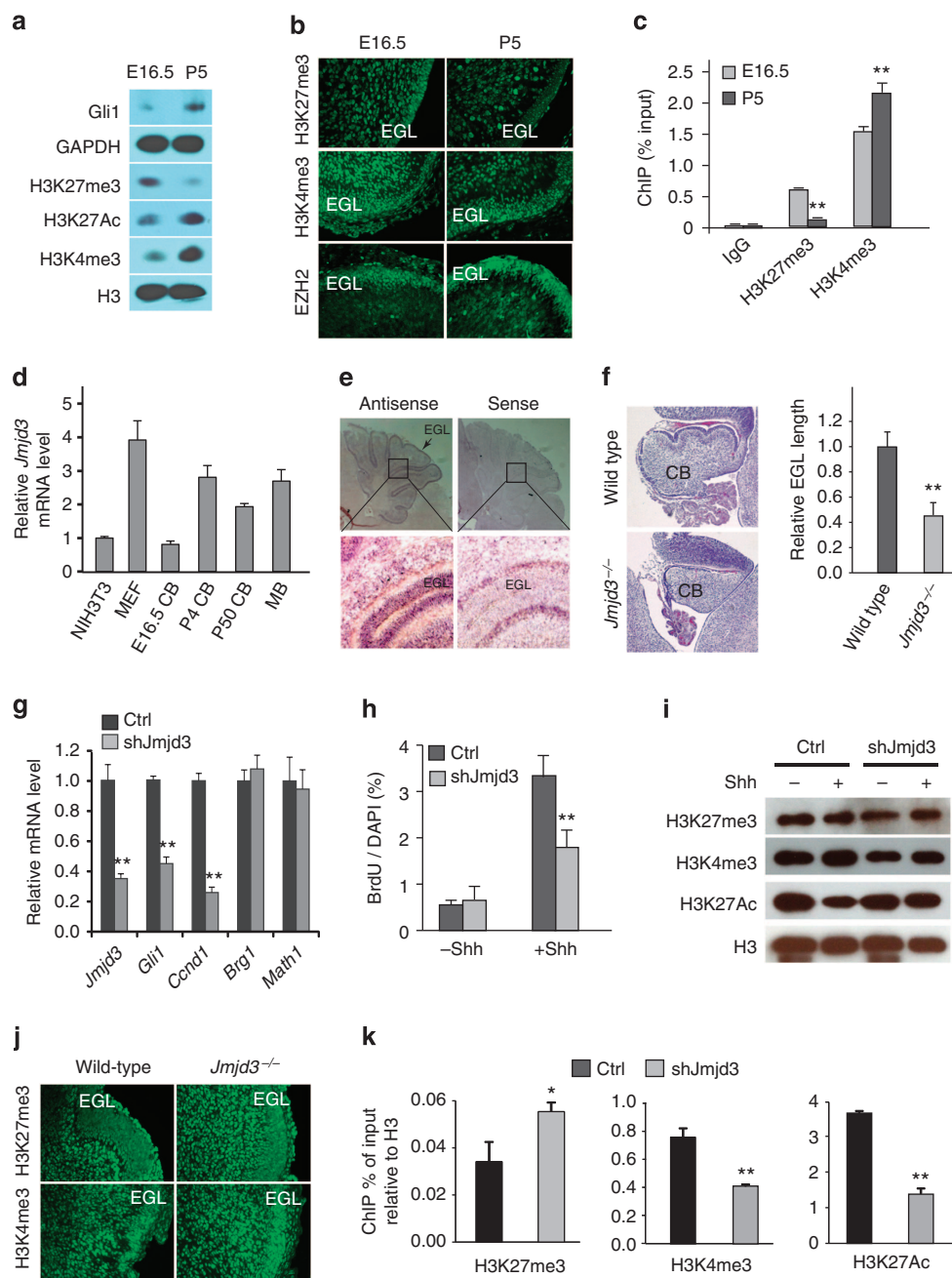


**Figure 5 | *Jmjd3* is required for Shh-dependent CGNP proliferation.** (a) Global changes of modified histone levels during cerebellum development evaluated by western blot. (b) Immunostaining of sections of E16.5 and P5 cerebella with antibodies against modified histones and EZH2. The EGL is the dense cell layer outlining the cerebellum. (c) Local changes of H3K27me3 and H3K4me3 at *Gli1* regulatory region in E16.5 and P5 cerebella (means  $\pm$  s.d.,  $n = 3$ ). (d) RT-qPCR analysis of *Jmjd3* in NIH3T3 and MEF cells and in cerebellum (CB) and medulloblastoma (MB) samples (means  $\pm$  s.d.,  $n = 3$ ). (e) In situ hybridization of P5 CB with *Jmjd3* antisense or sense probes. Note the enriched *Jmjd3* expression in EGL. (f) H&E staining of cerebella from E18.5 wild-type and *Jmjd3*<sup>-/-</sup> mice. The average length of EGL per cerebellum section is shown on the right (means  $\pm$  s.d.,  $n = 4$ ). (g) Inhibition of *Jmjd3* expression in cultured CGNPs results in defective Shh-induced gene expression as shown by RT-qPCR. (h) *Jmjd3* knockdown in cultured CGNPs decreases proliferation (as shown by BrdU incorporation) (means  $\pm$  s.d.,  $n = 3$ ). (i) Western blots indicating global histone modification levels in CGNP cultures in the absence and presence of Shh treatment with or without *Jmjd3* shRNA treatment. (j) Immunostaining of sections of E18.5 wild-type and *Jmjd3*<sup>-/-</sup> cerebella with antibodies against modified histones. (k) Decrease in *Jmjd3* levels in Shh-treated CGNP cultures by lentiviral-expressed shRNA resulted in significant changes of histone modifications at the *Gli1* regulatory region as shown by ChIP-qPCR. Histone H3 ChIP was used for normalization (means  $\pm$  s.d.,  $n = 3$ ). Significance was determined by Student's *t*-test; \*\* indicates  $P < 0.01$  and \* indicates  $P < 0.05$ .

requires the active signalling pathway<sup>4,47</sup>. Thus, as a key epigenetic coactivator of Shh target genes, *Jmjd3* might be targeted to inhibit medulloblastoma growth. We used a mouse model with a Cre-inducible *SmoM2* gene (a point mutation in *Smo*) to generate Shh-subtype medulloblastoma<sup>48</sup> (Fig. 6a).

*SmoM2*-induced medulloblastoma cells contain much lower H3K27me3 levels than normal cerebellar tissues (Fig. 6b,c). As a significant amount of EZH2 was expressed in *SmoM2*-induced medulloblastoma (Fig. 6b-d), the low H3K27me3 levels suggest that H3K27me3 demethylase is active in these tumour

cells. Notably, although *Jmjd3* is mutated in some cancers and even in non-Shh-type medulloblastoma<sup>47,49</sup>, it has not been found mutated in Shh-type medulloblastoma in several genome-wide exome-sequencing projects<sup>47,50–53</sup>, indicating a potential requirement of *Jmjd3* for these tumours.

To determine the function of *Jmjd3* in medulloblastoma, we first confirmed that in SmoM2 medulloblastoma the *Gli1* regulatory regions contain lower H3K27me3 levels and higher H3K4me3 and H3K27Ac levels than normal cerebellum (Fig. 6e). Reducing *Jmjd3* expression using virally expressed shRNA significantly impaired the expression of Shh target genes such as *Gli1*, *Ptch1*, *Ccnd1* and *N-myc* in cultured SmoM2 tumour cells (Fig. 6f). This defect was not due to the differentiation of tumour cells because the tumour progenitor marker *Math1* was not significantly reduced (Fig. 6f). Local H3K27me3 levels on the *Gli1* gene were significantly increased on inhibition of *Jmjd3* expression (Fig. 6g). The impaired Shh target gene expression in *Jmjd3*-deficient tumour cells led to a growth inhibition similar to that observed in *Gli1/2*-deficient tumour cultures as indicated by a cell survival assay (Fig. 6h). Therefore, as *Jmjd3* is required for Shh-subtype medulloblastoma growth, Shh-induced epigenetic switching events may be targeted to inhibit medulloblastoma growth.

## Discussion

In this report, we have identified a bivalent chromatin domain tightly associated with the poised states of Shh target genes. We have shown that Shh signalling induces a local epigenetic switch as well as the formation of a *Jmjd3*-centred epigenetic coactivator complex, which functions coordinately with GliA to resolve the bivalent domain and to activate transcription. We have also demonstrated the essential role of *Jmjd3* in regulating Shh-dependent developmental processes and tumour proliferation. The epigenetic mechanisms elucidated here significantly advance our understanding of Shh signalling and provide insights into the mechanisms of Shh-related cancers and diseases.

Activation of Shh signalling induces a local epigenetic switch from PRC2 to *Jmjd3* at Shh target genes to facilitate the resolution of bivalent chromatin domains. The removal of H3K27me3 in response to Shh likely resulted from both the recruitment of *Jmjd3* and the release of PRC2. We propose that, on Shh signalling stimulation, the activation and binding of Gli1/2 mediate the recruitment of *Jmjd3* and subsequently the coactivator complex, which displaces PRC2 at the regulatory regions, resolves bivalent domains and activates target genes (Supplementary Fig. 16). In the absence of *Jmjd3*, GliA binding

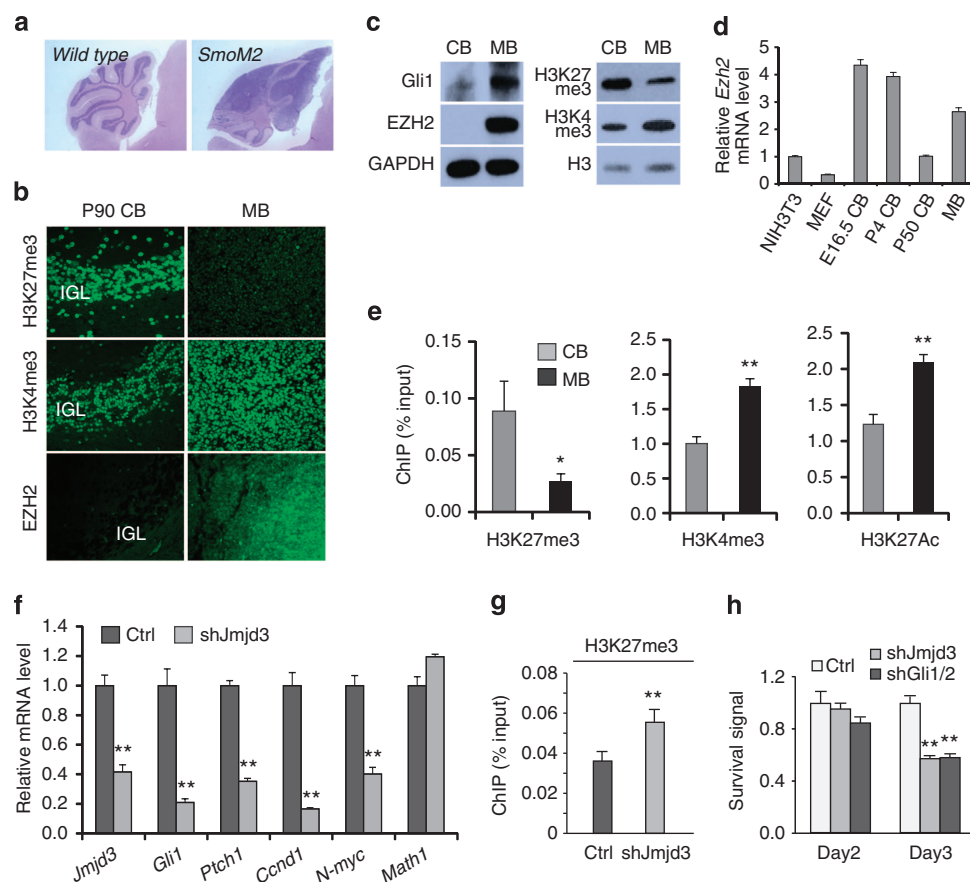


**Figure 6 | *Jmjd3* is required for Shh-subtype medulloblastoma cell growth.** (a) H&E staining of sections of a P90 normal cerebellum and one with a SmoM2-induced MB. (b) Levels of histone modifications and EZH2 in normal cerebellum (CB) and SmoM2-induced medulloblastoma (MB) were analysed by immunostaining. IGL = internal granule layers. (c) Western blots indicating global levels of histone modifications and EZH2 in normal CB and SmoM2 MB. (d) RT-qPCR analysis of *EZH2* in NIH3T3 and MEF cells and in CB and MB samples (means  $\pm$  s.d.,  $n = 3$ ). (e) ChIP-qPCR analysis of histone modification levels in the *Gli1* regulatory region in MB and normal CB. Histone H3 ChIP was used for ChIP normalization. (means  $\pm$  s.d.,  $n = 3$ ). (f) Cultured SmoM2 medulloblastoma tumour cells were infected with lentiviruses expressing either *Jmjd3* shRNA or scrambled control. Levels of Shh target genes and medulloblastoma progenitor marker *Math1* were measured with RT-qPCR (means  $\pm$  s.d.,  $n = 3$ ). (g) The H3K27me3 level in the *Gli1* gene regulatory region was increased after inhibition of *Jmjd3* expression (means  $\pm$  s.d.,  $n = 3$ ). (h) Cultured SmoM2 tumour cells were infected with viruses expressing control or shRNA targeting *Jmjd3* or *Gli1/2*. The survival rates of cells relative to the control culture were measured using the ATP cell viability assay (means  $\pm$  s.d.,  $n = 3$ ). Significance was determined by Student's *t*-test or ANOVA with *post hoc t*-test; \*\* indicates  $P < 0.01$  and \* indicates  $P < 0.05$ .

was not affected, but PRC2 release was impaired and Set1/MLL was not recruited. Although *Jmjd3* also functions in other pathways, in tissues that are predominantly dependent on GliA function, such as embryonic hair follicle, ventral neural tube, cerebellum, and Shh-type medulloblastoma, inhibition of *Jmjd3* expression and *Gli2* deletion led to similar phenotypes. Thus, *Jmjd3* plays an essential role in Shh-induced gene activation by coordinating the changes of chromatin environments. Shh signalling also significantly enhances the interactions between *Jmjd3* and Set1/MLL complexes. Although the biochemical bases for this Shh-induced interaction remain unclear, the possibility that Shh signalling directly modifies epigenetic cofactors and regulate their activities is intriguing.

Although the experiments were performed in populations of cells and we could not exclude the possibility that a fraction of the histone marks may exist in separate cells, our data strongly support the coexistence of H3K27me3 and H3K4me3 at the same loci and cooperative regulation of both marks by Shh signalling. The Shh-induced interaction between *Jmjd3* and MLL suggests that they function together to regulate both histone marks. Importantly, loss of *Jmjd3* not only affected the H3K27me3 levels at Gli target genes, but also impaired Shh-induced recruitment of Set1/MLL complexes and increase of H3K4me3 levels (Fig. 4f). In CGNPs, loss of *Jmjd3* also affected the levels of both histone marks at Shh target genes (Fig. 5k). These results could unlikely be explained if the two histone marks are in separate cells and regulated independently.

We propose that Shh-induced transcription factor exchange from GliR to GliA triggers the switch of the associated epigenetic complexes. Previous work and this report demonstrate that a complex epigenetic environment controls Shh target gene expression. It has been shown that Shh signalling also functions as switches for several epigenetic regulators that may coordinate with PRC2/*Jmjd3* to regulate transcription outcomes. We have previously reported that Shh activation enables Brg1-containing BAF chromatin remodelling complexes to switch from a repressor to an activator state, a switch likely mediated by interacting with different Gli transcription factors and other epigenetic regulators<sup>12</sup>. Brg1 may either antagonize or facilitate PRC2 function in a context-dependent manner in embryonic stem cell gene expression<sup>54</sup>. Brg1 has also been shown to interact with *Jmjd3* to induce specific target gene expression<sup>55</sup>. Thus, the Brg1 complex may coordinate with these histone modifiers to regulate Shh signalling. Indeed, deletion of *Brg1* resulted in altered histone modifications (ref. 12 and our unpublished data).

In addition, histone deacetylases (HDACs) and histone acetyl transferases (HATs) have been directly or indirectly linked to Shh signalling transcription regulation<sup>12,56–58</sup>. Interestingly, Shh signalling activities also alter HDAC function. In basal conditions, HDACs are likely involved in repressing the expression of Shh target genes by deacetylating histones<sup>12</sup>. However, on signal activation, HDAC1/2 function as activators of Shh target genes possibly by deacetylating and activating *Gli1/2* (refs 12,56). HDACs have been shown to tightly interact with Brg1 as well as PRC2 complexes<sup>12,59</sup>. Deletion of the gene encoding PRC2 subunit EZH2 led to global increase of H3K27Ac<sup>35,60</sup> (Supplementary Fig. 15). On Shh stimulation, the resolution of the bivalent domain is also accompanied with an increase of H3K27Ac at the regulatory regions (Supplementary Fig. 2). It is not clear whether the increased H3K27Ac is a byproduct of H3K27me3 loss or due to active recruitment of the H3K27 acetyltransferase p300/CBP<sup>60,61</sup>. In addition, *Jmjd3* has been shown to interact with proteins involved in transcription elongation<sup>62</sup>, which may also function to regulate Shh signalling.

During development, Shh can function as a mitogen or a morphogen. For the mitogenic function, Shh-induced GliA-

mediated transcription activation is required. In this study, we demonstrated that during cerebellum development, when active Shh signalling plays an essential role in CGNP proliferation, Shh activation is accompanied by a decrease of H3K27me3 and an increase of H3K4me3 levels. Shh-subtype medulloblastomas are characterized by low levels of H3K27me3. We have shown that a key epigenetic factor *Jmjd3* is required for the histone modification changes and Shh target gene activation in CGNPs and medulloblastoma cells. Deletion of *Jmjd3* affects cerebellum growth and CGNP proliferation. Inhibiting enzymatic and/or non-enzymatic activities of *Jmjd3* may effectively inhibit medulloblastoma growth.

In addition to the mitogenic function, Shh also functions as a morphogen to induce dosage-dependent expression of target genes<sup>2</sup>. The diverse outputs of Shh signalling are thought to be determined by the combination of activities of GliA and GliR<sup>6,7,63</sup>. Thus, the mechanisms that underlie basal versus signalling-induced conditions identified here might also function in more complicated Shh-responsive systems. The morphogenic activities of Shh signalling are largely mediated by antagonizing GliR function<sup>64,65</sup>. We identified PRC2 as a corepressor of Shh target genes. However, we believe that PRC2 is only part of a complex corepressor network associated with GliR. GliA activities are required in the areas receiving highest Shh signalling. We also showed modest but significant defects in *Jmjd3*<sup>-/-</sup> neural tubes in the most ventral area. Recent studies have revealed that the dosage-dependent transcription response to Shh results from different affinities for Gli-binding sites, other tissue-specific transcription factors, and functional interactions between different target genes<sup>6,7,63</sup>. It is likely that chromatin environment and epigenetic regulators also play important roles in determining the transcription outcomes of target genes in response to Shh. Additional genetic tools as well as more sensitive ChIP techniques will be needed to directly analyse the epigenetic regulation of the complex Shh-responsive systems.

In summary, our study revealed a novel epigenetic mechanism that regulates Shh-induced gene activation. We identified *Jmjd3* as a key regulator of Shh-activated gene expression and Shh-dependent developmental processes and tumour growth. In the future, the characterization of the components and analysis of the dynamics of epigenetic complexes downstream of Shh signalling will reveal the mechanisms underlying the diverse transcription activities of the signalling during development and in diseases.

## Methods

**Mice.** *Jmjd3*<sup>-/-</sup> MEFs were produced from E15.5 *Jmjd3*<sup>-/-</sup> embryos<sup>25</sup>. This allele deletes exons 14–21, which encode a region that includes the JmJC demethylase domain. RT-PCR primers *Jmjd3*\_koF1 and *Jmjd3*\_koR1 (Supplementary Information) were used to detect the deletion of the *Jmjd3* mRNA. E10.5 and E18.5 *Jmjd3*<sup>-/-</sup> embryos were produced from mice containing a *Jmjd3*/*Kdm6b*<sup>tm1(KOMP)Wisi</sup> allele (Shpargel and Magnuson, unpublished data). This allele with exons 11–20 replaced by a Neo cassette was targeted by Knockout Mouse Project (KOMP) in JM8 embryonic stem cells of C57BL/6N origin. Embryonic stem cells were injected into C57BL/6J-*Tyr*<sup>c-2j</sup>/J blastocysts. Following germline transmission, mice were maintained on the C57BL/6J background. Homozygotes were generated by heterozygous intercrosses. Both *Jmjd3* alleles delete a large portion of the protein, and these mice die at birth due to respiratory defects, which is similar to the phenotype of another *Jmjd3* knockout allele<sup>24</sup>. Both alleles also result in similar skin and cerebellum defects at E18.5 and are likely null alleles. *Jmjd3* conditional knockout allele was generated as previously described with exons 15 to 21 flanked by two LoxP sites<sup>46</sup>. SmoM2 mice<sup>48</sup> and CAG-CreER<sup>66</sup> mice were purchased from Jackson Laboratory. The SmoM2 CAG-CreER mice have a high rate of spontaneous medulloblastoma development before 2 months of age (~40%). These mice were maintained on a mixed genetic background at UT Southwestern Medical Center Animal Facility.

**Primary MEF, CGNP and medulloblastoma cell cultures.** Primary MEFs were cultured from E13.5 to E15.5 embryos as described previously<sup>12</sup>. In brief, embryo trunks were dissected, trypsinized, dissociated to single cells and cultured in DMEM



media with 10% fetal bovine serum. Primary CGNP cultures were derived from dissociated P4 mouse cerebella and cultured in DMEM/F12 media containing 25 mM KCl, N<sub>2</sub> and 10% FBS. For Shh stimulation, Shh-conditioned medium produced from Shh-CM 293T cells<sup>67</sup> was added at a 1:20 dilution to MEF and CGNP cultures. MEF cells were treated with Shh in low-serum media 24 h before harvesting. CGNP cells were treated with Shh in high-serum media for 2–3 days. BrdU was added 2 h before analyses. Tumour cells were derived from dissociated SmoM2 medulloblastoma and cultured in the media containing DMEM/F12, B27, N2, EGF and FGF2.

**Plasmid construction, virus preparation and transfection/infection.** The shRNA sequences targeting *Jmjd3* (5'-AGCACTCGATGCCTCATTCATA-3' (ref. 21), *Ash2L* (5'-CGAGTCTTGTTAGCCCTACAT-3'), *DPY30* (5'-GCGTTGA GAGAATAGTCGAAA-3'), *RbBP5* (5'-GCTCTATTGTATTACCCATT-3'), *WDR5* (5'-GCCGTTTCATTCAACCGTGAT-3'), *Gli1* (5'-GCTCAGCTGTGTGTAATTAC-3') and *Gli2* (5'-CCAACCAGAACAGCAGAACAA-3') were cloned into the PLKO lentiviral vector. The PLKO construct with a scrambled shRNA sequence was used as a negative control. Lentiviral vector pSin4-EF2-IRES-Puro was used to generate expression constructs for tagged Gli, Jmjd3, Ash2L, WDR5 and EZH2. GliDBD fusion proteins were generated by fusing the Gli3 Zinc-finger domains (aa 477–636) with EZH2, Jmjd3 full-length protein or the C-terminal fragment including JmJC domain (aa 1,141–1,641). Lentiviruses were prepared according to a previously described procedure<sup>12</sup>. PolyJet (Signagen) was used for plasmid transfection of cultured cells. Attached cultured cells were infected at a multiplicity of infection (MOI) of 5 for 24 h in media with 8  $\mu\text{g ml}^{-1}$  polybrene.

**RNA-seq.** Cultured primary MEFs (second passage) were treated with or without Shh-conditioned media for 24 h before harvesting. Total RNAs were extracted, and RNA-seq libraries were prepared using Illumina RNA-Seq Preparation Kit and sequenced by an HiSeq 2000 sequencer. RNA-seq reads were mapped using TopHat with default settings (<http://tophat.cbcb.umd.edu>). The mapped reads with the Phred quality score <20 were filtered out, whereas the duplicates were marked but not removed using SAMTOOLS<sup>68</sup> and PICARD (<http://picard.sourceforge.net>). Transcript assembly and transcript abundance quantification were carried out using CUFFLINKS, and then differential expression analysis between Shh-treated and untreated MEFs was performed using CUFFDIFF<sup>69</sup>. The differentially expressed genes with  $P < 0.05$  were selected for histone modification analyses (Supplementary Table 1).

**Immunoblotting.** For immunoblotting, cells or tissues were lysed in RIPA buffer (50 mM Tris, pH 8, 250 mM NaCl, 0.05% SDS, 0.5% DOC, 1% NP-40). Histone fractions were prepared with standard acid extraction (0.2 N HCl). Cell lysates or histone fractions were separated on SDS-PAGE (SDS-polyacrylamide gel electrophoresis) gels. Antibodies used were mouse monoclonal antibodies against Gli1 (#2643, Cell Signalling), HA (HA-7, Sigma), GAPDH (G9545, Sigma), H3K27me3 (#39536, Active Motif), H3H4me3 (ab8580, Abcam), H3K27Ac (ab4729, Abcam), histone H3 (ab1791, Abcam), Myc (9E10, Bishop), EZH2 (612667, BD Biosciences), SUZ12 (#3737, Cell Signalling) and FLAG (F1804, M2, Sigma). HRP-conjugated secondary antibodies were purchased from Jackson Immunology. Uncropped immunoblots are shown in Supplementary Fig. 17.

**Immunohistology and *in situ* hybridization.** Timed mouse pregnancies were determined by plugging date as day 0.5. Haematoxylin and eosin (H&E) staining and immunostaining were performed on paraffin sections. Antibodies used were against Olig2 (AB9610, Chemicon), NKX2.2 (74.5A5-s, DSHB, University of Iowa), FoxA2 (4C7-s, DSHB, University of Iowa), EZH2 (#3737, BD Bioscience), H3K4me3 (C42D8, Cell Signalling) and H3K27me3 (07-449, Millipore). The images were visualized using an Olympus BX50 microscope. *In situ* hybridization analyses were performed as described previously<sup>12</sup> on cryosections (P5 cerebellum) or paraffin sections (E10.5 neural tubes). The *Ptch1* and *Jmjd3* probes correspond to nucleotides (nts) 850–1,637 and nts 925–1,720 of their cDNAs, respectively.

**Co-immunoprecipitation experiments.** Antibodies were against the HA-tag (ab9110, rabbit, Abcam) or FLAG-tag (F2426, M2 beads, Sigma). Shh-responsive NIH3T3 cells were transiently transfected with plasmids expressing HA- or FLAG-tagged proteins using PolyJet (Signagen). Mock transfection was used as the negative control. Cells were harvested 24–48 h after transfection and were lysed with co-IP Lysis Buffer (50 mM Tris, pH 8.0, 150 mM NaCl, 1 mM EDTA, 1% Triton X-100, with protease inhibitor freshly added). Cell lysates were snap-frozen in liquid nitrogen and then thawed on ice followed by sonication to facilitate cell lysis. After centrifugation, appropriate antibodies were added to pre-cleared cell lysate and incubated at 4 °C overnight. Samples were incubated with protein A beads (GE Healthcare) for 1 h; beads were washed with co-IP buffer four times. Precipitated proteins were eluted by boiling in 2 × Sample Buffer before SDS-PAGE and western blot analysis. For  $\lambda$ -phosphatase treatment, 400 U of enzyme (Sigma) was added to cell lysates followed by 30 min incubation at 37 °C.

**Chromatin immunoprecipitation.** ChIP experiments were performed as described previously<sup>12</sup>. Dissociated cells were crosslinked with PFA or double crosslinked with DSG (Pierce) and PFA, and sonicated to fragments (200–1,000 bp). Antibodies used were against H3K27me3 (07-449, Millipore), H3K4me3 (ab8580, Abcam), H3K27Ac (ab4729, Abcam), histone H3 (ab1791, Abcam), SUZ12 (#3737, Cell Signalling), EZH2 (612667, BD Bioscience), Jmjd3 (ab85392, Abcam)<sup>70</sup>, WDR5 (A302-429A, Bethyl Laboratories), HA (ab9110, Abcam) and FLAG (F1804, M2, Sigma). Rabbit IgG was used as a negative control. Precipitated DNA was purified and subjected to real-time PCR.

**RT-PCR and q-PCR.** RNAs from cells or tissues were extracted with TRIZOL (Invitrogen) or the RNeasy kit (Qiagen). cDNAs were synthesized by reverse transcription using Superscript III (Invitrogen), followed by PCR or quantitative PCR analysis. An ABI-7500 real-time PCR system was used for quantitative PCR. Levels of *GAPDH* mRNA were used to normalize input RNA. Graphics shown are representative of experiments performed in triplicate. Experiments were repeated for at least three times. Standard errors were calculated according to a previously described method<sup>12</sup>. The primer sequences are listed in the Supplementary Information.

**Statistical analysis.** Data are expressed as means  $\pm$  s.d. Statistical analysis was performed by either analysis of variance with ANOVA *post hoc t*-test for multiple comparisons or a two-tailed unpaired Student's *t*-test. A *P* value of <0.05 was considered significant.

## References

- Jiang, J. & Hui, C. C. Hedgehog signaling in development and cancer. *Dev. Cell* **15**, 801–812 (2008).
- Fuccillo, M., Joyner, A. L. & Fishell, G. Morphogen to mitogen: the multiple roles of hedgehog signalling in vertebrate neural development. *Nat. Rev. Neurosci.* **7**, 772–783 (2006).
- Ingham, P. W., Nakano, Y. & Seger, C. Mechanisms and functions of Hedgehog signalling across the metazoa. *Nat. Rev. Genet.* **12**, 393–406 (2011).
- Barakat, M. T., Humke, E. W. & Scott, M. P. Learning from Jekyll to control Hyde: Hedgehog signaling in development and cancer. *Trends Mol. Med.* **16**, 337–348 (2010).
- Gilbertson, R. J. & Ellison, D. W. The origins of medulloblastoma subtypes. *Annu. Rev. Pathol.* **3**, 341–365 (2008).
- Oosterveen, T. *et al.* Mechanistic differences in the transcriptional interpretation of local and long-range shh morphogen signaling. *Dev. Cell* **23**, 1006–1019 (2012).
- Peterson, K. A. *et al.* Neural-specific Sox2 input and differential Gli-binding affinity provide context and positional information in Shh-directed neural patterning. *Genes Dev.* **26**, 2802–2816 (2012).
- Corrales, J. D., Rocco, G. L., Blaess, S., Guo, Q. & Joyner, A. L. Spatial pattern of sonic hedgehog signaling through Gli genes during cerebellum development. *Development* **131**, 5581–5590 (2004).
- Dahmane, N. & Ruiz i Altaba, A. Sonic hedgehog regulates the growth and patterning of the cerebellum. *Development* **126**, 3089–3100 (1999).
- Wallace, V. A. Purkinje-cell-derived Sonic hedgehog regulates granule neuron precursor cell proliferation in the developing mouse cerebellum. *Curr. Biol.* **9**, 445–448 (1999).
- Wechsler-Reya, R. J. & Scott, M. P. Control of neuronal precursor proliferation in the cerebellum by Sonic Hedgehog. *Neuron* **22**, 103–114 (1999).
- Zhan, X., Shi, X., Zhang, Z., Chen, Y. & Wu, J. I. Dual role of Brg chromatin remodeling factor in Sonic hedgehog signaling during neural development. *Proc. Natl Acad. Sci. USA* **108**, 12758–12763 (2011).
- Margueron, R. & Reinberg, D. The Polycomb complex PRC2 and its mark in life. *Nature* **469**, 343–349 (2011).
- Bernstein, B. E. *et al.* A bivalent chromatin structure marks key developmental genes in embryonic stem cells. *Cell* **125**, 315–326 (2006).
- Mills, A. A. Throwing the cancer switch: reciprocal roles of polycomb and trithorax proteins. *Nat. Rev. Cancer* **10**, 669–682 (2010).
- Voigt, P., Tee, W. W. & Reinberg, D. A double take on bivalent promoters. *Genes Dev.* **27**, 1318–1338 (2013).
- Cao, R. *et al.* Role of histone H3 lysine 27 methylation in Polycomb-group silencing. *Science* **298**, 1039–1043 (2002).
- Agger, K. *et al.* UTX and JMJD3 are histone H3K27 demethylases involved in HOX gene regulation and development. *Nature* **449**, 731–734 (2007).
- Lan, F. *et al.* A histone H3 lysine 27 demethylase regulates animal posterior development. *Nature* **449**, 689–694 (2007).
- Lee, M. G. *et al.* Demethylation of H3K27 regulates polycomb recruitment and H2A ubiquitination. *Science* **318**, 447–450 (2007).
- De Santa, F. *et al.* The histone H3 lysine-27 demethylase Jmjd3 links inflammation to inhibition of polycomb-mediated gene silencing. *Cell* **130**, 1083–1094 (2007).

22. Hong, S. *et al.* Identification of JmjC domain-containing UTX and JMJD3 as histone H3 lysine 27 demethylases. *Proc. Natl Acad. Sci. USA* **104**, 18439–18444 (2007).
23. Cho, Y. W. *et al.* PTIP associates with MLL3- and MLL4-containing histone H3 lysine 4 methyltransferase complex. *J. Biol. Chem.* **282**, 20395–20406 (2007).
24. Burgold, T. *et al.* The H3K27 demethylase JMJD3 is required for maintenance of the embryonic respiratory neuronal network, neonatal breathing, and survival. *Cell Rep.* **2**, 1244–1258 (2012).
25. Satoh, T. *et al.* The Jmjd3-Irf4 axis regulates M2 macrophage polarization and host responses against helminth infection. *Nat. Immunol.* **11**, 936–944 (2010).
26. Shpargel, K. B., Sengoku, T., Yokoyama, S. & Magnuson, T. UTX and UTY demonstrate histone demethylase-independent function in mouse embryonic development. *PLoS. Genet.* **8**, e1002964 (2012).
27. Wang, C. *et al.* UTX regulates mesoderm differentiation of embryonic stem cells independent of H3K27 demethylase activity. *Proc. Natl Acad. Sci. USA* **109**, 15324–15329 (2012).
28. Bilodeau, S., Kagey, M. H., Frampton, G. M., Rahl, P. B. & Young, R. A. SetDB1 contributes to repression of genes encoding developmental regulators and maintenance of ES cell state. *Genes Dev.* **23**, 2484–2489 (2009).
29. Taipale, J. *et al.* Effects of oncogenic mutations in Smoothened and Patched can be reversed by cyclopamine. *Nature* **406**, 1005–1009 (2000).
30. Lee, E. Y. *et al.* Hedgehog pathway-regulated gene networks in cerebellum development and tumorigenesis. *Proc. Natl Acad. Sci. USA* **107**, 9736–9741 (2010).
31. Vokes, S. A., Ji, H., Wong, W. H. & McMahon, A. P. A genome-scale analysis of the cis-regulatory circuitry underlying sonic hedgehog-mediated patterning of the mammalian limb. *Genes Dev.* **22**, 2651–2663 (2008).
32. Kallin, E. M. *et al.* Genome-wide uH2A localization analysis highlights Bmi1-dependent deposition of the mark at repressed genes. *PLoS Genet.* **5**, e1000506 (2009).
33. Mikkelsen, T. S. *et al.* Genome-wide maps of chromatin state in pluripotent and lineage-committed cells. *Nature* **448**, 553–560 (2007).
34. Su, I. H. *et al.* Ezh2 controls B cell development through histone H3 methylation and Igh rearrangement. *Nat. Immunol.* **4**, 124–131 (2003).
35. Wang, L., Jin, Q., Lee, J. E., Su, I. H. & Ge, K. Histone H3K27 methyltransferase Ezh2 represses Wnt genes to facilitate adipogenesis. *Proc. Natl Acad. Sci. USA* **107**, 7317–7322 (2010).
36. Wyngaarden, L. A., Delgado-Olguin, P., Su, I. H., Bruneau, B. G. & Hoppyan, S. Ezh2 regulates anteroposterior axis specification and proximodistal axis elongation in the developing limb. *Development* **138**, 3759–3767 (2011).
37. Di Meglio, T. *et al.* Ezh2 orchestrates topographic migration and connectivity of mouse precerebellar neurons. *Science* **339**, 204–207 (2013).
38. Pavletich, N. P. & Pabo, C. O. Crystal structure of a five-finger GLI-DNA complex: new perspectives on zinc fingers. *Science* **261**, 1701–1707 (1993).
39. Smith, E., Lin, C. & Shilatifard, A. The super elongation complex (SEC) and MLL in development and disease. *Genes Dev.* **25**, 661–672 (2011).
40. Ding, Q. *et al.* Diminished Sonic hedgehog signaling and lack of floor plate differentiation in Gli2 mutant mice. *Development* **125**, 2533–2543 (1998).
41. Lei, Q., Zelman, A. K., Kuang, E., Li, S. & Matise, M. P. Transduction of graded Hedgehog signaling by a combination of Gli2 and Gli3 activator functions in the developing spinal cord. *Development* **131**, 3593–3604 (2004).
42. Mill, P. *et al.* Sonic hedgehog-dependent activation of Gli2 is essential for embryonic hair follicle development. *Genes Dev.* **17**, 282–294 (2003).
43. De Santa, F. *et al.* Jmjd3 contributes to the control of gene expression in LPS-activated macrophages. *EMBO J.* **28**, 3341–3352 (2009).
44. Estaras, C. *et al.* Genome-wide analysis reveals that Smad3 and JMJD3 HDM co-activate the neural developmental program. *Development* **139**, 2681–2691 (2012).
45. Paus, R. *et al.* A comprehensive guide for the recognition and classification of distinct stages of hair follicle morphogenesis. *J. Invest. Dermatol.* **113**, 523–532 (1999).
46. Zhao, W. *et al.* Jmjd3 inhibits reprogramming by upregulating expression of INK4a/Arf and targeting PHF20 for ubiquitination. *Cell* **152**, 1037–1050 (2013).
47. Parsons, D. W. *et al.* The genetic landscape of the childhood cancer medulloblastoma. *Science* **331**, 435–439 (2011).
48. Mao, J. *et al.* A novel somatic mouse model to survey tumorigenic potential applied to the Hedgehog pathway. *Cancer Res.* **66**, 10171–10178 (2006).
49. Berger, M. F. *et al.* Melanoma genome sequencing reveals frequent PREX2 mutations. *Nature* **485**, 502–506 (2012).
50. Robinson, G. *et al.* Novel mutations target distinct subgroups of medulloblastoma. *Nature* **488**, 43–48 (2012).
51. Jones, D. T. *et al.* Dissecting the genomic complexity underlying medulloblastoma. *Nature* **488**, 100–105 (2012).
52. Northcott, P. A. *et al.* Subgroup-specific structural variation across 1,000 medulloblastoma genomes. *Nature* **488**, 49–56 (2012).
53. Pugh, T. J. *et al.* Medulloblastoma exome sequencing uncovers subtype-specific somatic mutations. *Nature* **488**, 106–110 (2012).
54. Ho, L. *et al.* esBAF facilitates pluripotency by conditioning the genome for LIF/STAT3 signalling and by regulating polycomb function. *Nat. Cell Biol.* **13**, 903–913 (2011).
55. Miller, S. A., Mohn, S. E. & Weinmann, A. S. Jmjd3 and UTX play a demethylase-independent role in chromatin remodeling to regulate T-box family member-dependent gene expression. *Mol. Cell* **40**, 594–605 (2010).
56. Canettieri, G. *et al.* Histone deacetylase and Cullin3-REN(KCTD11) ubiquitin ligase interplay regulates Hedgehog signalling through Gli acetylation. *Nat. Cell Biol.* **12**, 132–142 (2010).
57. Dai, P. *et al.* Sonic Hedgehog-induced activation of the Gli1 promoter is mediated by GLI3. *J. Biol. Chem.* **274**, 8143–8152 (1999).
58. Malatesta, M. *et al.* Histone acetyltransferase PCAF is required for Hedgehog-Gli-dependent transcription and cancer cell proliferation. *Cancer Res.* **73**, 6323–6333 (2013).
59. van der Vlag, J. & Otte, A. P. Transcriptional repression mediated by the human polycomb-group protein EED involves histone deacetylation. *Nat. Genet.* **23**, 474–478 (1999).
60. Pasini, D. *et al.* Characterization of an antagonistic switch between histone H3 lysine 27 methylation and acetylation in the transcriptional regulation of Polycomb group target genes. *Nucleic Acids Res.* **38**, 4958–4969 (2010).
61. Jin, Q. *et al.* Distinct roles of GCN5/PCAF-mediated H3K9ac and CBP/p300-mediated H3K18/27ac in nuclear receptor transactivation. *EMBO J.* **30**, 249–262 (2011).
62. Chen, S. *et al.* The histone H3 Lys 27 demethylase JMJD3 regulates gene expression by impacting transcriptional elongation. *Genes Dev.* **26**, 1364–1375 (2012).
63. Balaskas, N. *et al.* Gene regulatory logic for reading the Sonic Hedgehog signaling gradient in the vertebrate neural tube. *Cell* **148**, 273–284 (2012).
64. Rallu, M. *et al.* Dorsoventral patterning is established in the telencephalon of mutants lacking both Gli3 and Hedgehog signaling. *Development* **129**, 4963–4974 (2002).
65. Wijgerde, M., McMahon, J. A., Rule, M. & McMahon, A. P. A direct requirement for Hedgehog signaling for normal specification of all ventral progenitor domains in the presumptive mammalian spinal cord. *Genes Dev.* **16**, 2849–2864 (2002).
66. Hayashi, S. & McMahon, A. P. Efficient recombination in diverse tissues by a tamoxifen-inducible form of Cre: a tool for temporally regulated gene activation/inactivation in the mouse. *Dev. Biol.* **244**, 305–318 (2002).
67. Chen, J. K., Taipale, J., Young, K. E., Maiti, T. & Beachy, P. A. Small molecule modulation of Smoothened activity. *Proc. Natl Acad. Sci. USA* **99**, 14071–14076 (2002).
68. Li, H. *et al.* The Sequence Alignment/Map format and SAMtools. *Bioinformatics* **25**, 2078–2079 (2009).
69. Trapnell, C. *et al.* Transcript assembly and quantification by RNA-Seq reveals unannotated transcripts and isoform switching during cell differentiation. *Nat. Biotechnol.* **28**, 511–515 (2010).
70. Sen, G. L., Webster, D. E., Barragan, D. I., Chang, H. Y. & Khavari, P. A. Control of differentiation in a self-renewing mammalian tissue by the histone demethylase JMJD3. *Genes Dev.* **22**, 1865–1870 (2008).

## Acknowledgements

We thank Qiu Wang and Yu Chen for technical support, Dr Chao Xing for RNA-seq analyses and Dr Jin Jiang for reagents and critical discussion. This work was supported by grants from March of Dimes Foundation (J.W.), American Cancer Society (J.W.), NIH (R21MH102820, J.W.) and Department of Defense Visionary postdoc fellowship (X.S.).

## Author contributions

J.W., X.S. and Z.Z. designed the experiments. X.S., Z.Z., X.Z., M.C. and J.W. performed the experiments, collected the data and analysed the results. T.S., S.A., K.S., T.M., Q.L., R.W., C.W. and K.G. provided critical reagents. J.W. wrote the paper with help from all authors.

## Additional information

**Accession codes.** NCBI SRA SRP047495 for RNA-seq analyses of Shh-responsive genes in MEF cells.

**Supplementary Information** accompanies this paper at <http://www.nature.com/naturecommunications>

**Competing financial interests:** The authors declare no competing financial interests.

**Reprints and permission** information is available online at <http://www.nature.com/reprintsandpermissions/>

**How to cite this article:** Shi, X. *et al.* An Epigenetic switch induced by Shh signalling regulates gene activation during development and medulloblastoma growth. *Nat. Commun.* 5:5425 doi: 10.1038/ncomms6425 (2014).

Print


**ANNUAL  
MEETING 2014**
**HARNESSING  
BREAKTHROUGHS  
TARGETING  
CURES**

**April 5-9, 2014  
San Diego, CA**
**Category: Molecular and Cellular Biology**
**Session Title: Epigenetics 2**

**#404 Function of Brg1 chromatin remodeling factor in sonic hedgehog-dependent medulloblastoma development.** Xuanming Shi, Zilai Zhang, Qiu Wang, Jiang Wu. UT Southwestern Medical Ctr., Dallas, TX.

Medulloblastoma is the most common malignant pediatric brain tumor. Overactive Shh signaling in cerebellum granule neuron precursors (CGNPs) is the leading cause of the childhood medulloblastoma (Shh-subtype). Previously we have shown that chromatin remodeler Brg1 is required for Shh target gene expression, and Brg1 deletion reduced CGNP proliferation in developing cerebellum. Current study focuses on the function of Brg1 in mouse model of Shh-subtype medulloblastoma. In CGNP cultured from SmoM2 transgenic mice where Shh pathway is constitutively active, we found Brg1 is required for CGNP mitogenic target gene expression and proliferation. In SmoM2 medulloblastoma cultures, we observed that tumor cell growth was inhibited by conditional knockout of Brg1. In subcutaneous transplantation, we found that tumors were significantly shrunk upon induction of Brg1 deletion. Detailed analysis indicated that Shh-dependent mitogenic target genes decreased by loss of Brg1. Further evidences showed that medulloblastoma cell proliferation was significant inhibited by conditional knockout of Brg1. Effect of Brg1 on the chromatin environment of target genes during medulloblastoma development will be discussed. Our study will provide insights to the epigenetic mechanism of Shh-dependent tumor development and new therapeutic targets.

**Citation Format**

Shi X, Zhang Z, Wang Q, Wu J. Function of Brg1 chromatin remodeling factor in sonic hedgehog-dependent medulloblastoma development [abstract]. Proceedings of the 105th Annual Meeting of the American Association for Cancer Research; 2014 Apr 5-9; San Diego, CA. Philadelphia (PA): AACR; 2014. Abstract nr 404.

Copyright © 2014 American Association for Cancer Research. All rights reserved.

## Biographical Sketch

**Provide the following information for each individual included in the Research & Related Senior/Key Person Profile (Expanded) Form.**

NAME XUANMING SHI	POSITION TITLE INSTRUCTOR		
EDUCATION/TRAINING (Begin with baccalaureate or other initial professional education, such as nursing, and include postdoctoral training).			
INSTITUTION AND LOCATION	DEGREE (IF APPLICABLE)	YEAR(S)	FIELD OF STUDY
Anhui University, Hefei, China	B.S.	1999	Biochemistry
Sichuan Agricultural University & Institute of Microbiology, Chinese Academy of Science, China	M.S.	2005	Biochemistry & Molecular Biology
University of Rostock & Research Institute for the Biology of Farm Animals, Germany	Ph.D.	2009	Molecular Biology
University of Texas Southwestern Medical Center at Dallas	Postdoctoral	2010	Developmental Biology
<b>RESEARCH AND PROFESSIONAL EXPERIENCE:</b>  <u><b>Positions and Employment</b></u> 1999-2001     Assistant Engineer, BBKA Biochemistry Group Company, Bengbu, China. 2001-2002     Technician, Institute of Microbiology, Chinese Academy of Sciences, Beijing, China. 2002-2005     Graduate student, Sichuan Agricultural University and Institute of Microbiology, Chinese Academy of Sciences. Mentor: Prof. Dr. Yubi Huang & Prof. Dr. Keqian Yang 2005-2009     PhD student, University of Rostock & Research Institute for the Biology of Farm Animals, Germany. Mentor: Prof. Dr. Hans-Martin Seyfert 2010- 2014     Postdoctoral researcher, UT Southwestern Medical Center, Texas. Mentor: Dr. Jiang Wu 2015-           Instructor, UT Southwestern Medical Center, Texas.			



## HONORS AND AWARDS

DoD Postdoctoral Fellowship (2012-2015)

## Professional Associations/Affiliations

American Association of Cancer Research 2013-2015

## Peer-reviewed Publications (in chronological order)

1. **Shi, X.**, Wang, Q., Gu, J., Xuan, Z., Wu, J., Brg1/SmadA4 Coordinates Genetic and Epigenetic Networks Underlying Shh-type Medulloblastoma Development. *Oncogene* (In Press).
2. **Shi, X.**, Zhan, X., Wu, J., A Positive Feedback Loop between Gli1 and Tyrosine Kinase Hck Amplifies Shh Signaling Activities in Medulloblastoma. *Oncogenesis* (2015) 4, e176; doi:10.1038/oncsis.2015.38.
3. Zhang, Z., Cao, M., Chang, C., Wang, C., **Shi, X.**, Zhan, X., Birnbaum, S., Bezprozvanny, I., Huber, K., Wu, J., Autism-Associated Chromatin Regulator Brg1/SmadA4 is Required for Synapse Development and MEF2-mediated Synapse Remodeling. *Molecular and Cellular Biology* 2015 Oct 12. pii: MCB.00534-15.
4. **Shi, X.**, Zhang, Z., Zhan, X., Cao, M., Satoh, T., Akira, S., Shpargel, K., Magnuson, T., Wang, C., Ge, K., Wu, J. (2014). An Epigenetic Switch Induced by Sonic Hedgehog Signaling Regulates Gene Activation during Neural Development and Medulloblastoma Growth. *Nat. Commun.* 5:5425 doi: 10.1038/ncomms6425 (2014).
5. **Shi, X.**, Metges, C.C., and Seyfert, H.-M. (2013) Characterization of a far upstream located promoter expressing the acetyl-CoA carboxylase-alpha in the brain of cattle. *Gene*. 2013 Feb 25;515(2):266-71.
6. **Shi, X.**, Metges, C.C., and Seyfert, H.-M. (2012). Interaction of C/EBP and NF-Y factors constrains the promoter IA activity of the bovine acetyl-CoA carboxylase-alpha gene. *BMC Molecular Biology* 2012 Jun 27;13(1):21 doi:10.1186.
7. Zhan, X.#, **Shi, X.#**, Zhang, Z., Chen, Y., Wu, J.I. (2011) Dual Role of Brg Chromatin Remodeling Factor in Shh Signaling during Neural Development. *Proc Natl Acad Sci U.S.A.*, 2011 Aug 2;108(31):12758-63. # **Co-first author**.
8. Liu, S., Shi, X., Guenther, J., Bauer, I., Seyfert, H.-M. (2011). Lingual Antimicrobial Peptide and IL-8 expression are oppositely regulated by the antagonistic effects of NF-KB p65 and C/EBPb in Mammary Epithelial Cells. *Mol. Immunol.* 2011 March 48(6-7):895-908.
9. **Shi, X.**, Liu, S., Metges, C.C., and Seyfert, H.-M. C/EBP-beta drives expression of the nutritionally regulated promoter IA of the acetyl-CoA carboxylase-alpha gene in cattle. *Biochim. Biophys. Acta-gene regulatory mechanism* 1799 (2010) 561-567.
10. Muráni, E., Ponsuksili, S., Seyfert, H.-M., Shi, X., and Wimmers, K. (2009). Dual effect of a single nucleotide polymorphism in the first intron of the porcine Secreted phosphoprotein 1 gene: allele-specific binding of C/EBP beta and activation of aberrant splicing. *BMC Mol Biol.* 2009 Oct 21;10(1):96.